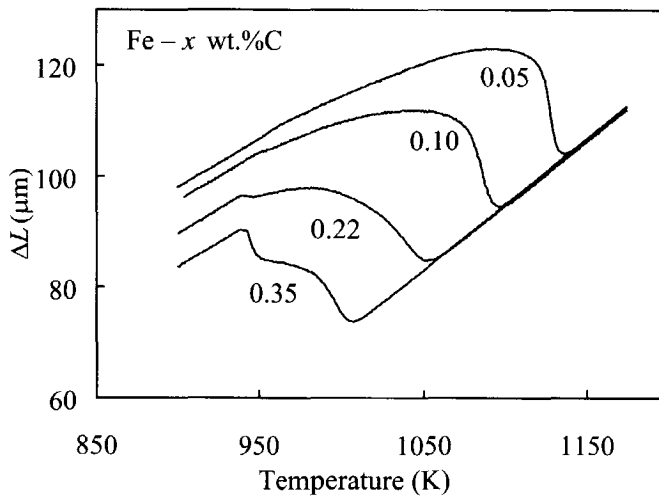# A dilatometric study of the austenite/ferrite interface mobility

Theo Kop

Stellingen

behorende bij het proefschrift

A dilatometric study of the austenite/ferrite interface mobility

Theo Kop
Oktober 2000, Delft

1. De aanname dat het proefstuk dat gebruikt wordt voor de studie van de austeniet/ferriet transformatiekinetiek isotroop uitzet is vaak onterecht.

2. Een grensvlakmodel is pas een zuiver grensvlakmodel als de drijvende kracht slechts gebaseerd is op de invloed van de atomen die op de plaats van het grensvlak aanwezig zijn.

3. De bepaling van de absolute waarde van de mobiliteit, M, van het austeniet–ferriet grensvlak is sterk afhankelijk van de waarde van een aantal andere grootheden, die niet nauwkeurig bepaald kunnen worden. Men dient zich daarom niet teveel op de absolute waarde van M te richten; trends in M–waarden zijn niettemin reëel.

4. Voor de modellering van de vorming van ferriet/perliet bandstructuren is een meer–korrelmodel nodig.
   S.W. Thompson, P.R. Howell, Mat. Sci. Techn. 8 (1992) 777

5. Wanneer twee verschillende benaderingen tot hetzelfde resultaat leiden betekent dit niet automatisch dat dit resultaat ook het juiste resultaat is.

6. Het opkomen van research naar de mogelijkheden van windenergie zal de definitieve doorbraak van kernfusie als energiebron uitstellen.

7. Het feit dat versnelde expositietesten klaarblijkelijk een goede indicatie geven voor "real-time" corrosieverschijnselen, toont aan dat de kinetiek van diffusieprocessen in het corroderende materiaal van ondergeschikt belang is.

8. Zowel voor de lager als de hoger geschoolde immigranten verloopt de integratie in het nieuwe thuisland voorspoediger als de lokale taal wordt beheerst.

9. Het feit dat het in Nederland ook mogelijk is de doctorsgraad te verkrijgen bij de verdediging van een proefschrift zonder stellingen toont aan dat een groot deel van de waarde van de stellingen ligt in het verhogen van het ceremoniële gehalte van de promotieplechtigheid.

A dilatometric study of the
austenite/ferrite interface mobility

THEO KOP

A dilatometric study of the austenite/ferrite interface mobility

Proefschrift
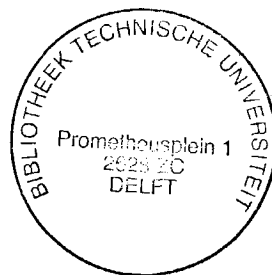
ter verkrijging van de graad van doctor
aan de Technische Universiteit Delft,
op gezag van de Rector Magnificus prof. ir K.F. Wakker,
voorzitter van het College voor Promoties,
in het openbaar te verdedigen op dinsdag 12 december 2000 om 16.00 uur

door

Theo Arnold KOP

doctorandus in de scheikunde
geboren te Rotterdam

Dit proefschrift is goedgekeurd door de promotor:
Prof. dr.ir. S. van der Zwaag

Toegevoegd promotor:
Dr. ir. J. Sietsma

Samenstelling promotiecommissie:

Rector Magnificus, voorzitter
Prof. dr. ir. S. van der Zwaag, Technische Universiteit Delft, promotor
Dr. ir. J. Sietsma, Technische Universiteit Delft, toegevoegd promotor
Prof. dr. ir. A. Bakker, Technische Universiteit Delft
Prof. dr. H. Zandbergen, Technische Universiteit Delft
Prof. H.K.D.H. Bhadeshia FRS, University of Cambridge, Engeland
Prof. Dr. –Ing. R. Kawalla, Technische Universität Bergakademie Freiberg, Duitsland
Prof. Dr. F. Sommer, Max Planck Institute for Metals Research, Stuttgart, Duitsland

Reservelid:
Prof. dr. S.J. Picken, Technische Universiteit Delft

Contents

1

General introduction

1.1. Introduction

Steelmaking has been practised for thousands of years. Its significance originates from the large amounts of iron ore present, and the good mechanical properties of steel products. Its long history makes it a well developed empirical technology. It used to be difficult to give a single, universally–accepted definition of the term "steel". For a long time steel was regarded "as a metal that was capable of being so hardened as to resist a common file" [1]. Others preferred a definition which was not so much related to the temperability: "iron which has been perfectly fused, and afterwards cast, while liquid, into a malleable ingot" [1]. Nowadays, a broadly accepted definition of steel is: "an alloy of iron and carbon, in which the carbon content amounts to 2 wt.% or less".

The discovery of X–ray diffraction, in 1895, made it possible to resolve crystal structures, and in 1912 the allotropy (changeable crystalline structure) of iron was discovered. It was found that the stable crystalline structure of iron up to 1185 K is a body centred cubic structure (bcc) and that the stable structure between 1185 K and 1667 K is a face centred cubic structure (fcc). The bcc–phase is called ferrite (α) and the fcc–phase is called austenite (γ). Steel owes many of its properties to this allotropy of iron in combination with the formation of additional phases which can occur upon alloying.

1.2. Scope of thesis

The austenite to ferrite phase transformation

This thesis relates to the behaviour of hypo–eutectoid steel grades. Hypo–eutectoid means that the carbon concentration is lower than 0.77 wt.% (figure 1.1). It is seen that the addition of carbon to iron causes the allotropic transition to shift in temperature; *e.g.* an alloy containing 0.1 wt.% C will start to transform at 1160 K, instead of at 1185 K. Furthermore, there is no longer a single transition temperature, but there is a transition region, the austenite/ferrite two–phase region, in which the austenite and ferrite are in equilibrium with each other. At temperatures below 1000 K the phase Fe_3C, called cementite, will be formed, giving rise to the ferrite/cementite two–phase region. The phase diagram gives the equilibrium phases. During processing the transitions do not occur at the equilibrium temperatures since the kinetics of the transformation play an important role. The austenite to ferrite transformation, like most solid state transformations, occurs via a nucleation and growth process. First the smallest stable aggregate of the new phase, the nucleus, has to form, and subsequently this nucleus can start to grow. Both these processes require a certain time. The time required for the transformation depends on a number of factors, one of them being the chemical composition of the phases present.

In general two types of alloying elements can be distinguished in accordance with their solubility in the iron matrix. Interstitially dissolved elements like carbon and nitrogen, are located in the octahedral vacancy sites of the iron lattice, while substitutionally dissolved elements like manganese and chromium are located at the same lattice sites as the iron atoms. In low alloy steel we can distinguish a third class of elements; the "micro–alloying elements", like niobium and titanium. These elements distinguish themselves by their tendency to form small precipitates at high temperatures. The different position and "role" of the alloying elements also cause a different influence on the transformation kinetics.

Transformation models

The kinetics of the austenite to ferrite phase transformation are highly dependent on the chemical composition, on the microstructure before transformation, *e.g.* austenite grain size and shape, the presence of additional phases (precipitates), and the stored deformation energy, and on the temperature at which the transformation occurs.

1185 K	
fcc	
bcc + fcc	fcc + θ
	1000 K
0.10 at.%	3.45 at.%
0.02 wt.%	0.77 wt.%
bcc + θ	
bcc	
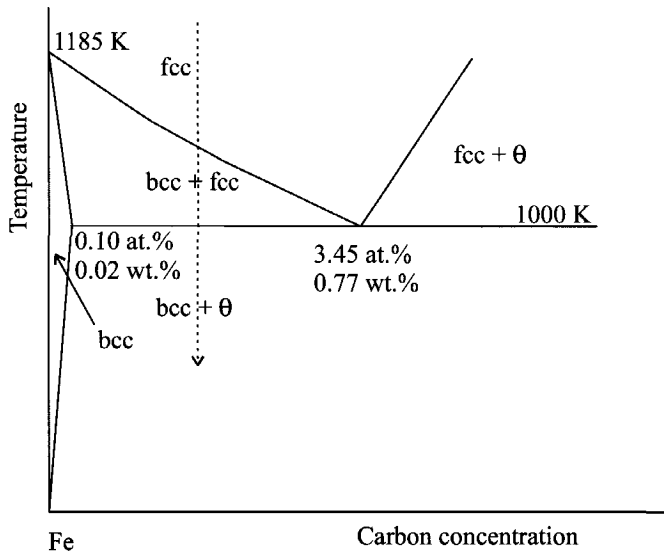
*Figure 1.1   Schematic drawing of a part of the Fe–C phase diagram. The austenitic (fcc)
and ferritic (bcc) area's are indicated as well as the region in which
cementite (θ) appears.*

To describe the kinetics of the austenite to ferrite phase transformation a number of models
has been developed. There are artificial neural network (ANN) models, semi–empirical
models, and models with a more physical approach. ANN models [2] and the semi–
empirical models [3] can be used to predict transformation behaviour for steels which are
closely related to the steels that are used to validate the model. These models, however, are
descriptive only and do not provide additional information about the processes governing
the transformation. They are therefore of little relevance when drastic changes in steel
grades [4–5] or steel production routes [6] are developed. The first austenite decomposition
models trying to incorporate physical features related to the ferrite growth process,
assumed that the rate of transformation was controlled by the diffusion of carbon [7].
Recent research acknowledged the fact that besides the diffusion of carbon, the kinetics of
the actual transformation of the fcc into the bcc lattice could play a role in the overall
transformation kinetics [8].

Dilatometry
To develop and validate models it is important to have reliable data. The evolution of the
austenite to ferrite transformation can be measured by a number of techniques, all with

3

their specific advantages and disadvantages. A convenient and often applied technique is dilatometry. A dilatometer measures the expansion behaviour of materials [9–11], by measuring a change in current brought about in a linear variable differential transformer (LVDT). This technique can register length changes of about 0.01%. Following the length change during the transition of the fcc to the bcc structure of iron, comprising in total of a volume change of about 1.6 %, can therefore be used to obtain data on the kinetics of the transformation. Although this technique is often used for studying phase transformations in steel, only a few studies on the validity of the conversion of length changes in volume fractions transformed have been published [12–13].

1.3. Contents of thesis

The industrial relevance of the kinetics of the austenite to ferrite phase transformation emerges via the possibility to control the formation of the microstructure; the microstructure which determines the mechanical properties. This means that both for the processing, *e.g.* at which temperature and with what force should the material be rolled, and for the development of the final microstructure, *e.g.* for the properties of the end–product, it is important to know how the microstructure depends on the production process variables: the temperature (change) and the degree of deformation. This thesis contributes to the development of a model for the austenite to ferrite phase transformation. The model is based on physical and microstructural features, thereby aiming to enlarge the insight into the physical processes occurring. By doing so, the results and insight gained are helpful in the development of new steel grades and steel production processes. The model [6, 14] describes the transformation via a nucleation and growth process. The growth is assumed to be controlled by the intrinsic mobility of the austenite/ferrite interface. Data on the austenite to ferrite transformation kinetics are mainly determined using dilatometry.

In the first part of this thesis the applicability of dilatometry for the determination of fractions transformed during the austenite decomposition of steel is treated in detail. The second part concentrates on the transformation kinetics of different steel systems. In general during the analysis of the dilatation signal two assumptions are made. First, it is assumed that the observed length change is proportional to the fraction transformed. Chapter 2 shows that this assumption is violated in the case of iron–carbon alloys. The influence of the carbon enrichment of the austenite during the transformation, and the difference in volume between ferrite and cementite are shown to be crucial factors. An

alternative method to analyse the dilatation signal during continuous cooling experiments of iron–carbon alloys is given. Chapter 3 discusses the validity of the second assumption, *i.e.* that the dilatation behaviour of the measured sample is isotropic. This is an important question for hot rolled steels which show a banded ferrite/pearlite structure. Dilatometric measurements on samples taken from the normal and the longitudinal rolling direction are performed and a model is presented to explain the observed dilatation behaviour. The implications for the determination of the fractions transformed are discussed.

Chapter 4 describes the transformation behaviour of pure binary substitutional iron alloys; Fe–X, with X denoting 1 or 2 at.% Al, Co, Cr, Cu or Mn. In this chapter the intrinsic mobility of the austenite/ferrite interface is determined. A range of alloys is used to obtain a range of transformation temperatures. Furthermore the cooling rate is varied. The data indicate a dependence of the intrinsic interface mobility on the nitrogen impurity of the samples. The interstitial nitrogen dependence is further investigated in chapter 5, which discusses the transformation kinetics of an Fe–1at%Si alloy. Samples are given various internal nitriding treatments to vary the nitrogen content. The ferrite fractions are experimentally determined and the model fraction curves are discussed. Chapter 6 deals with the transformation behaviour of lean carbon manganese steels. In this chapter the effect of the interstitials is incorporated via a "mean field approach", which effectively means that the transformation kinetics are solely determined by the interface mobility. In the discussion the role of carbon diffusivity in relation to the transformation kinetics is addressed, as well as the role of the nucleation process. Chapter 7 describes the effect of different austenitisation conditions on the transformation kinetics for a micro–alloyed steel. The interface mobility model as presented in chapter 4, in combination with the mean field approach as presented in chapter 6, is used to gain insight into the role of niobium on both the nucleation and the growth process.

References

1   J.S. Jeans, *Steel: its history, manufacture, properties and uses*, Spon, London (1880).

2   W.G. Vermeulen, P. van der Wolk, P.F. Morris, S. van der Zwaag, *Steel Research*, 68 (1997) 72.

3   S.V. Parker, "Modelling of Phase Transformations in Hot-Rolled Steels", PhD thesis, University of Cambridge, (1997).

4   European Patent Office, EP 0 750 049 A1.

5   P. Jacques, E. Girault, T. Calin, N. Geerlofs, T. A. Kop, S. van der Zwaag, F. Delannay, *Mat. Sci. Eng.* A273–275 (1999) 475.

6   Y. van Leeuwen, Ph.D. thesis, Delft University of Technology, (2000).

7   C. Zener, *J. Appl. Phys.* 20 (1949) 950.

8   G. P. Krielaart, J. Sietsma, S. van der Zwaag, *Mat. Sci. Eng.* A237 (1997) 216.

9   W. Gorski, *Dilatometrie–Grundlagen und Messverfahren*, Physicalisch Technische Bundesanstalt, Braunschweig (1996).

10   R.F. Speyer, *Thermal Analysis of Materials*, Marcel Decker, New York (1994).

11   G. Berger, *La dilatométrie différentielle appliquée a l'étude des aciers*, Dunod, Paris (1965).

12   M. Takahashi, H.K.D.H. Bhadeshia, *J. Mat. Sci. Lett.* 8 (1989) 477.

13   M. Onink, F.D. Tichelaar, C.M. Brakman, E.J. Mittemeijer, S. van der Zwaag, *Z. Metall.* 87 (1996) 24.

14   Y. van Leeuwen, S. Vooijs, J. Sietsma, S. van der Zwaag, *Met. Mat. Trans. A*, 29A (1998) 2925.

2

Dilatometric analysis of phase transformations in hypo–eutectoid steels

Dilatometry is a useful technique to obtain experimental data concerning transformation kinetics in ferrous alloys. This technique is commonly used in cooling experiments to study the austenite decomposition of hypo–eutectoid steel grades. In the standard analysis of the dilatation signal there are two factors that are normally neglected. During the pro–eutectoid ferrite formation the austenite enriches in carbon, resulting in a non–linear temperature dependence of the specific austenitic volume. Furthermore, the specific volume of the formed ferrite is considerably different from that of the formed pearlite. Not taking into account these two effects can lead to an error in the determined fraction ferrite of up to 25 %. A method is presented that takes into account the two above–mentioned factors. In order to determine both the fraction ferrite and the fraction pearlite, in the analysis the temperature range of the transformation is divided into a ferrite–formation range and a pearlite–formation range. Two possible criteria for this division are discussed, and it is shown that the choice between these two does not have an essential influence on the results.

2.1. Introduction

The production of hot–rolled steel plates with desired mechanical properties is a very complex process. A whole range of material properties, such as good formability or high strength, can be obtained by small variations in the amounts of alloying elements or in the process parameters, such as the temperature programme and the rolling parameters. Although there is a reasonable degree of empirical knowledge concerning steelmaking, the endeavour to produce superior qualities, whilst at the same time reducing costs, drives a considerable effort of fundamental research to obtain a more profound knowledge about the physical processes governing the austenite (γ) to ferrite (α) phase transformation. The importance of this research arises from the fact that it is this phase transformation that determines to a considerable extent the microstructure, and thereby the properties, of the final product.

Several models exist that predict the $\gamma \rightarrow \alpha$ transformation kinetics [1–7]. All models are developed by comparing and relating the model to experimental data. To obtain a reliable model it is therefore essential to have reliable experimental data. A technique often used to obtain information on the transformation kinetics, i.e. fractions austenite and ferrite as a function of temperature and time, is dilatometry [8–9]. Dilatometry registers length changes that occur during the heat treatment of a sample. A common method to determine the remaining fraction austenite as a function of temperature is to extrapolate the linear expansion behaviour from the temperature regions where no transformations occur, and to subsequently assume a proportionality between the fraction decomposed austenite and the observed length change. We will refer to this method as the lever–rule method. It should be realised, however that this approach is valid only if a single, non–partitioning phase transformation occurs. In the case of carbon–containing alloys, this method is not applicable for two reasons [10–12]: (1) the carbon redistributes between the forming ferrite and the remaining austenite, which increases the specific volume of the austenite, and (2) the formation of pearlite has a distinctly different volume effect than the formation of ferrite. In the present paper the dilatometric effects occurring during continuous cooling of carbon–containing steels are analysed taking these effects into account. In addition the effect of two different assumptions concerning the temperature range of the pearlite formation is shown. Experiments performed on steel alloys containing 0.2 – 2.1 at.%C (0.05 – 0.45 wt.%) are used to illustrate the method.

2.2. Theory

The applicability of dilatometry in phase transformation research is due to the change of the specific volume of a sample during a phase transformation. When a material undergoes a phase change, the lattice structure changes and this is in principle accompanied by a change in specific volume. Upon cooling of a pure iron sample from temperatures above the A_3–temperature, the austenite, having a face–centred cubic structure, will transform into ferrite, having the less closely packed body–centred cubic structure. This phase transformation will cause a volume expansion of about 1.6 %.

In the case of steel the iron is alloyed. The alloying gives rise to two–phase regions in the phase diagram. When a material transforms in such a two–phase region two processes occur. The lattice transformation takes place, but in addition there will be a redistribution of alloying elements. This means that the composition of the newly formed phase is not equal to the overall composition of the decomposing phase. Consequently, the composition of the decomposing phase changes. This gives rise to a change in the specific volume of the original phase. More specifically, a sample of a hypo–eutectoid carbon steel cooled from the austenite region, will cross the austenite/ferrite two–phase region. During the transformation the austenite will gradually transform into ferrite, in which the maximum solubility of carbon is limited, and the remaining austenite will enrich in carbon. Both the formation of ferrite and the enrichment of austenite cause an expansion of the sample. This can be seen in figure 2.1. Using the expressions for the lattice parameters for Fe–C alloys [10, 13–16], see table 2.1, the atomic volume V^γ of austenite as a function of the carbon concentration, ξ, is shown at an example temperature of 900 K. It can be seen that with increasing carbon content the austenitic volume increases. The maximum solubility of carbon in ferrite is approximately 0.09 at.%. The influence of carbon on the specific volume of ferrite is therefore limited. Upon further cooling the austenite decomposes into the equilibrium low–temperature phases ferrite and pearlite, a mixture of ferrite and cementite (Fe_3C).

The carbon–content dependence of the lattice parameters (table 2.1 and figure 2.1) has important implications for the volume effect of the transformation. The first is that the total volume effect of the transformation depends on the carbon content of the alloy. The second is that the volume effect of the ferrite formation from austenite significantly differs from the volume effect of pearlite formation. The third is that the volume effect of the transformation of austenite to ferrite depends on the carbon concentration of the austenite. The fourth is that this volume effect consists of two contributions, namely the specific–

volume difference between austenite and ferrite, and the increase of the austenite specific volume due to carbon enrichment.

Table 2.1   Lattice parameters of ferrite (α) and austenite (γ) and of the orthorombic phase cementite (θ) as a function of temperature T and the atomic fraction carbon ξ [10, 13–16].

Phase	Lattice parameters (Å)
α	$a_\alpha = 2.8863 \text{ Å} \cdot (1 + 17.5 \cdot 10^{-6} \text{ K}^{-1} \cdot [T - 800 \text{ K}])$ $800 \text{ K} < T < 1200 \text{ K}$
γ	$a_\gamma = (3.6306 + 0.78 \cdot \xi) \text{ Å} \cdot (1 + (24.9 - 50 \cdot \xi) \cdot 10^{-6} \text{ K}^{-1} \cdot [T - 1000 \text{ K}])$ $1000 \text{ K} < T < 1250 \text{ K}; \ 0.0005 < \xi < 0.0365$
θ	$a_\theta = 4.5234 \text{ Å} \cdot (1 + \{5.311 \cdot 10^{-6} - 1.942 \cdot 10^{-9} \text{ K}^{-1} \cdot T + 9.655 \cdot 10^{-12} \text{K}^{-2} \cdot T^2\} \text{ K}^{-1} \cdot [T - 293 \text{ K}])$ $b_\theta = 5.0883 \text{ Å} \cdot (1 + \{5.311 \cdot 10^{-6} - 1.942 \cdot 10^{-9} \text{ K}^{-1} \cdot T + 9.655 \cdot 10^{-12} \text{ K}^{-2} \cdot T^2\} \text{ K}^{-1} \cdot [T - 293 \text{ K}])$ $c_\theta = 6.7426 \text{ Å} \cdot (1 + \{5.311 \cdot 10^{-6} - 1.942 \cdot 10^{-9} \text{ K}^{-1} \cdot T + 9.655 \cdot 10^{-12} \text{ K}^{-2} \cdot T^2\} \text{ K}^{-1} \cdot [T - 293 \text{ K}])$ $300 \text{ K} < T < 1000 \text{ K}$

When the dilatation during the phase transformation is to be analysed the effects shown in figure 2.1 should be considered. The observed length change during the initial part of a measurement, due to the austenite to ferrite transformation, is the summation of two effects: the dilatation due to the lattice change and the enlargement of the remaining austenite due to carbon enrichment of this phase. The momentary dilatation effect therefore does not depend on the initial carbon concentration, but on the actual carbon concentration of the austenite, which depends on the degree of transformation.

The atomic volume of a sample is determined by the fractions of the phases present multiplied by their atomic volume, according to

$$V(T) = \sum_i f^i \cdot V^i(T), \tag{2.1}$$

where V is the average atomic volume of the sample, V^i is the atomic volume of phase i, f^i is the volume fraction of phase i, and T is the temperature. i can be α for ferrite, γ for

austenite or p for pearlite. The atomic volumes are related to the lattice parameters (table 2.1) by $V^{\alpha} = \frac{1}{2} a_{\alpha}^3$; $V^{\gamma} = \frac{1}{4} a_{\gamma}^3$; $V^p = (1-\rho)V^{\alpha} + \rho V^{\theta}$, with $V^{\theta} = 1/12 \, a_{\theta}b_{\theta}c_{\theta}$, and ρ the fraction cementite in the pearlite. In this study a constant value for ρ is used.

Equation (2.1) can be used to calculate the phase fractions from the volume change of a sample. However, the procedure is not completely straightforward, since only the length change is measured, from which data on three different phases are to be obtained.
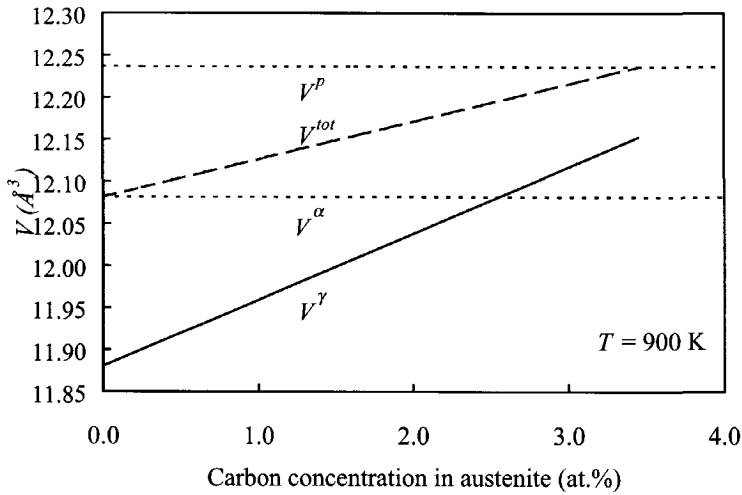
Figure 2.1   *The atomic volumes of austenite, V^{γ}, and of a system composed of equilibrium fractions ferrite and pearlite, V^{tot}, depending on the carbon concentration at a temperature of 900 K. The levels of the atomic volume of ferrite, V^{α}, and pearlite, V^p, are depicted as well.*

Two intrinsic factors prevent an unambiguous determination of the phase fractions: the simultaneous formation of two phases, *i.e.* ferrite and pearlite, and the carbon–concentration dependence of the atomic volume of austenite. As such, the dilatometer can not distinguish between the formation of pro–eutectoid ferrite and pearlite. If the formation of ferrite and pearlite is assumed to take place in separate temperature regions, as is expected from the equilibrium phase diagram, the dilatation of a sample can be analysed in two steps. The complication of the austenitic volume being carbon–concentration dependent is solved by using literature data for the austenite lattice [14].

The subsequent stages of the dilatation analysis will now be outlined. At high temperatures, in the beginning of the austenite to ferrite transformation, there is no pearlite. The fraction ferrite is then given by

$$f^\alpha = \frac{V - V^\gamma}{V^\alpha - V^\gamma},$$ (2.2)

which follows from equation (2.1), with $f^\alpha + f^\gamma = 1$.

In principle this equation can be solved with V evaluated from the dilatometer measurement, and V^α and V^γ from the literature (table 2.1). However, due to the carbon enrichment of the austenite, which depends on the momentary ferrite fraction, equation (2.2) can not be solved analytically. The fraction ferrite is therefore determined in an iterative process, for which the Newton–Raphson method is used.

In the second part of the transformation only pearlite can be assumed to form. This means that the ferrite fraction, f^α, is constant. No further austenite enrichment occurs, the austenitic volume is therefore only temperature dependent. The fraction pearlite is then readily found from

$$f^p = \frac{V - V^\gamma + f^\alpha \cdot (V^\gamma - V^\alpha)}{V^p - V^\gamma}.$$ (2.3)

The fraction ferrite as found from the analysis of the high–temperature part of the curve determines both the (constant) carbon concentration of the austenite during the pearlite formation and the ratio of cementite and ferrite in the pearlite.

In the case of assumed non–overlapping transformations, the temperature range of the transformation is divided into a temperature range $T > T_t$, in which the dilatation is to be analysed as due to ferrite formation, and a temperature range $T < T_t$, in which the dilatation is to be analysed as due to pearlite formation. Two assumptions can be made to define T_t. The first possible assumption is that pro–eutectoid ferrite formation takes place until the final equilibrium fraction ferrite, f^α_{eq} is obtained. The temperature T_t then equals the temperature at which $f^\alpha = f^\alpha_{eq}$. A second possible criterion for the transition from the ferrite analysis to the pearlite analysis is to choose T_t as the temperature at which the (second) point of inflection occurs in the length change with respect to the temperature. The point of inflection indicates an increased transformation velocity, which is expected at

the start of the pearlite formation. (The first inflection point corresponds to the start of the ferrite formation.)

The distinction of temperature ranges for ferrite formation and for pearlite formation is somewhat artificial, but necessary to deduce different phase fractions from a single measurement. Simultaneous formation of ferrite and pearlite in a limited temperature range is in principle possible, but cannot be distinguished by dilatometry. Both methods to determine T_t, however, have their drawbacks. Using the equilibrium ferrite fraction can easily lead to small errors for two reasons. First, due to higher cooling rates, the ferrite fraction that is actually formed can be different from the equilibrium ferrite fraction. And secondly, small deviations, due to experimental inaccuracies, in the determined ferrite fraction can lead to relatively large shifts in the pearlite start temperature T_t. Using the point of inflection in the measured dilatation data to determine T_t seems more appropriate but is not always possible, especially at high cooling rates.

2.3. Dilatometry

The volume change of a sample can be monitored by means of a dilatometer. The dilatometer measures length changes. For the analysis of the data it is assumed that the expansion/contraction is isotropic. For small relative volume changes the measured length change is related to the volume change by

$$\frac{\Delta L}{L_0} = \frac{1}{3} \cdot \frac{\Delta V^S}{V_0^S} = \frac{1}{3} \cdot \frac{\Delta V}{V_0} \ , \tag{2.4}$$

where ΔL is the measured length change, $L_0 = 10.0$ mm the initial length, ΔV^S and $V^S{}_0$ the volume change and the starting volume of the sample, and ΔV and V_0 the average atomic volume change and the initial average atomic volume, respectively. In order to introduce the measured dilatation ΔL in the equations (2.1) and (2.2), the average atomic volume V can be written as

$$V = \kappa \cdot V_0 \cdot \left(\frac{3\Delta L}{L_0} + 1 \right), \tag{2.5}$$

13

where κ, a scaling factor, ideally equals 1. In practice, however, some non–idealities occur. First, it is possible that there is a contribution from the dilatation measuring system to the measured signal. Another effect that can occur is a net length change of the sample due to effects of transformation plasticity in combination with non–isotropic conditions [17–18]. To compensate for such effects, in equation (2.5) the scaling factor κ is introduced. In the ideal case the ferrite and pearlite volume fractions can be determined using equations (2.2) through (2.5), with $\kappa = 1$.

In the non–ideal case of a dilatometric experiment, the scaling factor can be determined by considering the dilatation signal just before (eqs. (2.1) and (2.5) with $f^\gamma = 1$) and after (eqs. (2.3) and (2.5) with $f^\alpha = f^\alpha_{eq}$ and $f^P = f^P_{eq}$) the transformation. Due to the lack of detailed information on the transformation–plasticity effects, the scaling factor is varied linearly between the values found directly before and after the transformation.

The analysis presented here will be compared to the most widely used method to analyse dilatometry data, the lever–rule method. In the latter method the formation of a single phase is assumed, and the length change of the sample is assumed to be proportional to the fraction of this phase. For the application of this method the dilatation from the higher and lower temperature part of the dilatation curve are extrapolated (see figure 2.2). The fraction transformed determined by this method, ϕ, which is the sum of the ferrite and pearlite fractions, is then assumed to be given by the ratio of the observed dilatation to the maximum possible dilatation at each temperature, and calculated by

$$\phi = \frac{\Delta L - \Delta L^\gamma_e}{\Delta L^\alpha_e - \Delta L^\gamma_e} \,, \tag{2.6}$$

where ΔL^γ_e and ΔL^α_e represent the extrapolated dilatations in the high–temperature and low–temperature range respectively.

In using this method two implicit assumptions are made:
(1) the effect of carbon enrichment of the austenite is negligible, and
(2) the atomic volumes of ferrite and pearlite are equal.
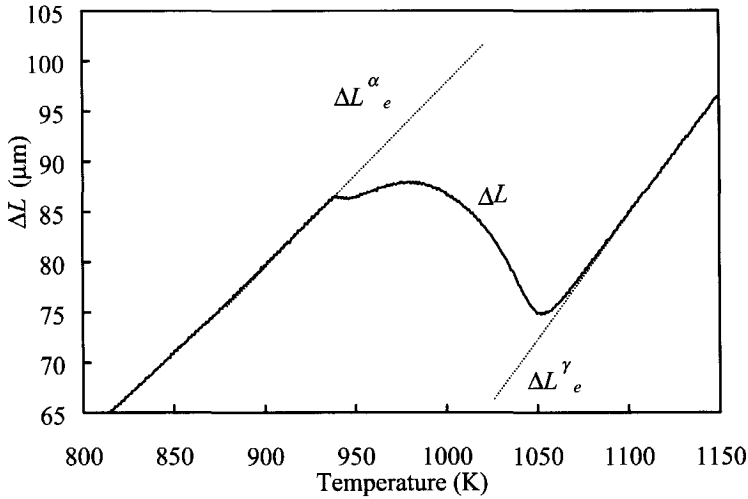
Figure 2.2   *Example dilatation curve during cooling. The straight lines are the extrapolated austenitic length change and the ferritic–pearlitic length change. The fraction transformed according to the lever–rule method (ϕ) is given by the ratio of the apparent dilatation change, $\Delta L - \Delta L^{\gamma}_{e}$, to the maximum possible dilatation change, $\Delta L^{\alpha}_{e} - \Delta L^{\gamma}_{e}$.*

In order to illustrate the difference between the lever–rule method and the current method, the fractions transformed obtained by both methods from an artificial dilatation curve have been compared. The dilatation curve is calculated for iron alloyed with 1.0 at.%C (0.22 wt.%C), assuming transformation under equilibrium conditions and using the lattice parameters given in table 2.1. Figure 2.3 shows the results of the analyses of the dilatation curve up to the equilibrium fraction ferrite. For this artificial case, the presently discussed method yields the exact transformation curve. The relative error ε_L in the lever–rule results is defined by

$$\varepsilon_L = \frac{\phi - f^{\alpha}}{f^{\alpha}} \ . \tag{2.7}$$

ϕ is the fraction obtained from the lever–rule approach (eq. (2.6)) and f^{α} the true fraction ferrite. It can be seen in figure 2.3 that the relative error is largest at the beginning of the

15

transformation, while of course the absolute error (visible as the difference between the two fraction curves) is largest at the end of the ferrite formation. The error is mainly due to neglecting the difference in the ferritic and pearlitic specific volume. In the present method the dilatation signal is related to the specific–volume difference of the austenite phase and the ferrite phase, while in the lever–rule approach an average volume of ferrite and pearlite is used. Since in reality the pearlitic volume is larger than the ferritic volume, the effect of pearlite formation is underestimated, and therefore the extent of ferrite formation is overestimated. The difference increases with increasing carbon concentration. In the course of the transformation this error is slightly compensated by not taking the enrichment of the austenite into account. Therefore during the transformation there is a slight and continuous decrease in ε_L. The analysis of the error connected to the application of the lever rule has been performed for several carbon concentrations.
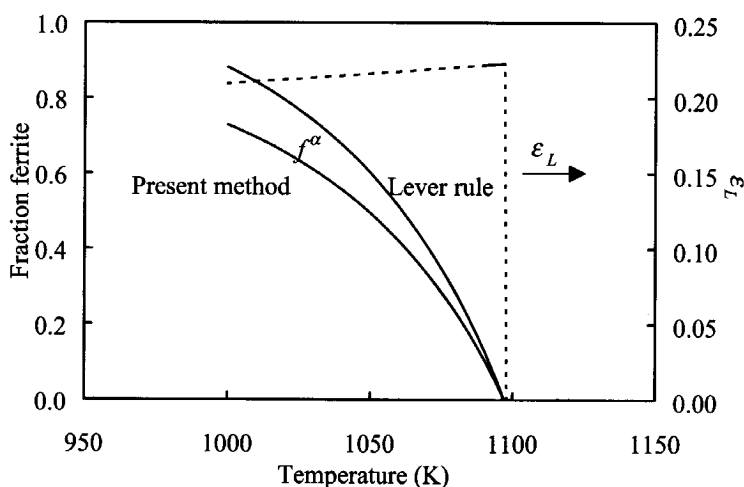
Figure 2.3   The fractions transformed determined from a calculated dilatation curve of a steel sample containing 1.0 at.%C by the lever rule and by the presently discussed method, and the resulting relative error, ε_L, in the fraction ferrite.
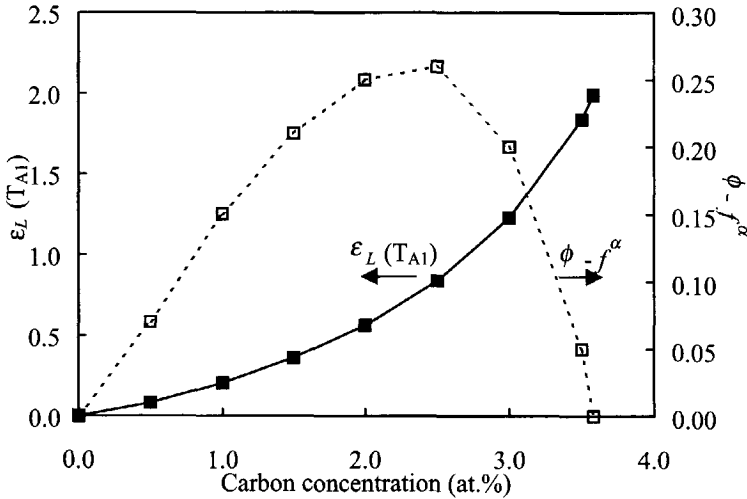
Figure 2.4   The relative and absolute maximum difference between the fraction ferrite determined by the lever rule and by the present approach at the A_1–temperature as a function of the carbon concentration.

In figure 2.4 the value of ε_L at the pearlite–formation temperature T_{A1} for several alloys with varying carbon concentration is given. It can be seen that there is a progressively increasing relative error, $\varepsilon_L(T_{A1})$, with increasing carbon concentration. For higher carbon concentrations less ferrite is formed and therefore the maximum absolute difference, $\phi - f^\alpha$, in the determined ferrite fraction diminishes.

For the pearlite formation a similar comparison can be made and the argumentation for the fractions ferrite applies for the pearlite fractions as well. For clarity of the discussion only the results of the comparison of the fractions ferrite are given and discussed. It should be noted that in principle the lever rule only gives the amount of transformed austenite and does not give information over individual fractions ferrite and pearlite.

2.4. Experimental

In order to test the presently proposed method, transformation experiments on a series of steels with different carbon contents have been performed. The composition of the samples is given in table 2.2.

Table 2.2   Compositions of the alloys in weight percentages. For carbon the atomic percentages are given as well (in brackets).

alloy	C (at.%)	Mn	Si	Cu	Cr	Ni	Mo	Sn	P	S
C05	0.055 (0.26)	0.237	0.008	0.009	0.023	0.024	0	0.002	0.011	0.013
C07	0.072 (0.33)	0.365	0.007	0.010	0.024	0.024	0.002	0	0.012	0.013
C10	0.103 (0.48)	0.490	0.006	0.009	0.018	0.021	0	0	0.01	0.014
C22	0.214 (0.99)	0.513	0.200	0.086	0.021	0.049	0.003	0.003	0.019	0.031
C35	0.364 (1.67)	0.656	0.305	0.226	0.177	0.092	0.016	0.017	0.014	0.021
C45	0.468 (2.14)	0.715	0.257	0.231	0.193	0.144	0.017	0.013	0.002	0.031

The dilatation of the samples as a function of temperature is determined using a Bähr 805A/D dilatometer. Figure 2.5 gives a schematic representation of the instrument. The sample is 10.0 mm long with a diameter of 4.0 or 5.0 mm. Two thermocouples, type S, are spot welded onto the sample, which is clamped between quartz push rods. One thermocouple is used to control the heating power and one serves as a reference to verify the temperature homogeneity. The temperature differences between the two thermocouples remain within 10 K. In the present experiments, each sample is heated by induction to a temperature of 1223 K, austenitised for 5 minutes and subsequently cooled at a rate of 20 K/min.

The temperature of the push rods does not remain constant during the measurement due to thermal conductivity effects from the sample. Due to the small expansion coefficient of

quartz, $0.5 \cdot 10^{-6}$ K^{-1} (the expansion coefficient of steel is approximately $10 \cdot 10^{-6}$ K^{-1}), the contribution of the push rods to the measured length is limited. The length change of the sample plus push rods is recorded by a linear variable differential transformer.
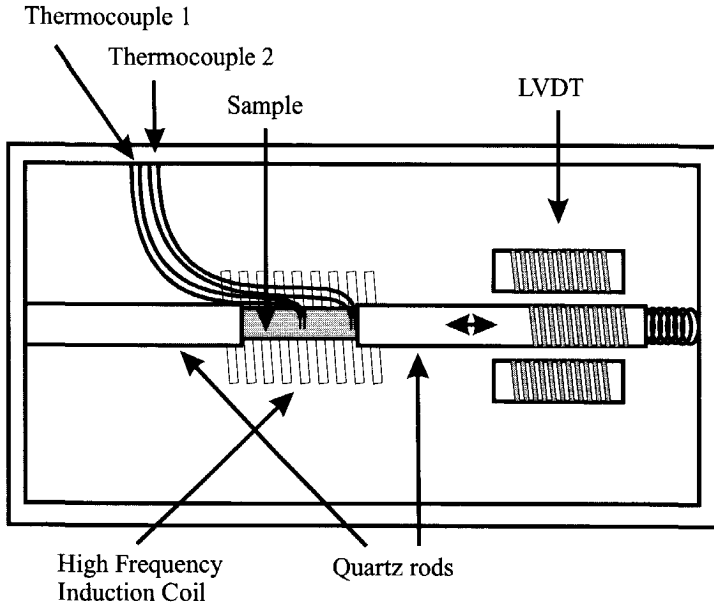
Figure 2.5   Schematic representation of the dilatometer configuration.

During the experiment, the heating power is also registered. This provides a means to have an independent absolute temperature reference, since a ferromagnetic material, ferrite at $T < T_C$ (T_C is the Curie temperature), is more easily heated by induction than a paramagnetic material, austenite or ferrite at $T > T_C$. Therefore, a distinct drop in the power required to keep the sample at the scheduled temperature appears when the sample transforms from the paramagnetic to the ferromagnetic state. The Curie temperature of steel is known to be almost independent of the carbon concentration, but it depends strongly on the manganese concentration. From thermodynamic data it follows that this dependence can be expressed by the relation

$$T_C = 1042 \text{ K} - x_{Mn} \cdot 1500 \text{ K}, \tag{2.8}$$

with x_{Mn} the weight fraction manganese.
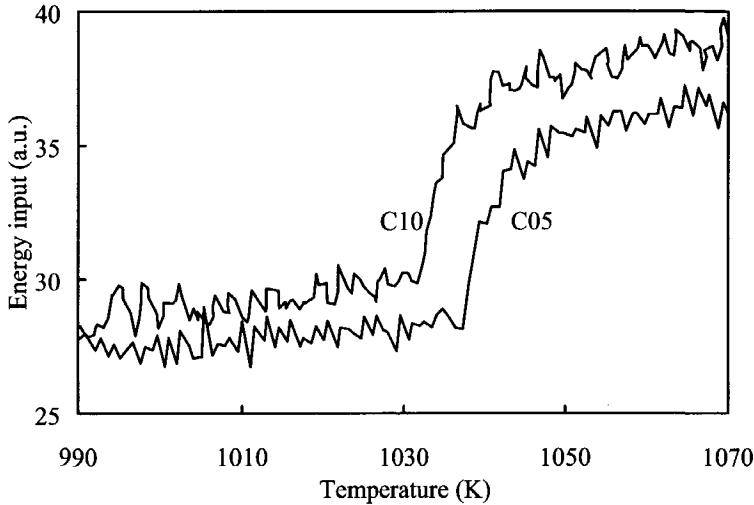
Figure 2.6   The required power to follow the scheduled temperature programme for the samples C05 and C10. The change in the required power corresponds to the Curie transition.

Figure 2.6 gives two examples of such internal temperature checks. The steel C05 contains 0.24 at.%Mn (table 2.2), which implies that T_C = 1038 K. Steel C10, with more manganese, 0.50 at.%, should have a lower Curie temperature, namely 1034 K. The temperatures at which the heating power drops during the measurements indicate that the dilatometer temperature measurement system yields correct absolute temperature values.

2.5.   Results and discussion

Figure 2.7 depicts the measured dilatation curves, represented as $\Delta L/L_0$ vs. T, for the six steel compositions given in table 2.2. The curves have been shifted along the $\Delta L/L_0$ – axis in order to make them coincide in the austenite region. It is observed that at higher carbon levels, going from sample C05 to C45, the transformation–start temperature shifts towards lower temperatures. This tendency is readily understood from the phase diagram. Furthermore, it can be seen that the length change caused by the transformation becomes less with increasing carbon content. This was already predicted in the Theory section and

is readily understood from figure 2.1. In figure 2.8 the dilatation difference $(\Delta L - \Delta L^{\gamma}{}_{e})$ at a temperature of 900 K is depicted against the calculated length change at the same temperature. It can be seen that the measured length change is consistently smaller than the calculated length change. This is consistent with the observation that the length of the sample after a complete transformation cycle is less than at the beginning of the experiment. The most likely explanation of these observations is that they are due to transformation plasticity.
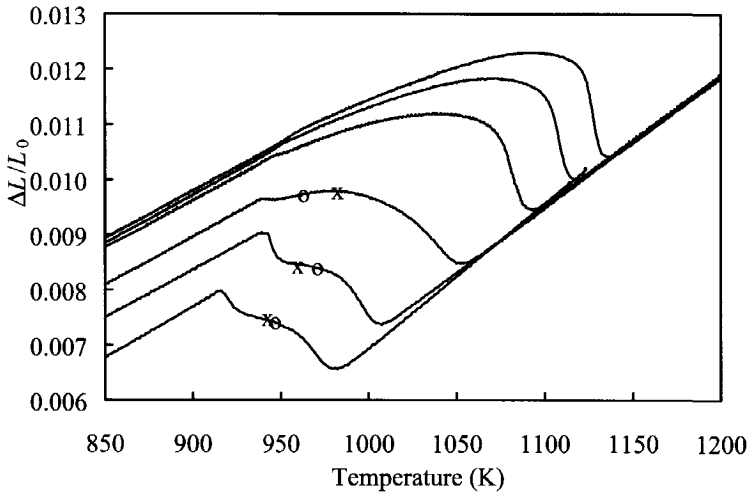
Figure 2.7   The measured dilatation curves for the six alloys of table 2.2. The curves are shifted along the $\Delta L/L_0$ – axis in order to coincide in the austenite region. The crosses and circles indicate the T_t temperatures, according to the two criteria used.

The scaling factor κ (equation (2.5)) is determined from each measurement as described in the Dilatometry section. The values found for κ are given in table 2.3. It can be seen that only a slight correction is needed, between 0.4 and 0.8 %. The difference between the two κ–values within each measurement never exceeds $7 \cdot 10^{-4}$. Despite the variations being only slight, it is essential to introduce a factor κ to get consistent values for the phase fractions.
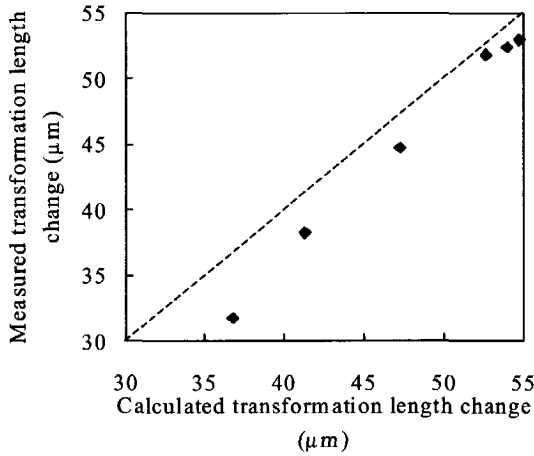
Figure 2.8   The calculated vs. measured apparent dilatation caused by the transformation for the six compositions determined at 900 K.

Table 2.3   Experimental scaling factor κ in the ferrite/pearlite and the austenite region.

alloy	κ in ferrite/pearlite region	κ in austenite region
C05	1.0073	1.0078
C07	1.0056	1.0058
C10	1.0037	1.0038
C22	1.0078	1.0075
C35	1.0060	1.0054
C45	1.0046	1.0039

In order to deduce the ferrite and pearlite fractions from the dilatation curves the temperature T_t is chosen, indicating the distinction between the temperature ranges of ferrite and pearlite formation. As previously stated, two approaches are used. In the first approach it is assumed that ferrite is formed until the equilibrium fraction is reached, and that subsequently only pearlite forms. The resulting fractions for the measurements of figure 2.7 are shown in figure 2.9a. The transition from ferrite to pearlite is marked with an cross, x, both in figure 2.7 and figure 2.9a. It can be seen that for C05 and C07 there is a temporary decrease in the fraction at the end of the ferrite formation. This is probably due to the application of the linear variation of the scaling factor. As explained before, one of

the spurious effects that influences the dilatation curve is transformation plasticity. The plasticity effect is different for the austenite/ferrite transformation and the austenite/pearlite transformation. Therefore, the linear variation of κ during the complete transformation that is assumed in the analysis, should be seen as a first–order approximation. For low carbon concentrations the difference between the measured volume change and the ferritic volume –the numerator in equation (2.2)– is small, and therefore very sensitive to the value of κ. The transition temperature T_t in figure 2.9a coincides well with the temperatures at which an accelerated transformation rate is observed. There is a considerable variation in the pearlite start temperatures of the several materials. This variation in the Ar_1–temperature seems large in view of the variation in chemical composition of the alloys and their reaction kinetics.

Figure 2.9b gives the results when using the second approach for the choice of T_t. Now, the pearlite start temperatures as indicated by the inflection point in the dilatation curve (figure 2.7, marked with an o) are used to switch to the pearlite analysis. Comparing with the results depicted in figure 2.9a, the pearlite start temperatures have shifted significantly (see table 2.4 and figure 2.7), especially for low carbon contents, causing the Ar_1–temperatures for the six alloys to be within a smaller range. Nevertheless, the deviations in the ferrite fraction between the results for the two different transition criteria are only slight. The unrealistic drop in the fraction curves for lower carbon contents does not appear in figure 2.9b. All in all, the choice of using the point of inflection to determine T_t leads to more consistent transformation curves than determining T_t through the equilibrium ferrite fraction. Nevertheless, the differences between both approaches are not very large, especially when considering the ferrite formation. This is of importance when the point of inflection cannot accurately be determined, for instance at high cooling rates. As an illustration, the difference in the transformation curves resulting from the two approaches is shown for C22 in figure 2.10. The ferrite parts of the transformation curves coincide up to the formation of pearlite for the equilibrium–fraction choice. Both the amount of pearlite and the pearlite formation rate are significantly influenced by the criterion for T_t. Also given in figure 2.10 is the transformation curve resulting from the application of the lever rule to the same experimental data. The error in the transformation curve is considerable. In a small temperature range the calculated fraction even exceeds the calculated equilibrium fraction.

23
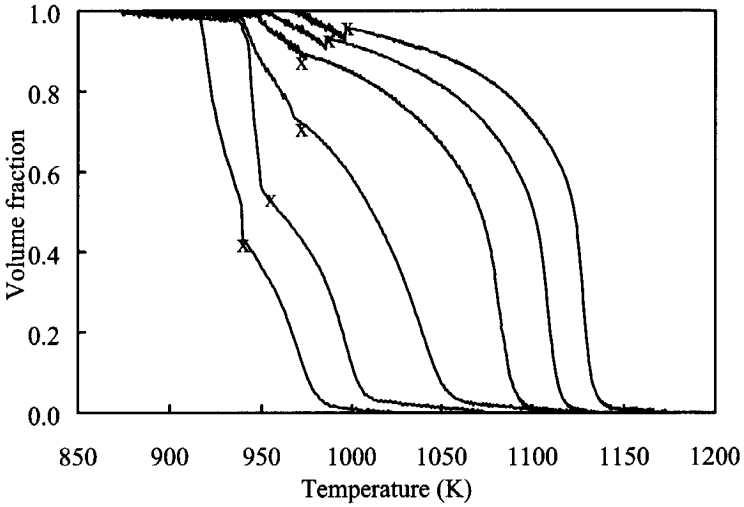
(a)
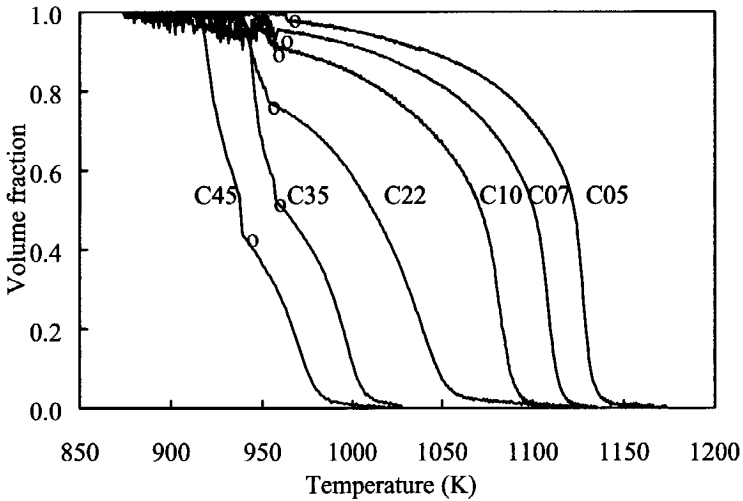
(b)

Figure 2.9   *The fraction curves obtained from the present analysis. a) As the criterion to*
             choose T_t the equilibrium ferrite fraction was used. The crosses indicate the
             temperature to switch to the pearlite analysis. b) As the criterion to choose T_t
             the point of inflection in the ΔL vs. temperature plot was used. The circles
             indicate the temperature to switch to the pearlite analysis.

Table 2.4   *Pearlite start temperatures as obtained from the criteria "equilibrium fraction ferrite" and "point of inflection" (see text).*

Alloy	Equilibrium fraction	Point of inflection
C05	996 K	963 K
C07	986 K	958 K
C10	973 K	958 K
C22	967 K	953 K
C35	949 K	956 K
C45	941 K	943 K
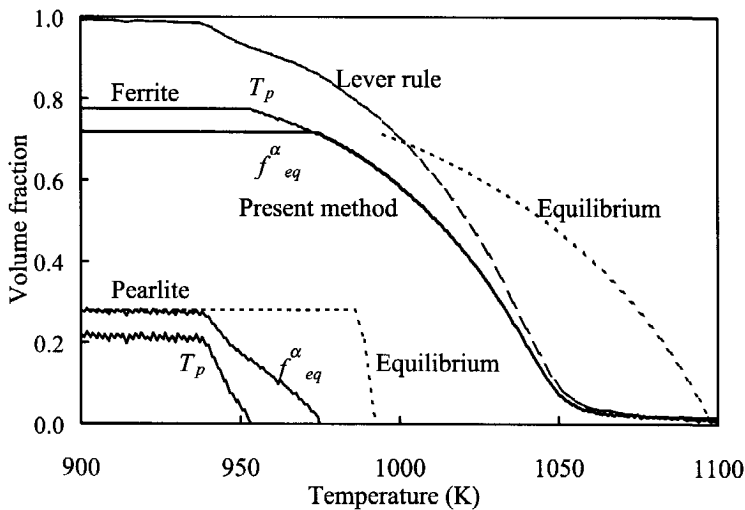
Figure 2.10   *The fraction curves obtained from a measurement by applying the present analysis (solid lines), once with the equilibrium ferrite fraction criterion (f^{α}_{eq}) and once with the inflection point criterion (T_p). The results from applying the lever rule are represented by the dashed line. Furthermore fraction curves for sample C22 according to equilibrium (short dashed lines) are given.*

Figure 2.10 is an adequate summary of the effects that have been presented in this paper: the discussed method yields an accurate determination of the ferrite and pearlite formation

from a dilatometry experiment, where the distinction between ferrite and pearlite formation is only slightly influenced by the criterion for T_t.

2.6. Conclusions

Dilatometry can effectively be used to obtain data concerning the austenite decomposition of pro–eutectoid steel grades. Both the carbon enrichment of the austenite during the primary ferrite formation and the difference in atomic volume of ferrite and pearlite are quantitatively taken into account. This rigorous approach necessitates a division of the transformation into a ferrite–formation range and a pearlite–formation range. In principle, two different criteria can be used for this choice. It is shown that this choice does not significantly affect the ferrite–formation curve. Significant errors are shown to result from neglecting the carbon enrichment and the difference in ferritic and pearlitic atomic volume.

References

1   J.W. Johnson, R.F. Mehl, *Trans. AIME* 135 (1939) 416.

2   M. Avrami, *J. Chem. Phys.* 7 (1939) 1103.

3   M. Avrami, *J. Chem. Phys.* 8 (1940) 212.

4   M. Avrami, *J. Chem. Phys.* 9 (1941) 177.

5   W.T. Reynolds, Jr. M. Enomoto, H.I. Aaronson, Proc. Conf. Phase Transformations in Ferrous Alloys, Metall. Soc. AIME and ASM, Philadelphia, PA (1983), 155.

6   R.A. Vandermeer, *Acta Metall. Mater.* 38 (1990) 2461.

7   G.P. Krielaart, J. Sietsma, S. van der Zwaag, *Mater. Sci. Eng.* A237 (1997) 216.

8   Robert F. Speyer, "Thermal analysis of materials", Marcel Dekker, Inc., New York (1994).

9   C. García de Andrés, F.B. Cabellero, C. Capdevila, H.K.D.H. Bhadeshia, *Scr. Mat.* 39 (1998) 791.

10   M. Onink, C. M. Brakman, E.J. Mittemeijer, S. van der Zwaag, *Z. Metall.* 87 (1996) 24.

11   M. Takahashi, H.K.D.H. Bhadeshia, *J. Mat. Sci. Lett.* 8 (1989) 477.

12   T.A. Kop, J. Sietsma, S. van der Zwaag, Proceedings from Materials Solutions '97 on Accelerated Cooling/Direct Quenching Steels, 15-18 September 1997, Indianapolis, Indiana, ASM International, Materials Park Ohio (1997), 159.

13   H. Stuart, N. Ridley, *J.I.S.I.* 204 (1966) 711.

14   M. Onink, C.M. Brakman, F.D. Tichelaar, E.J. Mittemeijer, S. van der Zwaag, J.H. Root, N.B. Konyer, *Scr. Metal. Mat.* 29 (1993) 1011.

15   C. Qui, S. van der Zwaag, *Steel Research* 68 (1997) 32.

16   R.C. Reed, J.H. Root, *Scr. Mat.* 8 (1998) 95.

17   J.B. Leblond, G. Mottet, J.C. Devaux, *J. Mech. Phys. Solids* 34 (1986) 395.

18   R. Kennedy, A.I. Grant, A.J. Kinnear, I.M. Kilpatrick, *J.I.S.I.* 208 (1970) 601.

3

The anisotropic dilatation behaviour of hot rolled steels showing a banded structure

Dilatation measurements on cylindrical samples taken from the longitudinal and the normal direction of a hot rolled C–Mn strip, are performed and show rather different results for those heat treatments which lead to a banded ferrite/pearlite microstructure. Under those conditions the standard methods of deriving the fractions transformed from the dilatation signal give rise to systematic errors. A model describing the anisotropic dilatation behaviour for such an evolving banded structure is presented. The model reproduces the experimentally observed differences as a function of the band orientation semi–quantitatively. The model calculations indicate that the description of the anisotropic dilatation behaviour during transformation of a forming banded structure should be based on a time dependent model rather than on models that do not account for the phase transformation history. Furthermore the consequences for the determination of the fractions transformed are discussed.

3.1. Introduction

Dilatometry [1–2], the measurement of the length changes of a sample as a function of time and temperature, is quite successful in studying the kinetics of the austenite decomposition, since the transformation can be investigated in situ, and over a wide range of cooling rates. Although the derivation of transformation data from a dilatation curve seems to a first approximation quite easy, an accurate quantitative determination is rather complicated [3–5]. In the analysis of dilatometry data generally two assumptions are made: (1) the material is macroscopically isotropic, and (2) the observed length change is linearly related to the fraction transformed. The combination of both assumptions leads to the well known lever–rule method in which the fraction transformed is taken to be proportional to the temperature–corrected fractional length change. In the case of carbon–containing non–eutectoid ferrous alloys it has been shown [3–5] that assumption (2) does not hold and the lever rule cannot be applied. The violation of assumption (2) is due to: (1) the carbon redistribution between the forming ferrite and the remaining austenite, which increases the specific volume of the austenite, and (2) the formation of pearlite having a distinctly different volume effect than the formation of ferrite. By assuming that the dilatation curve can be split into two sequential parts, corresponding to the ferrite formation and the pearlite formation, respectively, the fractions transformed can still be derived quite accurately [5].

The present paper concentrates on the microstructural anisotropy of hot rolled C–Mn strip and its effect on the dilatation behaviour during transformation. Due to the segregation of alloying elements, such as manganese, during continuous casting and the subsequent hot rolling and controlled cooling, the final material contains a microscopically inhomogeneous –banded– distribution of alloying elements [6–7]. In the manganese enriched bands the transformation start is delayed with respect to the neighbouring manganese–poor regions. Those regions, initially remaining austenitic, enrich in carbon when the other regions transform to ferrite. The carbon–enriched areas will eventually transform to pearlite. The often observed banded structure [6–9] thus indicates a non–uniform transformation in time.

It is the purpose of this paper to investigate the effects of spatially inhomogeneous and anisotropic transformation behaviour on the dilatation behaviour of samples used for dilatometric measurements, and on the consequences for the accuracy of the determined fractions transformed. A model describing the dilatation behaviour of a banded structure,

incorporating the effects of the strain due to the phase change and an anisotropic contribution due to the banded structure, is presented.

3.2. Theory

3.2.1. Austenite decomposition and volume changes

The nature of the austenite decomposition strongly depends on the chemical composition and on the cooling rate imposed. For low to medium carbon–manganese steels cooled at moderate rates it holds that an equi–axed ferrite/pearlite structure is formed. During the formation of the primary ferrite the austenite will enrich in carbon, as can be seen in the Fe–C phase diagram. When the driving force for pearlite formation becomes large enough, the enriched austenite will transform to pearlite. Each of these processes, ferrite formation, carbon enrichment of the austenite, and pearlite formation, is accompanied by a temperature–dependent volume change. Besides the temperature dependence of the dilatation effects, the dilatation is also dependent on the carbon concentration since the austenitic volume depends on the carbon concentration.

Table 3.1   Lattice parameters of ferrite (α) and austenite (γ) and of the orthorombic phase cementite (θ) as a function of temperature T and the atomic fraction carbon (ξ) [4, 10–13].

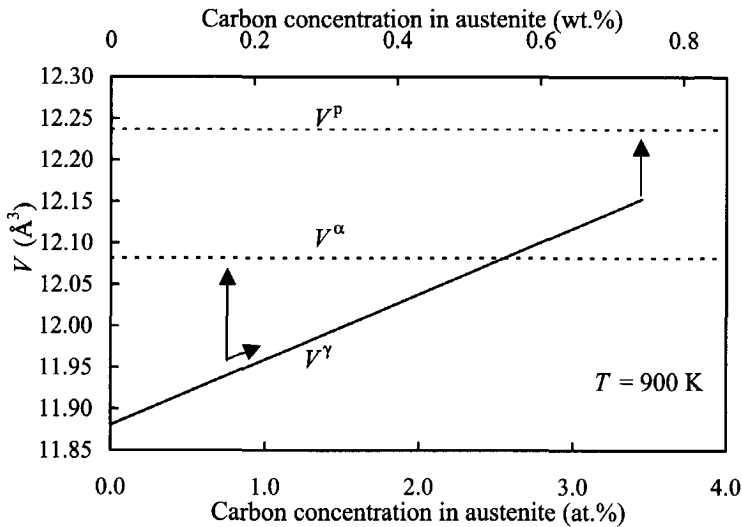| Phase	Lattice parameters (Å)
α	$a_\alpha = 2.8863 \text{ Å} \cdot (1 + 17.5 \cdot 10^{-6} \text{ K}^{-1} \cdot [T - 800 \text{ K}])$ $800 \text{ K} < T < 1200 \text{ K}$
γ	$a_\gamma = (3.6306 + 0.78 \cdot \xi) \text{ Å} \cdot (1 + (24.9 - 50 \cdot \xi) \cdot 10^{-6} \text{ K}^{-1} \cdot [T - 1000 \text{ K}])$ $1000 \text{ K} < T < 1250 \text{ K}; \ 0.0005 < \xi < 0.0365$
θ	$a_\theta = 4.5234 \text{ Å} \cdot (1 + \{5.311 \cdot 10^{-6} - 1.942 \cdot 10^{-9} \text{ K}^{-1} \cdot T + 9.655 \cdot 10^{-12} \text{K}^{-2} \cdot T^2\} \text{ K}^{-1} \cdot [T - 293 \text{ K}])$ $b_\theta = 5.0883 \text{ Å} \cdot (1 + \{5.311 \cdot 10^{-6} - 1.942 \cdot 10^{-9} \text{ K}^{-1} \cdot T + 9.655 \cdot 10^{-12} \text{ K}^{-2} \cdot T^2\} \text{ K}^{-1} \cdot [T - 293 \text{ K}])$ $c_\theta = 6.7426 \text{ Å} \cdot (1 + \{5.311 \cdot 10^{-6} - 1.942 \cdot 10^{-9} \text{ K}^{-1} \cdot T + 9.655 \cdot 10^{-12} \text{ K}^{-2} \cdot T^2\} \text{ K}^{-1} \cdot [T - 293 \text{ K}])$ $300 \text{ K} < T < 1000 \text{ K}$

Carbon concentration in austenite (wt.%)

Figure 3.1   *The atomic volume of austenite, V^{γ}, depending on the carbon concentration at a temperature of 900 K. The levels of the atomic volume of ferrite, V^{α}, and pearlite, V^{p}, are depicted as well. The arrows indicate the instantaneous change in atomic volume at the beginning of the ferrite formation and during the pearlite formation for a sample with an initial carbon concentration of 0.7 at%.*

Figure 3.1 shows the calculated atomic volumes of the different phases per iron atom at 900 K for binary Fe–C alloys, using the lattice constants given in table 3.1 [4, 10–13]. The austenitic atomic volume, V^{γ}, is dependent on its carbon concentration. It can be seen that at 900 K alloys with an initial carbon concentration less than 2.6 at.%C (= 0.6 wt.%) experience an expansion when the first ferrite is formed from the austenite. At the same time the austenite will expand due to the carbon enrichment. When the carbon concentration in the austenite exceeds 2.6 at.% at a temperature of 900 K, the austenite atomic volume is larger than the ferrite atomic volume. The carbon concentration for which $V^{\gamma} = V^{\alpha}$ is temperature dependent due to different thermal expansion coefficients of austenite and ferrite. The dilatation effect of a sample in which the carbon concentration in the austenite exceeds this threshold concentration will be a summation of the contraction due to the ferrite formation and an expansion due to a further carbon enrichment of the austenite. The formation of the pearlite from the enriched austenite causes an increase in

volume. Using the equations for the temperature–dependent lattice parameters given in table 3.1, the volume change corresponding to the phase transformations can be calculated.

3.2.2. Geometrical model and anisotropic dilatation behaviour

In general it is assumed that the observed dilatation corresponds with the volume change and that there is no contribution to the volume change from plastic effects due to a constraining effect of the matrix on the expanding phase. Although it is unrealistic that plastic effects cause a volume change it is possible that they cause a change in geometry, resulting in an orientation dependent length change. In order to analyse the dilatation behaviour of dilatometry samples with a banded structure, a model description for the dilatation is developed. The essence of the layered character of the microstructure is the layered variation in manganese concentration, causing a layered variation in Ar$_3$–temperature [6]. Consequently the transformation proceeds layer by layer. Two geometrical situations have to be distinguished: the layers are perpendicular (figure 3.2a, cylindrical sample taken of the normal direction of rolling) or parallel (figure 3.2b, cylindrical sample taken from the longitudinal or transverse rolling direction) to the axis of the cylindrical sample.

The dilatation behaviour of such a sample can be calculated on the basis of the lattice parameters. For the perpendicular case (figure 3.2a) it holds that the length, l, of the sample at an arbitrary moment, at which it consists of layers that are either ferritic (α), pearlitic (p) or austenitic (γ), is given by the sum of the lengths of the contributions of the three phases, according to

$$l = \sum_i l_i \, , \tag{3.1}$$

where i stands for ferrite, austenite or pearlite. Note that the phase fractions f^i are related to l_i by $f^i = l_i / l$. The fractions of ferrite, pearlite and austenite depend on the time–temperature path.

Volume changes of the sample can be due to either a temperature, compositional or phase change. The one–dimensional expansion behaviour of phase i, ε_i, is deduced from the atomic volumes of the phase, and approximately given by

$$\varepsilon_i = \frac{1}{3} \cdot \left(\frac{V^i - V_0}{V_0} \right), \tag{3.2}$$

in which V denotes the atomic volume. When there is no interaction between the layers, the total length of phase i, l_i, depends on its fraction and on the dilatation relative to the start of the transformation:

$$l_i = f^i \cdot l_0 \cdot (1 + \varepsilon_i), \tag{3.3}$$

in which l_0 denotes the length at the start of the transformation. The change in length relative to l_0 at the start of the transformation is then easily determined by

$$\Delta l = l - l_0. \tag{3.4}$$

In practice however, there is bound to be interaction between the various layers. In the model presented here the effects of the interaction are incorporated by assuming that the integral of the stress over the surface of the sample is zero, that there are no discontinuities at the surface of the sample, *i.e.* the surface energy is large compared to the energy necessary for the change of shape of the sample, and that there are no strain gradients in the phases, *i.e.* the diameter and length are the same over the entire sample.
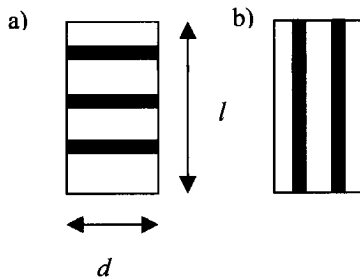
Figure 3.2   Schematic representation of dilatometer samples showing the orientation of the band structure with respect to the main axis of the cylindrical sample.

The diameter, d, of the sample will then be constrained due to the interactions between the layers (see figure 3.3). The value d depends on the expansion of the several layers and on the interactions between the layers through

$$d = d_0 \cdot (1 + \varepsilon_{av}), \tag{3.5}$$

with

$$\varepsilon_{av} = K_\alpha \varepsilon_\alpha + K_\gamma \varepsilon_\gamma + K_p \varepsilon_p, \tag{3.6}$$

and

$$K_\alpha + K_\gamma + K_p = 1. \tag{3.7}$$

K_i can be seen as a weighting factor for the expansion behaviour regarding phase *i*. A large weighting factor for phase *i* means that the expansion behaviour, in the constrained direction, is largly governed by phase *i*. ε_{av} can either be completely determined by the expansion behaviour of one of the phases or by an average of the expansion behaviour of the phases.
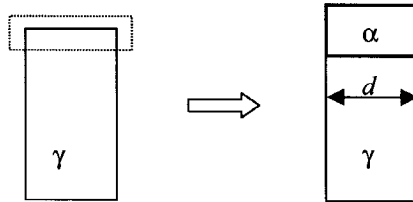
Figure 3.3   Schematic representation of the formation of a ferrite layer, which complies with the austenitic expansion behaviour.

The constraint in the diameter of the sample will influence the length of the sample. When the constraints between the several layers are taken into account the total length of phase *i*, $l_{i,mod}$, follows, through the assumption that there is no volume change, from

$$l_{i,mod} = l_i \cdot \left(\frac{d_i}{d}\right)^2, \tag{3.8}$$

where d_i is given by

$$d_i = d_0 \cdot (1 + \varepsilon_i). \tag{3.9}$$

Two different approaches for the calculation of ε_{av}, a continuous and a discrete approach, are described to show the two extremes. The difference between the two approaches reveals itself by the dependence on the development of the geometry of the sample. The continuous approach is defined such that there is no dependence of the geometrical shape change at a certain time on the geometrical shape at the moment just before, it only depends on the initial length, l_0. In the discrete approach there is a dependence on the shape change that occurred in the previous time step.

In the continuous approach there is a gradual change of the austenite weighting factor with the fraction primary ferrite formed, defined by

$$K_\gamma = \left(1 - \frac{f^\alpha}{f^{\alpha,\max}} \right)^n . \tag{3.10}$$

The parameter n is an adjustable parameter and influences the course of K_γ *vs.* f^α. The fraction $f^{\alpha,\max}$ denotes the maximum ferrite fraction that is formed in the sample. The pearlite is assumed to adjust itself to the behaviour of the more abundant ferrite: $K_p = 0$. By applying this scheme, the calculation of the diameter of the sample at a certain moment during the transformation, and therefore the calculated length change, depends on the fractions present and on the temperature at that moment.

The discrete approach is based on a transition point, rather than a gradual change, for the austenite weighting factor. It is assumed that while $f^\alpha < f^\alpha_t$ the weighting factors have the values $K_\gamma = 1$ and $K_\alpha = 0$, with f^α_t the transition fraction, and that for larger ferrite fractions $K_\gamma = 0$ and $K_\alpha = 1$. By applying this scheme the diameter of the sample, and therefore the calculated length change, not only depends on the fractions present and on the temperature, but also on the transition point, f^α_t. At the transition point the diameter, at that instant determined by the austenite phase, will be fixed and subsequently will be only temperature dependent. The temperature dependence is given by the expansion coefficient of the ferrite. Since the fixed diameter is given by the austenitic phase, the fraction austenite at which the switching occurs has a large influence on the total dilatation signal.

The calculation of the length change for the parallel case (figure 3.2b) is based on the same assumptions as made for the perpendicular case. The result is straightforward. The

calculation of the length in the parallel case equals the calculation of the diameter in the perpendicular case (eq. (3.5)). It follows that the calculated change in length in the parallel case is given by

$$\Delta l = l_0 \cdot (1 + \varepsilon_{av}) - l_0 = l_0 \cdot \varepsilon_{av}$$ (3.11)

Using the abovementioned equations, the change in length for the two geometrical situations can be calculated as a function of the temperature and the fractions f^i.

3.3. Experimental

In order to investigate the dilatation effect as a function of the directionality of the sample several lean carbon–manganese steels have been investigated. The results presented here are those obtained for an alloy containing 0.147 wt.%C and 0.926 wt.% Mn. The chemical composition of the alloy is given in table 3.2. The material was hot rolled to a thickness of 12 mm.

Table 3.2   Chemical composition of the alloy in wt.%.

C (at.%)	Mn	Si	Nb	Al	Cr	Mo	Ni
0.147 (0.684)	0.926	0.009	0.002	0.043	0.027	0.004	0.026

Figure 3.4 shows a compilation of micrographs showing the presence of the banded structure. Samples with three different orientations were taken and studied. A sample of which the longitudinal axis coincides with the normal to the plane of rolling is indicated as an n–sample (corresponding to the perpendicular case), while a specimen of which the longitudinal axis coincides with the longitudinal rolling direction is indicated as an l–sample (the parrallel case). Comparison of dilatation measurements on samples from the longitudinal and the transverse direction did not show significant differences. Therefore, only the measurements on the n– and l–samples will be shown.

Length changes were measured with a Bähr 805 A/D dilatometer. Samples, 10.0 mm long with a diameter of 4.0 mm, were heated in vacuum to the austenitisation temperature,

1123 K or 1323 K, held for 20 minutes and subsequently cooled at a fixed rate of 20 K/min. The samples were held between two quartz pushrods. By measuring the temperature at two positions along the length of the sample it was established that temperature gradients over the sample were within 5 K. Nital etching and optical microscopy were performed to observe the microstructures.
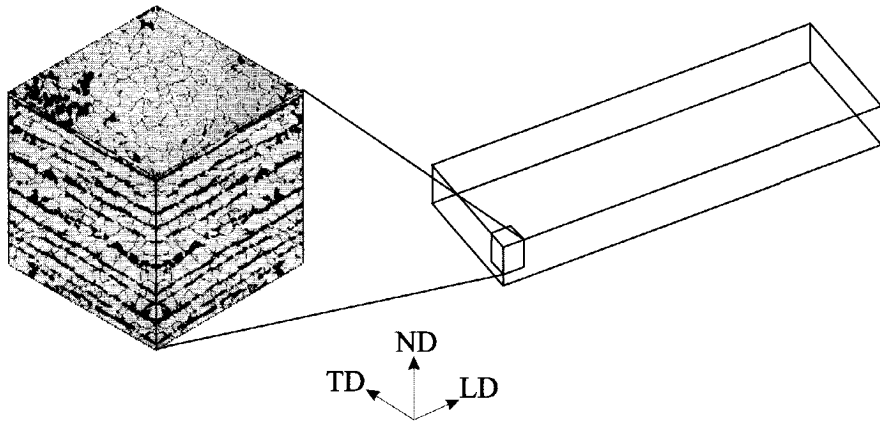
Figure 3.4   Micrographs showing the macroscopic inhomogeneity in respect to the rolling direction. The rolling directions are indicated.

3.4. Results

Figure 3.5a shows the dilatation curves during cooling of an n– and of an l–sample, following austenitisation at 1123 K. For clarity the curves are shifted along the ΔL–axis in such a way that they coincide in the austenite region. During the first part of the transformation the two measured curves coincide. Thereafter the measured dilatation of the n–sample increases faster than the dilatation of the l–sample. It is observed that the total measured dilatation due to the phase transformation in the n–sample is more than twice that of the l–sample. This effect occurs for both the ferrite and the pearlite formation. Apparently the sensitivity of the dilatation behaviour for the transformation processes is higher for n–samples. The third curve in figure 3.5a represents a theoretical dilatation curve, based on a transformation according to equilibrium and based on isotropic dilatation behaviour.

(a)

(b)
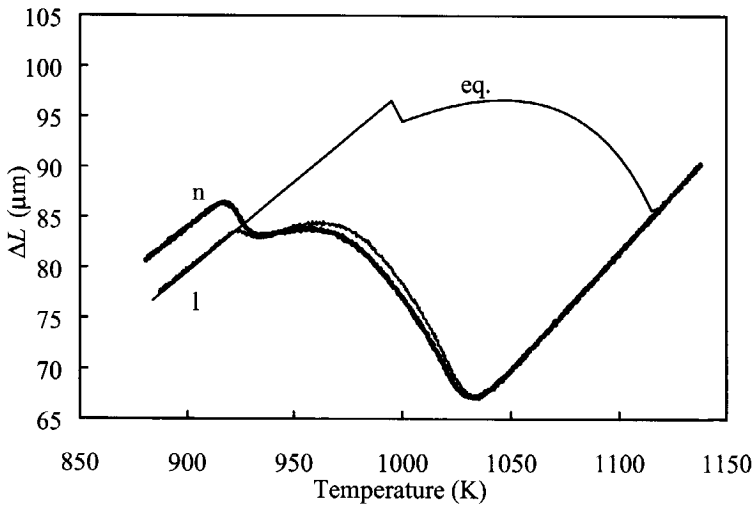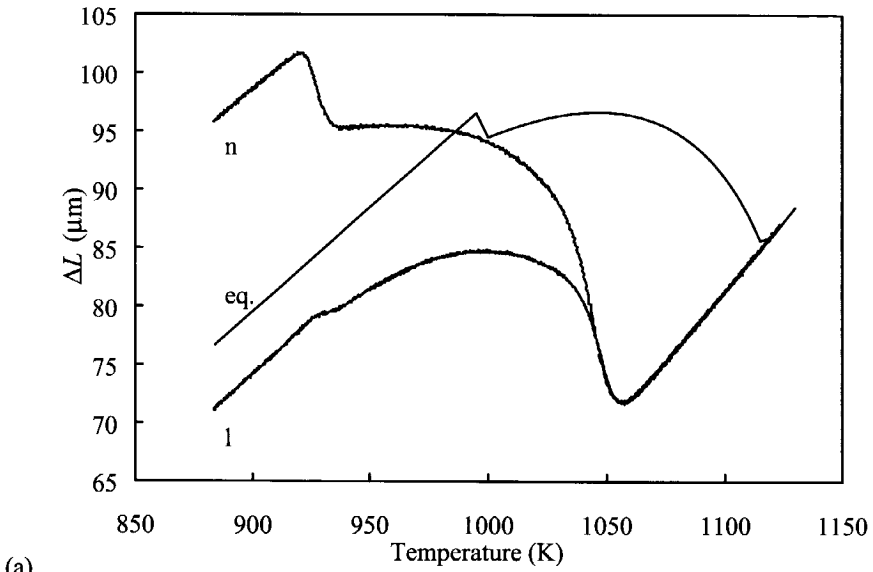
Figure 3.5   *Dilatation curves measured on an n– and an l–sample. A calculated dilatation curve based on equilibrium transformation and isotropic dilatation behaviour is also shown. The samples were austenitised a) at 1123 K, and b) at 1323 K.*

The isotropic dilatation due the transformation is smaller than the measured dilatation of the n–sample and larger than the measured dilatation of the l–sample. Figure 3.5b shows the same results for the same material austenitised at 1323 K. In this case the difference between the measured dilatations is much smaller. The dilatation effect during the ferrite formation is approximately the same for both sample orientations, whilst the dilatation effect corresponding to the pearlite transformation does show an orientation dependence.
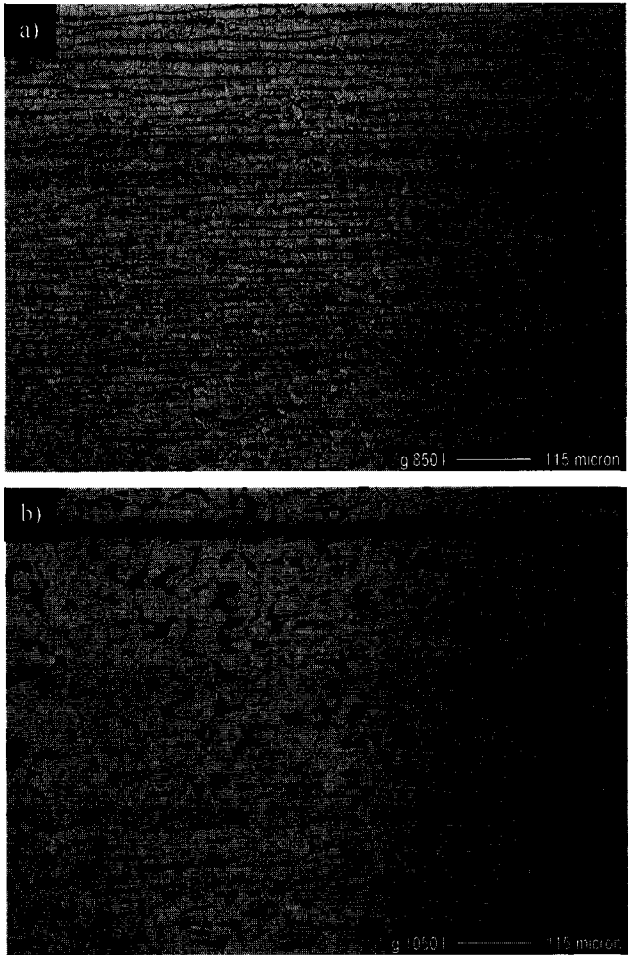
Figure 3.6   Microstructures showing ferritic–pearlitic band structure after the heat treatment. a) Austenitised at 1123 K, and b) austenitised at 1323 K.

Figure 3.6 shows the microstructures resulting from both austenitisation conditions. Although it is hard to quantify the degree of banding in the structure [9,14], it can be seen that in the sample austenitised at 1123 K the banded structure is more pronounced than in the sample austenitised at 1323 K. The bands are more continuous and finer; the banding wavelength, the distance between the pearlite bands, is about 20 μm *vs.* 45 μm. The microstructures suggest that the anisotropic dilatation behaviour (figure 3.5) is indeed related to the degree of banding.

3.5. Discussion

From the experimental dilatation curves in figure 3.5a the fractions ferrite and pearlite are determined using the lever–rule method. With the fractions ferrite and pearlite as a function of temperature thus determined, the dilatation curves are recalculated using the procedure described and the appropriate lattice parameters (table 3.1). Figure 3.7a and 3.7b show the experimental and the model dilatation curves using the continuous and the discrete approach, respectively.

The model curves of figure 3.7a are obtained with $n = 0.6$. The value of n is chosen such that the measured and the calculated dilatation curves coincide in the beginning of the ferrite formation. For a lower value of n the calculated expansion for the n–sample is too large and for a higher n–value the expansion is too small. It is seen that the model curves show a difference in dilatation behaviour between the normal and the longitudinal samples which is similar to that for the experimental curves. The features of the expansion behaviour during the pearlite formation are adequately modelled. The calculation for the l–sample shows no dilatation effect corresponding with the pearlite formation while for the n–sample a relatively large dilatation effect is shown. Due to the gradual transition of the weight factors K_i between the beginning and the end of the ferrite formation there is a point where the calculations for both orientations give the same results as for the isotropic behaviour. This is where the dilatation of the n–sample and the l–sample are equal. Note that such a point does not occur for the experimental curves. The observed absolute dilatation effect of the ferrite formation for the normal sample is not reached by the model curve.
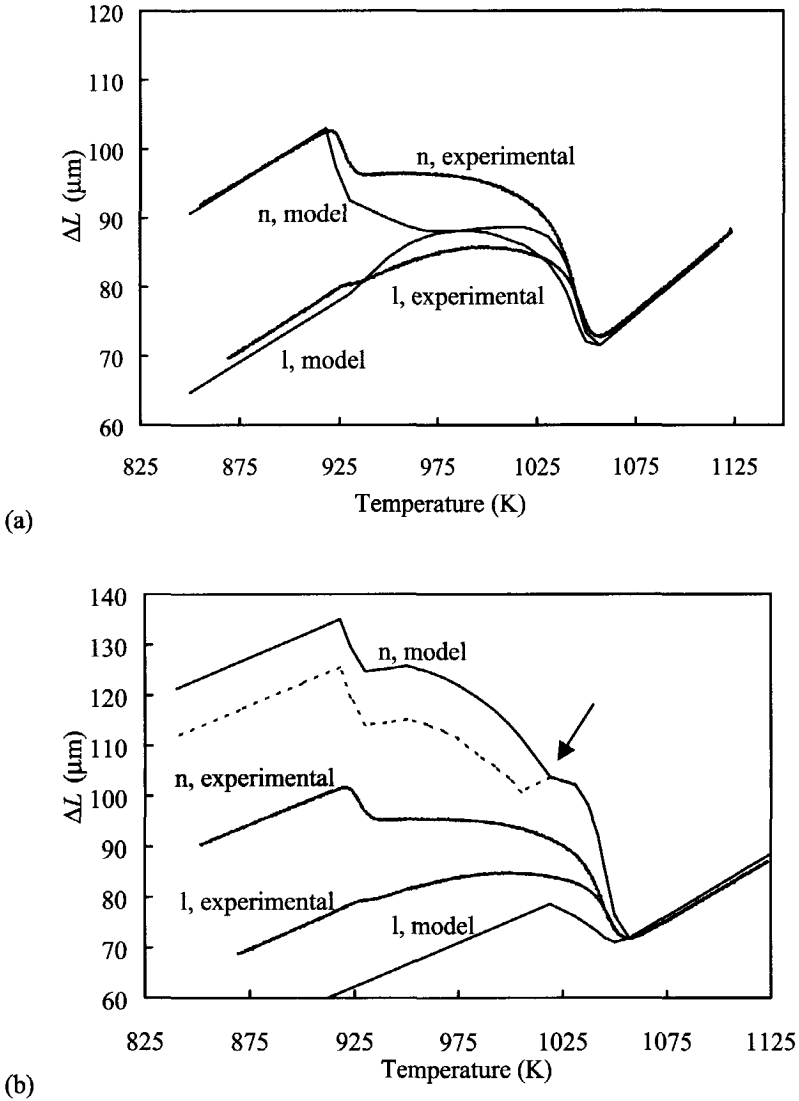
41

(a)

(b)

*Figure 3.7   The experimental and model dilatation curves after austenitising at 1123 K.
The curves for both the normal and the longitudinal samples are shown. a)
Using the continuous approach with n = 0.6, and b) using the discrete
approach with the transition at $f^{\alpha}_t = 55$ % (or at $f^{\alpha}_t = 60$ %, indicated by the
dotted line).*

Figure 3.7b shows the model dilatation curves using the discrete step in weighting factors. The transition point at $f^{\alpha}_t = 55$ %, indicated by the arrow in figure 3.7b, is chosen in order to maintain for the n–sample a continuously increasing dilatation curve. Choosing a larger ferrite fraction for the transition results for the n–sample, as indicated by the dotted line, in a reduction in length (caused mainly by the temperature effect) before a further increase occurs. Using the discrete approach the calculated length change for the n–sample can be larger than the measured dilatation. Combining figures 3.7a and 3.7b it can be concluded that the correct way to model the geometry change of a material during transformation considers the time–dependent development of the geometry change during the transformation. The physical factors governing which phase dominates the expansion behaviour at which moment are not well understood.

Neglecting the fact that the measured dilatation depends on the macroscopic inhomogeneity of the sample has consequences for the determination of the fractions transformed by means of dilatometry. Figure 3.8 shows the fractions transformed after austenitisation at 1123 K and 1323 K (see figure 3.5) determined by the lever–rule method (see chapter 2) from measurements on n– and l–samples. Figure 3.8a shows a difference of about 15 % in the determined fractions. The difference in the determined fractions for the sample austenitised at 1323 K, corresponding to the less banded structure, is distinctly smaller. Although the dilatation during the ferrite formation was identical (figure 3.5b) there is a difference in the ferrite fraction, which is caused by the difference in dilatation behaviour during the pearlite formation.

Not only the fractions as determined by the lever–rule method are affected. Also the results of analyses which are based on the atomic volumes of the transforming phases [3–5] are influenced. An analysis method that is based solely on the lattice parameters of the transforming phases would result in significant errors. It can been seen (figure 3.5a, equilibrium curve) that a transformation dilatation of 40 μm at 990 K would correspond to complete transformation. The dilatation of the l–sample, austenitised at 1123 K will always be smaller, while the n–sample already at 985 K has caused such a dilatation (figure 3.5a). Figure 3.9 shows the fraction curves obtained from the dilatation curves shown in figure 3.5, applying the method incorporating the effects of the carbon, as explained in chapter 2 [5]. The temperature at which the equilibrium ferrite fraction is reached, is taken as the transition criterium from ferrite formation to pearlite formation.

(a)

(b)
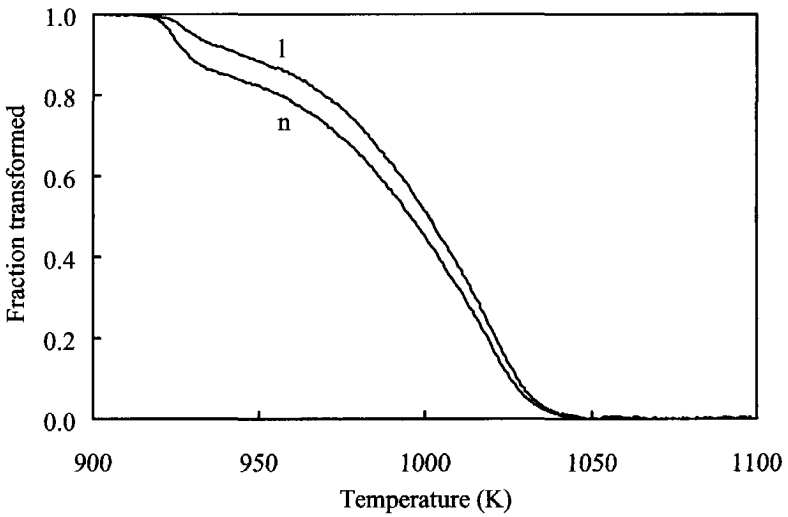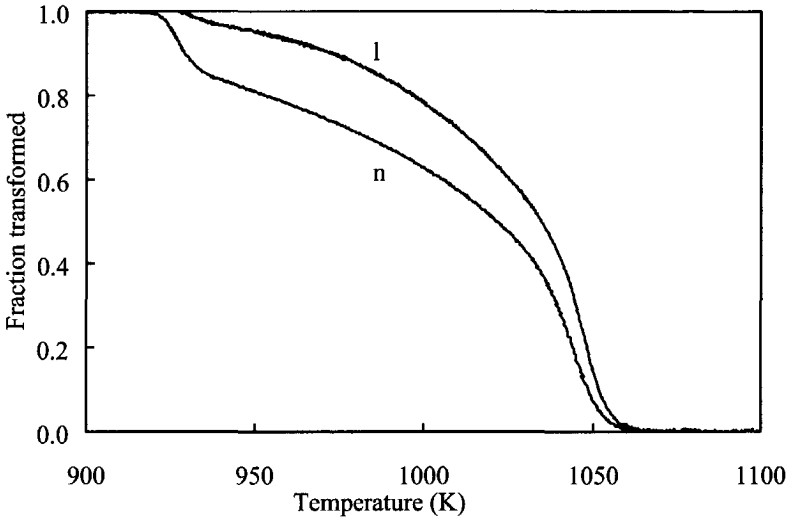
Figure 3.8   Fractions transformed obtained using the lever–rule method after austenitisation at a) 1123 K, and b) 1323 K, determined on the n– and l– sample measurements.
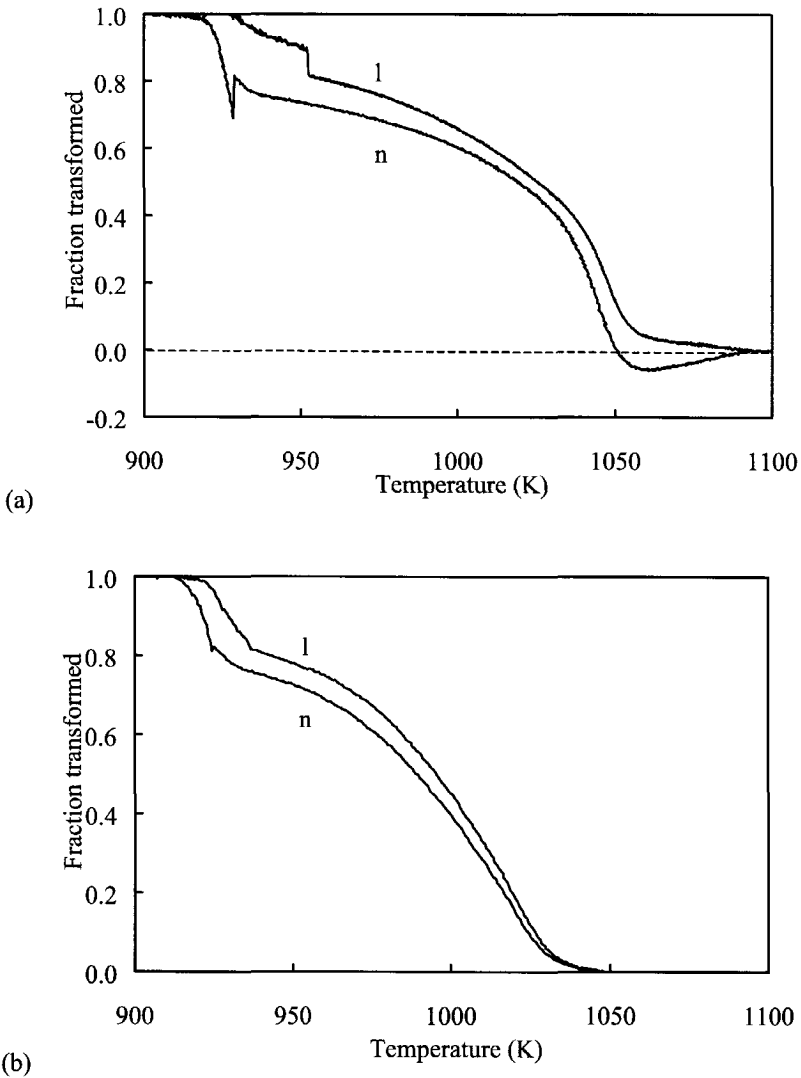
(a)

(b)

Figure 3.9   Fractions transformed obtained using the method proposed in chapter 2 [5] after austenitisation at a) 1123 K, and b) 1323 K, determined on the n– and l–sample measurements.

In figure 3.9a several anomalies are observed. The fraction transformed as deduced from the n–sample becomes negative even before the transformation has really started, and there

are abrupt transitions corresponding to the transition from ferrite formation to pearlite formation. These features result from the scaling factor that was introduced in the analysis. The method is based on the determination of the scaling factor, κ, which accounts for deviations of the isotropic dilatation behaviour, at two temperatures; one in the austenitic region and one in the ferritic/pearlitic region. The value of κ for intermediate temperatures is obtained by a linear interpolation. In figure 3.9a, changes in the fraction ferrite at temperatures above 1060 K are observed. From the dilatation signal (fig. 3.5a) it is clear that this change in fraction is due to the analysis and does not correspond to an actual change in fractions. Both this change in fraction and the jumps in the fraction curves, indicating the transition to the pearlite formation, are due to the linear variation of κ. Apparently the geometric shape change induced by the layered transformation is not linearly related with temperature. Figure 3.9b shows that when the measured dilatation effects approach isotropic circumstances, the anomalies in the determined fractions disappear.

In the case of banded structures both the lever rule and methods based on the lattice parameters do not yield reliable results. However, when it is realised that the dilatation measurement is influenced when a banded structure is formed, a qualitative indication of the error can be given. For example, in practice the samples for dilatometric investigation are most often machined such that the longitudinal axis of the specimen coincides with the plane of rolling. If the dilatation signal of such a specimen is analysed with the lever–rule method (figure 3.8a) the fractions transformed are certainly overestimated. Further work, quantifying the degree of banding [9,14] and relating it to the calculated phase fractions, will make it possible to make a quantitative correction of the measured fraction curves for the anisotropic dilatation effect.

3.6. Conclusions

It has been shown that the assumption of macroscopic isotropic behaviour of dilatometry samples, which is made during the analysis of dilatometry data, is not valid for banded structures. When a banded structure is present, there is a distinct difference in dilatation behaviour between a sample taken from the plane of rolling and a sample taken from a direction normal to the plane of rolling. The model presented here reproduces the experimentally observed differences as a function of the band orientation semi–quantitatively. The model calculations indicate that the description of the anisotropic

dilatation behaviour during transformation of a forming banded structure should be based on a time dependent model rather than on models that do not account for the phase transformation history. The consequences for the determination of transformation kinetics from dilatometry curves are significant, both for a lever–rule analysis, and for the analysis on the basis of lattice constants.

References

1   Robert F. Speyer, "Thermal analysis of materials", Marcel Dekker, Inc., New York (1994).

2   G. Berger, *La dilatométrie différentielle appliquée a l'étude des aciers*, Dunod, Paris (1965).

3   M. Takahashi, H.K.D.H. Bhadeshia, *J. Mat. Sci. Lett.* 8 (1989) 477.

4   M. Onink, C. M. Brakman, E.J. Mittemeijer, S. van der Zwaag, *Z. Metall.* 87 (1996) 24.

5   T.A. Kop, J. Sietsma, S. van der Zwaag, accepted for publication in *J. Mat. Sci.* (chapter 2 of this thesis).

6   S.W. Thompson, P.R. Howell, *Mat. Sci. Techn.* 8 (1992) 777.

7   R. Grossterlinden, R. Kawalla, U. Lotter, H. Pircher, *Steel Research* 63 (1992) 331.

8   F.A. Khalid, M. Farooque, A. ul Haq, Q. Khan, *Mat. Sci. Techn.* 15 (1999) 1209.

9   J. Komenda, R. Sandström, *Mater. Char.* 31 (1993) 143.

10   H. Stuart, N. Ridley, *J.I.S.I.* 204 (1966) 711.

11   M. Onink, C.M. Brakman, F.D. Tichelaar, E.J. Mittemeijer, S. van der Zwaag, J.H. Root, N.B. Konyer, *Scr. Metal. Mat.* 29 (1993) 1011.

12   C. Qui, S. van der Zwaag, *Steel Research* 68 (1997) 32.

13   R.C. Reed, J.H. Root, *Scr. Mat.* 8 (1998) 95.

14   A. From, R. Sandström, *Mater. Char.* 41 (1998) 11.

4

A study on the austenite to ferrite phase transformation in binary substitutional iron alloys

The massive transformation from austenite to ferrite in binary substitutional Fe–X alloys, where X represents successively 1 or 2 % of Co, Cu, Mn, Cr or Al, is experimentally investigated by means of dilatometry. The resulting transformation curves have been modelled by an interface–controlled growth model, taking the characteristics of the austenitic microstructure into account. The assumption of an Arrhenian temperature dependence of the interface mobility, defined as the ratio between the interface velocity and the driving force, is found to give a consistent picture of the observations with an activation energy for atoms crossing the interface of 140 kJ/mol. The spurious presence of interstitial nitrogen is shown to have a significant effect on the mobility, as large as a factor 8 at concentration levels on the order of 10^{-4}.

4.1. Introduction

The properties of steels are controlled by and are highly sensitive to the chemical composition and the microstructure of the material [1–3]. In hot–rolled steel grades the microstructure is essentially formed during the austenite to ferrite phase transformation. The understanding of the mechanisms controlling the austenite to ferrite phase transformation, and a model that allows the microstructure to be calculated as a function of steel composition and processing history, is therefore not only of fundamental interest, but also of great practical importance. Consequently, a considerable number of studies has appeared on this subject (*e.g.* [4–6]). In many studies in the literature semi–empirical relationships, for instance based on the Johnson–Mehl–Avrami equation [7–8], are proposed to quantify the effect of composition and the austenite microstructure on the transformation kinetics. A more fundamental approach has been followed in models that consider diffusion kinetics, more specifically the diffusion of carbon, to be rate determining for the phase transformation. A landmark paper for this type of models is the early work by Zener [9]. Whereas the Zener approach has proven to be fairly successful for carbon–containing steels, for modern steel grades containing extremely small amounts of interstitially solved elements it cannot be applied. For such compositions the influence of the actual lattice–transformation rate, assumed to be infinite in the Zener approach, becomes of essential importance. This transformation rate has been considered to determine the intrinsic mobility of the interface between the old and the newly forming phase [10]. In a series of recent studies [11–12] a mixed–mode model for the austenite to ferrite phase transformation has been developed, taking into account both the diffusion kinetics and the interface mobility. Although satisfactory results were obtained with this approach, the actual nature of the interface mobility and its dependence on composition has not been fully unraveled. The present research has therefore been concentrated on the phase transformation in binary iron alloys involving a massive austenite to ferrite phase transformation, in which the interface mobility is rate determining.

The austenite to ferrite phase transformation in binary iron alloys has been analysed during cooling at a constant rate. The alloys under consideration are Fe–X alloys, where X is 1 or 2 % of a substitutionally dissolved element, in particular Co, Cu, Mn, Cr or Al. These alloys are selected because the austenite to ferrite transformation, on cooling at a moderate rate, can be assumed to be diffusive but compositionally invariant, which means that the transformation does not involve a change in chemical composition at the interface. Consequently, the phase–transformation kinetics are entirely dependent on the interface

mobility. Experimentally obtained fractions of ferrite and austenite as a function of temperature, determined by dilatometry, are compared to model transformation curves that are calculated on the basis of the interface–mobility model, taking into account the prior–austenite microstructure as proposed in ref. [13]. The transformation kinetics of the Fe–Co and Fe–Cu alloys has also been studied by means of calorimetry [14].

4.2. Theoretical background

4.2.1. Interface migration

The nucleation of ferrite (α) in austenite (γ) can be assumed to be heterogeneous in character, taking place mainly at austenite grain boundaries and resulting in an α/γ–phase interface. Subsequently, this interface migrates normal to itself, which causes the growth of the ferrite phase. The growth takes place continuously along the entire interface: atoms detach from one crystalline region, cross the interface, and attach to the crystalline region on the other side of the interface. The resulting velocity v with which the interface moves is, according to Christian [10], given by

$$v = \frac{\delta f^*}{RT} \exp\left(-\frac{Q}{RT}\right) \Delta G^{\gamma/\alpha}, \tag{4.1}$$

in which Q and f^* are the activation energy and frequency for the atoms crossing the interface, δ is the atomic diameter, R the universal gas constant, T the temperature, and $\Delta G^{\gamma/\alpha}$ the driving force for the transformation, for which the free–energy difference between the ferrite phase and the austenite phase is taken. In the derivation of equation (4.1) it is taken that $\Delta G^{\gamma/\alpha} \ll RT$, a condition that is usually satisfied in practice. Equation (4.1) can be written as

$$v = M \cdot \Delta G^{\gamma/\alpha} = M_0 \exp\left(-\frac{Q}{RT}\right) \Delta G^{\gamma/\alpha}, \tag{4.2}$$

where M is the interface mobility, with a pre–exponential factor $M_0 = \delta f^*/RT$. With $\delta = 0.3$ nm and $f^* = kT/h$ (k is the Boltzmann's constant and h is Planck's constant), it follows that, as an order of magnitude, $M_0 \approx 0.8$ molm/Js.

51

The picture of the interface motion that is sketched by equation (4.2) is implicitly accounting for a number of factors that influence the phase–transformation kinetics. Some of the most pronounced of these complicating effects are the interatomic interactions at the interface, the strain energy caused by density differences between the two phases, the segregation of solute atoms at the interface, and solute–drag effects. Consequently, the quantities M_0 and Q should be seen as effective parameters. Indications for the values of these quantities are the abovementioned 0.8 molm/Js for M_0 and 144 kJ/mol for Q, the value that was found in ref. [15] as the activation energy for recrystallisation in iron.

As stated before, for the driving force $\Delta G^{\gamma/\alpha}$ the Gibbs free–energy difference $G^{\gamma} - G^{\alpha}$ is taken, where G^{γ} and G^{α} are the molar Gibbs free energies of the austenite and ferrite phase in the unconstrained bulk condition. Quantitative data for $\Delta G^{\gamma/\alpha}$ as a function of temperature have been obtained from the thermodynamical database programme MTDATA.

4.2.2. Austenite grain geometry

The austenite microstructure is a crucial parameter for the austenite to ferrite phase transformation in steel. In the first place the austenite grain boundaries are the principal nucleation sites for the ferrite. Also during the growth of the ferrite phase the austenite microstructure is of importance, since the shape and dimensions of the three–dimensional grains determine the effect of the basically one–dimensional interface velocity on the volume fraction of ferrite. In order to determine the interface velocity as a function of temperature, information about the geometry of the austenite grains is required, which should adequately be incorporated in the model. Therefore, a realistic three–dimensional model geometry is necessary. A tetrakaidecahedron, with its dimension a defined as the distance between opposite square faces, is selected as the model grain for the austenite microstructure (figure 4.1) [13,16]. This geometry combines the topological features of a random Voronoi distribution, which can be seen as the optimal mathematical representation of a metal microstructure, with the advantages of single–grain model calculations. It is assumed in the model that nucleation takes place heterogeneously at the grain corners [17–18] (see figure 4.1), with a nucleus density that is derived from microscopic observations of the austenite and ferrite microstructures. From these nuclei the ferrite grows spherically into the grain with the interface velocity given by equation (4.2). During the modelling of the transformation, the ferrite volume fraction in the tetrakaidecahedron is evaluated by numerical integration.
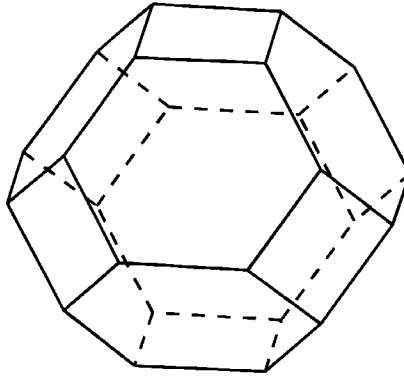
Figure 4.1   The tetrakaidecahedron, which is used in this study as a model austenite grain. Ferrite grains grow from the grain's corners.

4.3. Experimental

4.3.1. Material

The iron alloys were produced by arc–melting high–purity iron under an argon flow while adding the desired amount of alloying element, followed by furnace cooling to room temperature. The alloy material originally consisted of discs with a diameter of 100 mm and a thickness of 10 mm. The discs were hot–rolled to a thickness of 5 mm, after which the oxide layer and segregation was removed from the surface. As a homogenisation treatment, the alloys were annealed at 1500 K for 160 hours in quartz tubes, filled with a 20 kPa Ar/5%H_2 gas mixture. The chemical compositions of the alloys are listed in table 4.1. Cylindrical samples with a length of 10 mm and a diameter of 3 mm were prepared from the homogenised alloys to be used in the dilatometry experiments.

4.3.2. Dilatometry experiments

Dilatometry is a technique in which the length change of a sample is measured as a function of temperature. It can be applied in a study of the austenite to ferrite phase transformation because of the density difference between austenite and ferrite. This density difference gives rise to an observable dilatation during the transformation that is different from the normal linear expansion effect. Assuming the volume changes to occur isotropically, the volume fraction ferrite can be obtained from a curve of the relative length change as a function of temperature [19]. At each temperature during the transformation,

the observed length change of the sample, ΔL, is related to the limiting values ΔL^{α}, obtained by linear extrapolation of the low–temperature data, and ΔL^{γ}, obtained by linear extrapolation of the high–temperature data. Since in the present experiments only two phases are involved, without composition changes taking place, the volume fraction ferrite, f^{α}, is determined from

$$f^{\alpha} = \frac{\Delta L - \Delta L^{\gamma}}{\Delta L^{\alpha} - \Delta L^{\gamma}}. \tag{4.3}$$

For the experiments in this study, each sample is heated in the dilatometer, at a pressure of less than 1×10^{-7} bar, to 1223 K (1298 K for 1Al) at a constant rate of 50 K/min, followed by austenitising for 1 hour at this temperature. After this heat treatment the sample is cooled using one of three cooling rates β: 20, 40 or 60 K/min.

Table 4.1   *Composition of the Fe–X alloys used in the experiments, and the temperature T_0 at which austenite and ferrite of the nominal composition have equal free energies.*

alloy	X (at.%)	C (at.%)	Si (at.%)	Ni (at.%)	S (at.%)	N (appm)	T_0 (K)
1Co	0.95	0.009	<0.002	0.006	0.003	4	1186
2Co	1.99	0.009	<0.002	0.008	0.003	8	1187
1Cu	0.79	0.009	<0.002	0.004	0.003	40	1155
2Cu	1.67	0.009	<0.002	0.005	0.003	110	1126
1Mn	0.81	0.014	<0.002	0.006	0.005	30	1140
2Mn	1.90	0.005	<0.002	0.007	0.003	440	1086
2Cr	1.84	0.005	<0.002	0.006	0.003	410	1161
1Al	1.03	0.005	0.004	0.006	0.002	300	1253

4.3.3. Grain–size distribution

In order to model the transformation kinetics quantitatively, the austenite grain–size distribution of the specimen is determined. The austenite grain boundaries are made visible by oxidation at high temperature. To this aim cylindrical samples, of which one side is polished, are heated in the dilatometer to the austenitising temperature, and held at this temperature for 1 hour. After 40 minutes some oxygen is introduced into the dilatometer to mark the austenitic microstructure. For the metallographic study of the ferrite

microstructure, samples were prepared by 2 % nital etching. Optical microscopy is applied to determine the grain–size distribution, using a Zeiss Jenavert microscope equipped with a Leica quantitative image analysing system with a 1024×1024 pixel CCD camera.

The area distribution $p_A(A)$ that results from quantitative microscopy is to be converted into a distribution $p_a(a)$ of the tetrakaidecahedron size a in order to apply it to the model calculations. To do so, the observed area distributions are deconvoluted by a relatively simple method, assuming the largest observed area, A_{max}, to be the most probable cross–sectional area for grains from the largest size class, for which $a = a_{max}$. The distribution of cross–sectional areas belonging to this size class is then subtracted from the observed distribution. Subsequently the second–largest class is treated in the same way. This results in a set of equations that relates the grain sizes to the observed distributions of areas [20]. Using a vector notation for the N–bin histograms that give the distributions, the relation between the area distribution $p_A(A/A_{max})$ and the grain–size distribution $p_a(a/a_{max})$, is given by

$$p_A = \alpha \times p_a, \qquad\qquad (4.4)$$

with α a matrix that is related to the shape of the tetrakaidecahedron. To determine this matrix, the expected area distribution of sectional planes through a tetrakaidecahedron of constant size has been determined by a Monte–Carlo method. The area of an arbitrarily chosen sectional plane through a tetrakaidecahedron, representing the surface of a microscopy sample, depends on the distance from the centre of the tetrakaidecahedron and on the orientation of the tetrakaidecahedron with respect to the plane. The distribution resulting from this study is in agreement with the distribution that was determined 'by hand' in the fifties [21], with the most probable cross–section equalling approximately $0.64a^2$. Using 6–bin histograms for the distributions p_a and p_A, the matrix α is then given by

$$\alpha = \begin{pmatrix} 1 & 0.396 & 0.260 & 0.202 & 0.167 & 0.137 \\ 0 & 0.604 & 0.281 & 0.194 & 0.146 & 0.123 \\ 0 & 0 & 0.459 & 0.227 & 0.165 & 0.136 \\ 0 & 0 & 0 & 0.377 & 0.204 & 0.145 \\ 0 & 0 & 0 & 0 & 0.318 & 0.184 \\ 0 & 0 & 0 & 0 & 0 & 0.275 \end{pmatrix}$$

4.4. Results

4.4.1. Experimental

An example of the austenitic grain structure is given in figure 4.2a for the 2Cu alloy. From this picture the austenite grain boundaries are traced by hand, resulting in figure 4.2b. The figure shows that the austenitic microstructure is rather coarse, due to the high purity of the alloys. An average austenite grain size on the order $d_\gamma \approx 300 - 400$ μm is observed for all alloys (except $d_\gamma = 80$ μm for 2Mn), with a relative standard deviation of the distribution for d_γ of $60 - 70$ %. The ferrite microstructure was generally found to be slightly finer than the austenite, with the average grain size decreasing, as expected, with increasing cooling rate. The nucleus density n_n is derived from the average ferrite grain size d_α by $n_n = (d_\alpha)^{-3}$, which results in approximately 1 to 7 nuclei per austenite grain for the different alloys. The data for the microstructures and the resulting nucleus densities are given in table 4.2.
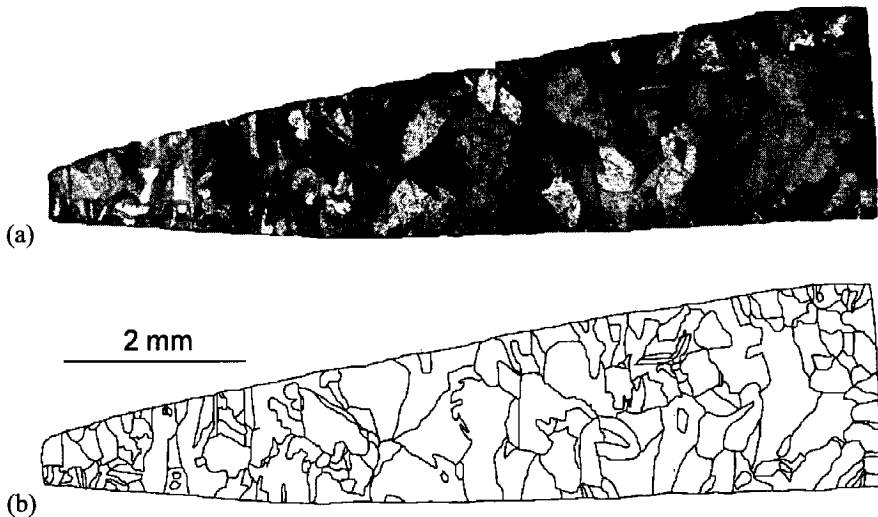

(a)

2 mm

(b)

Figure 4.2   *The austenitic microstructure of the 2Cu alloy. Picture (a) gives an assembly of microscopic pictures, picture (b) gives the grain boundaries, as derived by hand.*

Table 4.2   *The experimentally observed microstructural parameters; d_γ and σ_γ are the average and standard deviation of the austenite grain–size distribution, β is the cooling rate during the dilatometry experiment, d_α is the average ferrite grain size after cooling, and n_n is the nucleus density.*

alloy	d_γ (μm)	σ_γ (μm)	β (K/min)	d_α (μm)	n_n (10^{10} m^{-3})
1Co	440	340	20	450	1.1
			40	360	2.2
			60	320	2.9
2Co	450	340	20	590	0.49
			40	480	0.93
			60	470	0.99
1Cu	360	270	20	430	1.3
			40	310	3.3
			60	290	4.1
2Cu	440	340	20	600	0.47
			40	460	1.0
			60	400	1.5
1Mn	360	260	20	380	1.8
			40	350	2.3
			60	310	3.4
2Mn	80	56	20	100	98
			40	83	180
			60	77	210
2Cr	270	190	20	200	12
			40	190	15
			60	180	17
1Al	260	190	20	350	2.3
			40	340	2.6
			60	340	2.6

The relative dilatation, $\Delta L/L_0$, with L_0 the initial length of the sample, is measured as a function of temperature for the alloys of table 1 at each of the cooling rates $\beta = 20$, 40 and 60 K/min. From the measured dilatometry curves the fraction ferrite is calculated using

equation (4.3). For each alloy the measurement has been performed in duplicate, resulting in two transformation curves that in general showed a difference of several Kelvin in the position along the temperature axis. The temperatures at corresponding ferrite fractions in each set of two measurements were averaged, resulting in a single transformation curve for each alloy.
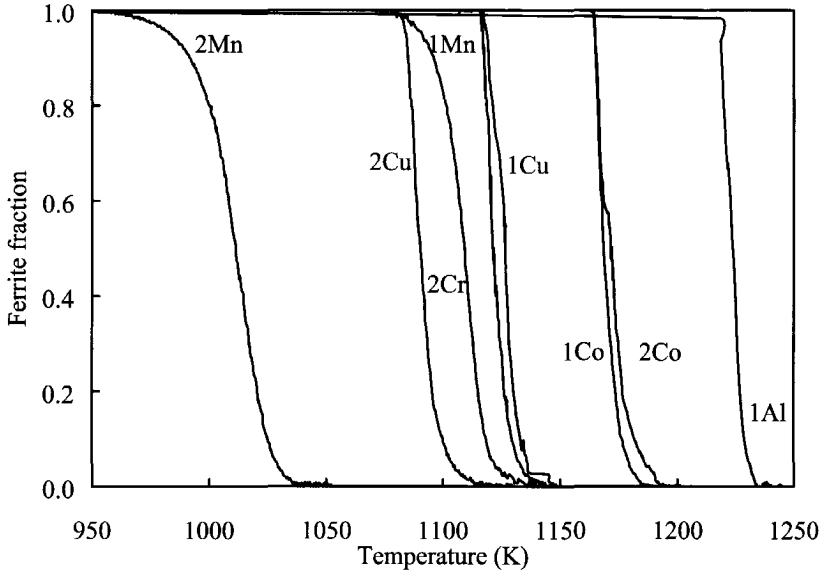
Figure 4.3   The ferrite volume fractions as a function of temperature, derived from measurements at the cooling rate $\beta = 20$ K/min.

In figure 4.3 the experimental transformation curves, for the cooling rate $\beta = 20$ K/min, are given in a single graph. The temperature ranges of the transformations for the different alloys extend over some 200 K, due to both the composition dependence of the temperature T_0, at which austenite and ferrite of the nominal alloy composition have the same free energy, and the differences in transformation kinetics for the different alloys. The ferrite fractions are plotted against the undercooling $T_0 - T$, again for the cooling rate of 20 K/min, in figure 4.4. This graph separates the two aforementioned influences, and directly shows the different transformation kinetics. Nevertheless, also figure 4.4 does not specifically show the influence of the composition on the interface mobility, since the transformations take place at different temperatures, implying a different atomic mobility

and a different driving force. Figure 4.4 clearly shows that the undercooling required to start the transformation depends on the alloy composition.
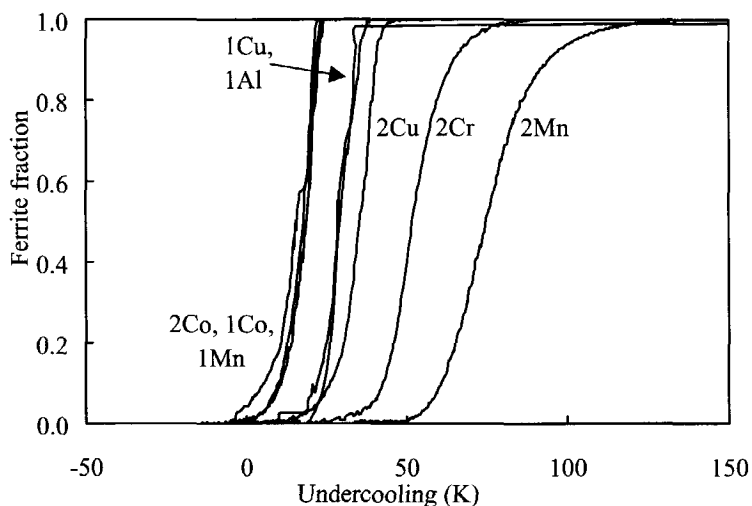
Figure 4.4   The ferrite fractions of figure 4.3, given as a function of the undercooling $T_0 - T$.

4.4.2. Model

In order to derive the mobility for the different alloys, the experimentally measured fractions are compared to the calculated ferrite fractions applying the interface–mobility model with the tetrakaidecahedron as the model austenite grain. The observation of the austenite and ferrite microstructure is used to determine the austenite grain–size distribution and the nucleus density, which are both used as input parameters in the model. The values of $\Delta G^{\gamma/\alpha}$ as a function of composition and temperature are calculated using MTDATA. The remaining parameters M_0, the pre–exponential factor for the mobility, and Q, the activation energy, can in principle be derived from a fit of the model transformation curves to the experimental ones, but the temperature range for each transformation is too small to determine both parameters with a reasonable accuracy. Therefore, for Q the value of 140 kJ/mol was chosen, in accordance with literature data for recrystallisation [15] and transformation [11] in iron alloys.

Table 4.3 *Model parameters for the different alloys, using Q = 140 kJ/mol. The error in the undercooling $T_0 - T_s$ is estimated from the duplicated measurements. The temperature T_m is the approximate temperature at a ferrite fraction of 50%. The parameter $M_0{}^{\grave{}}$ is fitted to data for different cooling rates separately, and gives an indication of the quality of the fit of a single M_0–value for three cooling rates. The error in M_0 is estimated at 30 %.*

alloy	β (K/min)	$T_0 - T_s$ (K)	T_m (K)	$M_0{}^{\grave{}}$ (molm/Js)	M_0 (molm/Js)
1Co	20	0 ± 3	1168	2.1	2.4
	40	13 ± 5	1163	2.8	
	60	18 ± 7	1154	2.3	
2Co	20	0 ± 2	1172	2.2	2.5
	40	0 ± 1	1175	2.5	
	60	0 ± 2	1178	2.9	
1Cu	20	17 ± 4	1127	1.5	2.1
	40	0 ± 2	1131	2.1	
	60	0 ± 5	1129	2.6	
2Cu	20	20 ± 3	1091	1.3	1.5
	40	28 ± 5	1081	1.6	
	60	35 ± 2	1067	1.6	
1Mn	20	0 ± 1	1122	2.2	3.5
	40	0 ± 1	1121	3.8	
	60	0 ± 1	1120	4.6	
2Mn	20	41 ± 3	1011	0.15	0.25
	40	54 ± 2	1006	0.24	
	60	54 ± 1	1004	0.36	
2Cr	20	33± 5	1109	0.27	0.37
	40	34± 2	1105	0.34	
	60	35± 3	1103	0.50	
1Al	20	20± 1	1224	0.75	1.2
	40	21± 3	1224	1.3	
	60	22± 2	1220	1.5	

To account for the undercooling occurring before the onset of the transformation, in the model calculations nucleation is assumed to occur instantaneously at a temperature T_s, implying an undercooling $T_0 - T_s$. From that moment the nuclei grow with the velocity v given by equation (4.2). After each time step, the ferrite volume fraction is calculated by numerical integration over the grain volume.

The cooling rate β, the undercooling $T_0 - T_s$, the temperature T_m at which 50 % of the ferrite has formed, and the parameter M_0 to fit the experimental data to the transformation model are given in table 4.3 for the different Fe–X alloys. Although the interface mobility cannot be assumed to depend on the cooling rate, in table 4.3 also values are given for $M_0\grave{}$, obtained from separate fits to data for different cooling rates. These data are merely presented because the variation in $M_0\grave{}$ contains an indication of the consistency of the fit with a single M_0–value for each alloy. A tendency of $M_0\grave{}$ increasing with increasing cooling rate can be observed. As an example, in figure 4.5 the experimental transformation curves for the 2Cu alloy are given together with the curves fitted to these measurements for each of the three cooling rates applied with a single value for M_0.
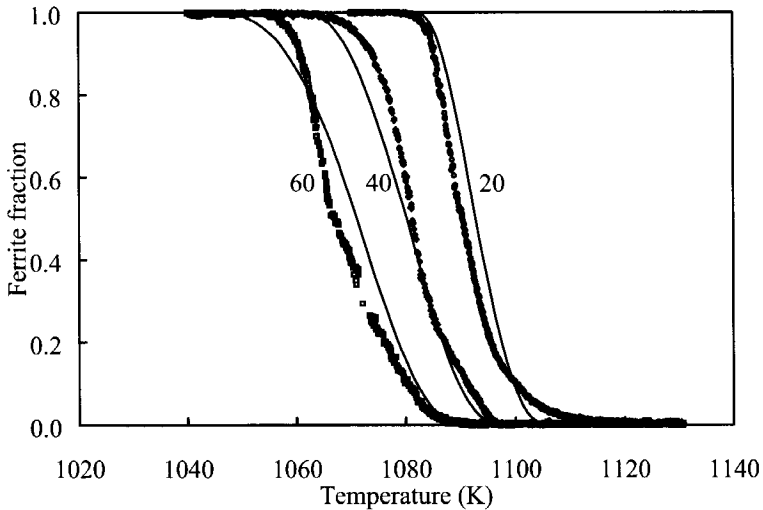

Figure 4.5   *The ferrite fraction for 2Cu at the three cooling rates (K/min) indicated. The symbols give the experimental results, the lines give the modelled transformation curves (M_0 = 1.5 molm/Js).*

In the model calculations, the Gibbs free–energy difference $\Delta G^{\gamma/\alpha}$ between the austenite and the ferrite structure provides the driving force for boundary migration. During the transformation however, this Gibbs free energy can be reduced by other circumstances, like stress build–up near the interface or solute–drag effects [22]. As a consequence, the actual driving force for boundary migration can effectively be smaller than $\Delta G^{\gamma/\alpha}$ used in the calculations and the mobilities found in this work are to be considered minimum values.

In comparison with the results on Fe–Co and Fe–Cu in ref. [14], the same tendencies of M_0 with temperature and composition are found, but the numeric values show distinct differences due to the use of different experimental techniques. This shows that the determination of the mobility is very sensitive to systematic experimental errors, which is of importance when considering the general applicability of these results.

4.5. Discussion

The investigation of the mobilities, M, of the different alloys aims to determine the dependence of M on composition and on temperature. In figure 4.6 the mobility determined from the model calculations is shown in an Arrhenius plot as a function of the temperature at 50% of the transformation, T_m. The error bars indicate the estimated accuracy of 30% in the mobility. Each symbol refers to an alloy composition and one of the three cooling rates. It is seen that the mobility of the entire set of alloys cannot be described by a single Arrhenius relation. The global temperature dependence of the mobility would indicate an activation energy that is distinctly larger than the previously mentioned values from the literature [11,15].

Inspecting figure 4.6 more closely, one notices that the results seem divided in two groups, the alloys 1Al, 2Cr and 2Mn displaying lower–than–average mobilities and the other alloys displaying higher mobilities. This division appears to be related to the nitrogen content of the alloys (table 4.1), which ranges from 4 appm for 1Co to over 400 appm for 2Cr and 2Mn. The effect of nitrogen on the transformation kinetics is generally two–fold: (1) the nitrogen content affects the driving force $\Delta G^{\gamma/\alpha}$, and (2) the presence of nitrogen causes a solute–drag effect, with nitrogen atoms located preferentially at the interface, thus hindering the motion of the interface. The influence of the first effect on the mobilities determined from the experiments can be estimated by calculating $\Delta G^{\gamma/\alpha}$ with and without nitrogen at the temperature range of the transformation. These calculations show that the

driving forces for the three 'slow' alloys 1Al, 2Cr and 2Mn are only about 10% lower due to the presence of approximately 400 appm nitrogen (segregation of nitrogen at the interface is not taken into account). This means that the *M*–values presented in figure 4.6 are 10% lower than the values that would be obtained if nitrogen were taken into account in the calculation of the driving force. This deviation is not significant in view of the estimated accuracy, and much smaller than the observed deviations. The effect of nitrogen therefore appears to be mainly a solute–drag effect, affecting the mobility of the α/γ–interface.
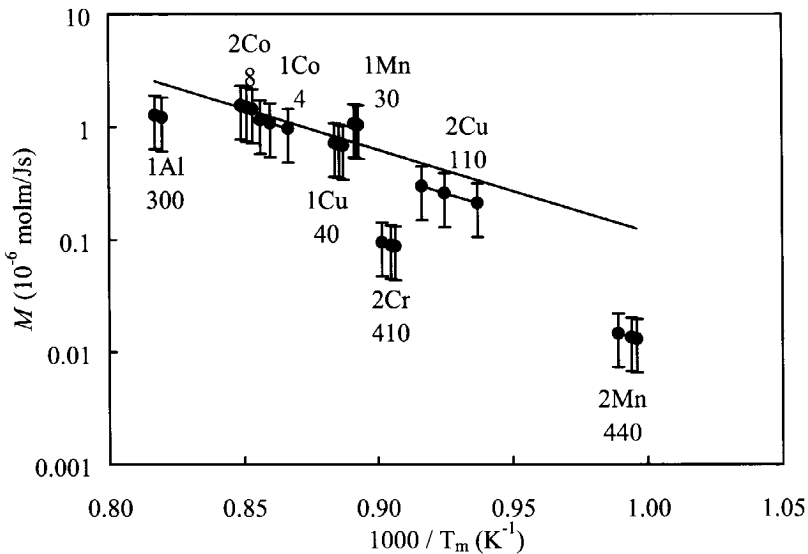

Figure 4.6   The mobilities M as a function of temperature in an Arrhenius plot. The solid line gives the best fit for the data for low nitrogen contents ($M_0 = 2.4$ molm/Js, $Q = 140$ kJ/mol). The nitrogen contents are given in appm.

An unambiguous determination of the mobility as a function of the nitrogen content is not feasible, but the present data indicate that the parameters for the interface mobility are indeed significantly affected by the nitrogen content, which varies over the alloys. In fact, the solid line in figure 4.6 (describing the data for the four alloys containing 40 appm N or less, with the parameter values $M_0 = 2.4$ molm/Js and $Q = 140$ kJ/mol) shows that the data indicate an activation energy of 140 kJ/mol, a value that is typical for grain–boundary processes, and a pre–exponential factor M_0 that is continuously decreasing with increasing

nitrogen content. Figure 4.7 gives the relative deviation of the observed mobility M from the model value M_{fit} calculated with $M_0 = 2.4$ molm/Js and $Q = 140$ kJ/mol, as a function of the nitrogen content. This graph clearly shows the significant and monotonous decrease of the mobility with increasing nitrogen content. A quantitative indication of the effect is seen in the M_0–values for the Fe – Co alloys, containing practically no nitrogen ($M_0 \approx 2.4$ molm/Js) and the M_0–values for the alloys 2Cr and 2Mn, containing on the order of 400 appm nitrogen ($M_0 \approx 0.3$ molm/Js). Of course it should be noted that these concentrations denote the average concentrations in the sample; the local concentration at the interface can be considerably higher, but cannot be determined experimentally. In the present interpretation it is assumed that higher overall nitrogen concentrations lead to proportionally higher concentrations at the austenite/ferrite interfaces.

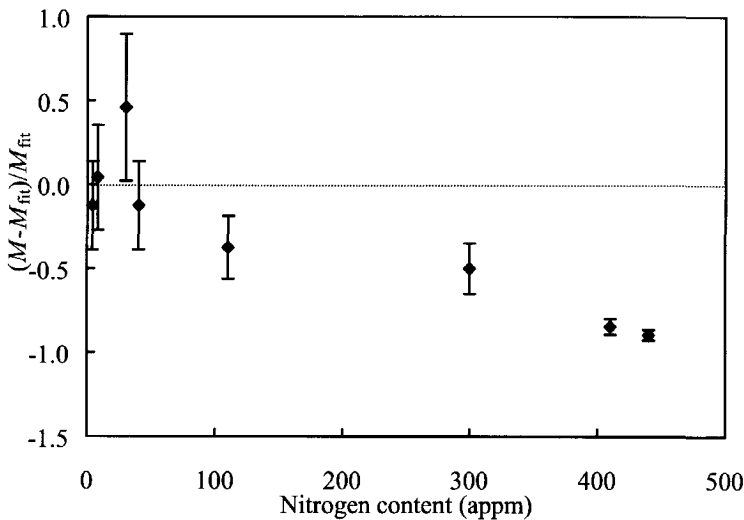*Figure 4.7   The relative deviation of the mobilities of figure 4.6 from the model value M_{fit}*
(solid line in figure 4.6).

4.6. Conclusions

The kinetics of massive growth of ferrite in substitutional iron alloys during the decomposition of austenite can be satisfactorily described by the interface–mobility model. The interface mobility determined for a range of iron alloys containing 1 or 2% of a

substitutional element shows a temperature dependence that cannot be described with a single Arrhenius relation. However, the transformation kinetics appear to be sensitive to the nitrogen content of the samples, causing an apparent scatter in the mobility data. It is shown that an activation energy of 140 kJ/mol, typical for grain–boundary processes, fits well to the low–nitrogen data. The pre–exponential factor M_0 shows a continuous decrease with increasing nitrogen content, decreasing by a factor of 8 for an overall concentration of 400 appm nitrogen.

References

1   D.A. Porter, K.E. Easterling, *Phase transformations in metals and alloys*, 2nd edition, Chapman & Hall, London, 1992.

2   *Steel, a handbook for Material Research and Engineering*, Springer Verlag, Berlin, 1992.

3   R.W.K. Honeycombe, H.K.D.H. Bhadeshia, *Steels Microstructure and Properties*, Edward Arnold, London, 1995.

4   R.A. Vandermeer, *Acta Metall. Mater.* 38 (1990) 2461.

5   M. Enomoto, *ISIJ Intern.* 32 (1992) 297.

6   R.C. Reed, H.K.D.H. Bhadeshia, *Mater. Sci. Technol.* 8 (1992) 421.

7   J.W. Johnson, R.F. Mehl, *Trans. A.I.M.E.* 135 (1939) 416.

8   M. Avrami, *J. Chem. Phys.* 7 (1939) 1103.

9   C. Zener, *J. Appl. Phys.* 20 (1949) 950.

10   J.W. Christian, *The theory of phase transformations in metals and alloys*, 2nd edition, Pergamon Press, Oxford, 1981.

11   G.P. Krielaart, S. van der Zwaag, *Mater. Sci. Techn.* 14 (1998) 10.

12   G.P. Krielaart, J. Sietsma, S. van der Zwaag, *Mater. Sci. Eng.* A 237 (1997) 216.

13   Y. van Leeuwen, S.I. Vooijs, J. Sietsma, S. van der Zwaag, *Metall. Mater. Trans.* A 29 (1998) 2925.

14   S.I. Vooijs, Y. van Leeuwen, J. Sietsma, S. van der Zwaag, *Metall. Mater. Trans.* A 31 (1999) 379.

15   M. Hillert, *Metall. Trans.* A 6 (1975) 5.

16   T. Gladman, *The Physical Metallurgy of Microalloyed Steels*, 1st edition, Institute of Materials, London, 1997, 144.

17   W. Huang, M. Hillert, *Metall. Mater. Trans.* A 27 (1996) 480.

18   C. Zurek, E. Suchova, H.P. Hougardy, *Abschlussbericht project COSMOS*, Max–Planck Institut für Eisenforschung, Düsseldorf, 1993.

19   T.A. Kop, J. Sietsma, S. van der Zwaag, accepted for publication in *J. Mat. Sci.* (2000) (Chapter 2 of this thesis).

20   J.C. Russ, *Practical Stereology*, Plenum Press, New York, 1986, 64.

21   F.C. Hull and W.J. Houk, *Trans. AIME*, April 1953, 565.

22   Z.K. Liu, *Acta Mater.* 44 (1996) 3855.

5

The influence of nitrogen on the austenite/ferrite interface mobility in Fe–1%Si

In this chapter the inferred relation between nitrogen content and the mobility of the austenite/ferrite interface (chapter 4) is explored further. Samples of an Fe–1at.%Si alloy were given various internal nitriding treatments, leading to samples containing nitrogen concentrations between 20 and 3000 appm. Dilatometric measurements indicate a clear shift in the transformation curves. The transformation is shifted to lower temperatures and is slowed down with higher nitrogen contents. The transformation kinetics are modelled using an interface mobility model in combination with the tetracaidecahedron as a representation of the austenite grain. For nitrogen concentrations smaller than 500 appm there is a good agreement between experimental and model fraction curves, using an exponential relation for the nitrogen dependence of the pre–exponential mobility factor, M_0. For higher nitrogen levels M_0 decreases less rapidly. Moreover, only the first part of the ferrite formation is accurately modelled. Towards the end of the transformation the discrepancy between experimental and model fraction curves increases. This suggests that for the determination of the driving force in the case of higher nitrogen concentrations long range diffusion of nitrogen should be taken into account.

5.1. Introduction

In chapter 4 the transformation behaviour of binary substitutional iron alloys was described [1] by an interface–mobility model [2–3], based on the driving force given by the Gibbs free–energy difference between the austenite and the ferrite, using the tetracaidecahedron geometry as the model austenite grain [4–5]. Although only small amounts of nitrogen (less than 500 appm) were present in the samples used in chapter 4, a relation between the nitrogen content and the mobility resulted from the modelling of the experimental fraction curves. It is the aim of this chapter to further investigate this relation. To this end dilatation experiments on binary Fe–1at.%Si samples with different nitrogen concentrations are performed. The resulting experimental fraction curves are compared with model fraction curves, based on the interface–mobility model and using the pre–exponential factor of the mobility, M_0, as the varying parameter, to derive the effect of nitrogen on the interface mobility.

5.2. Experimental

The composition of the base material is shown in table 5.1. Hollow cylindrical dilatometry samples, 10.0 mm long with an outer and inner diameter of respectively 4.0 and 3.0 mm, were machined. The samples were given an internal nitriding treatment in an NH$_3$/H$_2$ atmosphere [6–7] to establish the nitrogen content. An internal nitriding treatment is a nitriding treatment in which the nitriding potential is kept below the value required to form iron nitrides. The nitriding potential r_N is defined as

$$r_N = \frac{p_{NH_3}}{(p_{H_2})^{3/2}} ,$$

(5.1)

in which p_i is the partial pressure of gas i. The formation of internal precipitates depends on the nitrogen affinity of the alloying elements and on the nitriding potential, temperature and time. The applied treatments are given in table 5.2. The amount of added nitrogen was determined by measuring the increase in weight of the samples, using a Sartorius balance with an accuracy of 0.0001 mg, which corresponds with about 2 appm N.

The fractions transformed were determined in dilatometry experiments at a 40 K/min cooling rate after austenitisation at 1300 K for 15 minutes. The dilatometry setup described

in chapter 2 [8] was used. Two thermocouples attached to the surface of the sample were used, the control thermocouple being located in the centre and the reference thermocouple at the end of the sample. The temperature gradients along the length of the specimen are larger for the hollow samples than for the massive samples used in chapter 4. This is caused by different contributions of the heat conduction and radiation due to the difference in volume–area ratio's between hollow and massive samples, and due to differences in the induced magnetic field in the samples, since the induced field depends on the sample geometry. The second thermocouple readings indicate differences up to 25 K with respect to the first thermocouple. The austenite grain size was determined by optical microscopy after thermal etching, and the ferrite microstructure was revealed using a 2 % nital etch and optical microscopy.

Table 5.1   Composition of the base alloy.

Alloy	Si (at.%)	Si (wt.%)	Ni (wt.%)	Cu (wt.%)	C (wt.%)	S (wt.%)	N (wppm)	N (appm)
1Si20N	0.96	0.48	0.006	0.002	0.001	0.002	5	20

Table 5.2   Nitriding conditions and nitrogen content x_N for the different samples.

Sample	x_N (appm)	Nitriding temperature (K)	Nitriding time (h)	Nitriding potential, r_N (10^{-4} Pa$^{-1/2}$)
1Si20N	20	–	–	–
1Si260N	260	773	1	2.17
1Si740N	740	773	4	2.17
1Si1180N	1180	773	120	3.63
1Si2940N	2940	861	6	3.63

Figure 5.1a shows a part of the Fe–Si phase diagram, calculated by the thermodynamical database program MTData. It is seen that silicon is a ferrite stabiliser. For silicon concentrations larger than 3.8 at.% the austenite region disappears completely. Figure 5.1b shows the thermodynamic influence of nitrogen on the Fe–1%Si system. It is seen that at the austenitisation temperature all nitrogen is in solid solution when equilibrium circumstances are reached. The nitrogen enlarges the austenite–ferrite two–phase region and for temperatures below 1125 K, silicon nitride is a thermodynamically stable phase in the iron matrix. The indicated T_0–line corresponds with the temperature for which the

Gibbs free energies G of the austenite and the ferrite phase, with identical compositions, are equal: $G^{\gamma} = G^{\alpha}$.

5.3. Results and discussion

Figure 5.2 shows the dilatation behaviour of the samples during the complete thermal cycle. In the dilatation cycle the T_0–values are indicated by asterisks and the Ae_3– and Ae_1–temperatures are marked by the ends of the horizontal bars. The ferrite to austenite transformation kinetics, given by the heating part of the dilatation curves, do not show a strong influence of nitrogen for the four lowest nitrogen concentrations. The onset temperature of the austenite formation decreases slightly with increasing nitrogen content. The decrease in onset temperature more or less corresponds with the decrease in T_0. The dilatation curve of the 1Si2940N sample however starts to deviate at temperatures well below the T_0–temperature. The large difference between the heating curves of the 1Si1180N and the 1Si2940N samples suggests that in the 1Si2940N sample different processes are taking place. According to the phase diagram the relatively large amount of nitrogen present results in Si_3N_4 precipitates. The difference in the dilatation curves during heating suggests that during the internal nitriding treatment indeed Si_3N_4 precipitates are formed. The finish temperature of the austenite formation is approximately the same for all samples. For the 1Si2940N sample this means that there is a significant retardation of the transformation, extending it to temperatures well above the Ae_3–temperature. This is probably also related to the presence of silicon nitrides.

During cooling there is an influence of the nitrogen over the entire austenite to ferrite transformation range. The cooling parts of the dilatation curves show that the ferrite–start temperature is reduced and that the total transformation time increases with increasing nitrogen content. The transformation–finish temperature for the 1Si20N, 1Si740N and the 1Si1180N samples is within 25 K below the Ae_1–temperature. The transformation–finish temperature of the 1Si260N and the 1Si2940N samples do not follow this trend. The deviation of the 1Si260N sample should be seen in the light of the accuracy of the temperature control. The second thermocouple reading for this experiment suggests that the control thermocouple underestimates the real temperature of the sample.
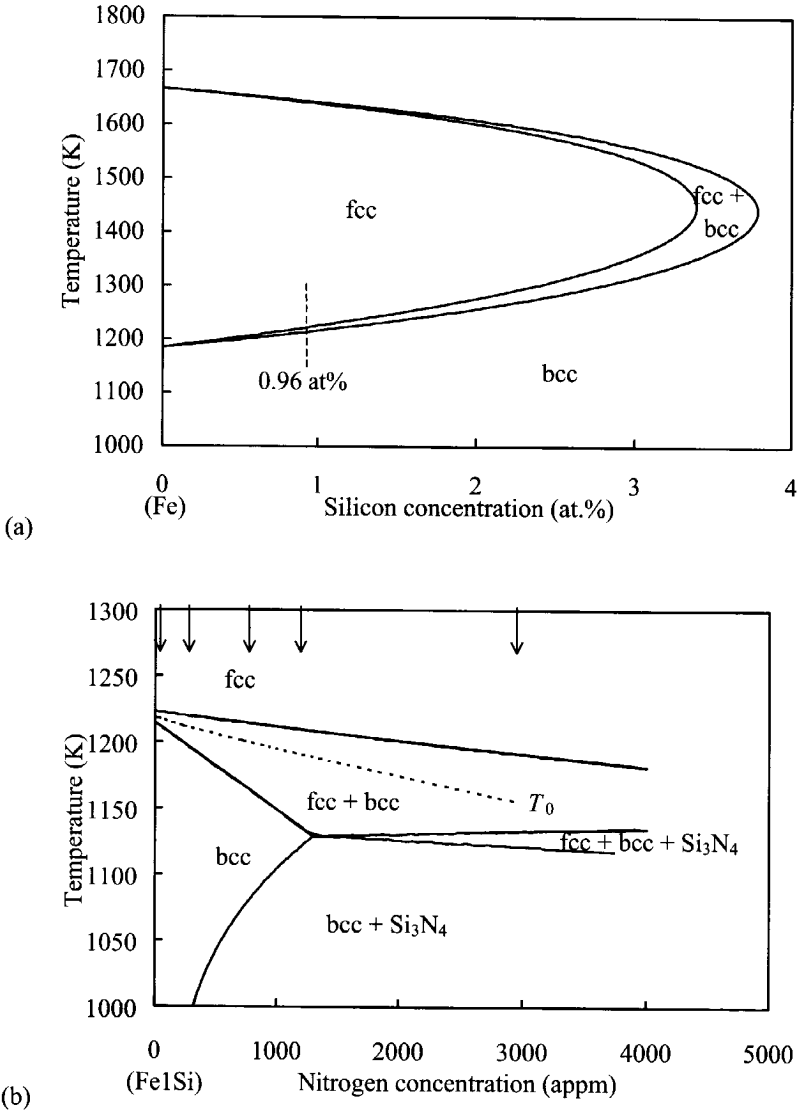
(a)

(b)

Figure 5.1   *Phase diagrams calculated with MTData. a) A part of the Fe–Si phase diagram, and b) a binary cross–section of the Fe–Si–N phase diagram at x_{Si} = 0.96 at.%. The compositions of the used samples are indicated by the arrows at the austenitisation temperature (x_N, 1300 K). T_0 is the temperature for which the free energies for ferrite and austenite are equal.*
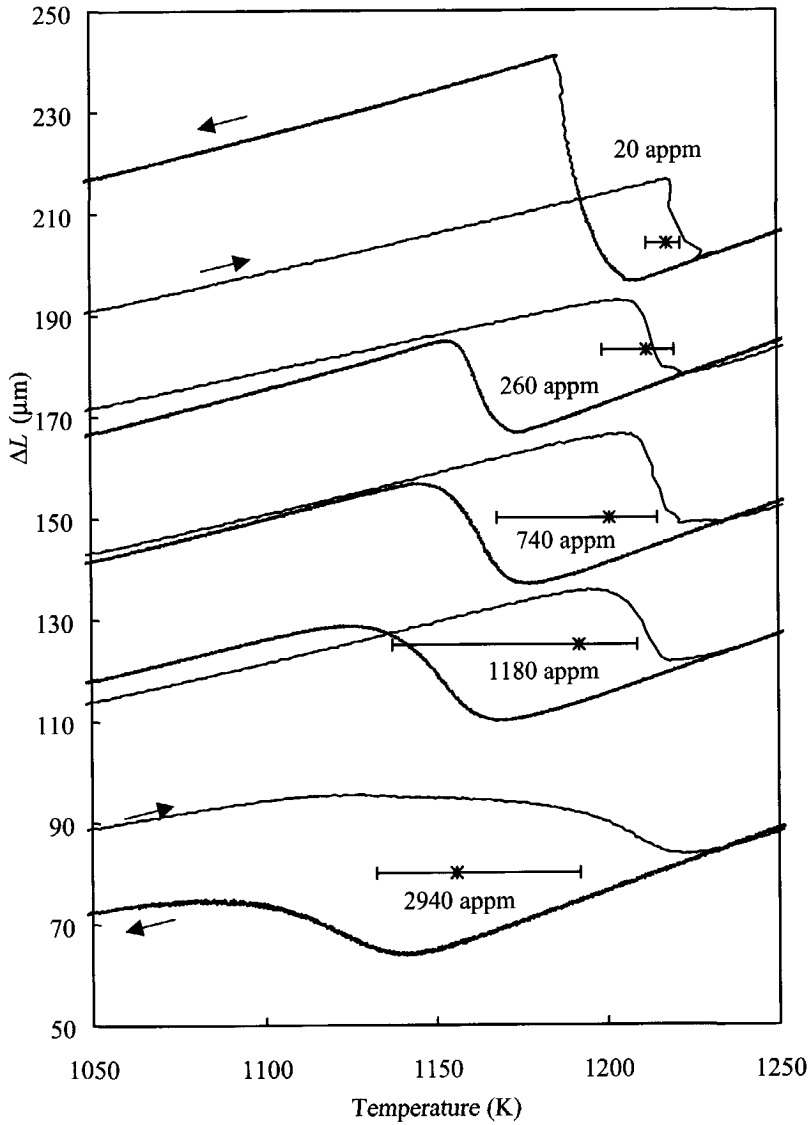
Figure 5.2   The measured change in length vs. temperature for the 5 samples of table 5.2. The nitrogen content is indicated, as well as the two–phase region in the phase diagram. The asterisks denote T_0. The curves have been shifted along the ΔL–axis for clarity.
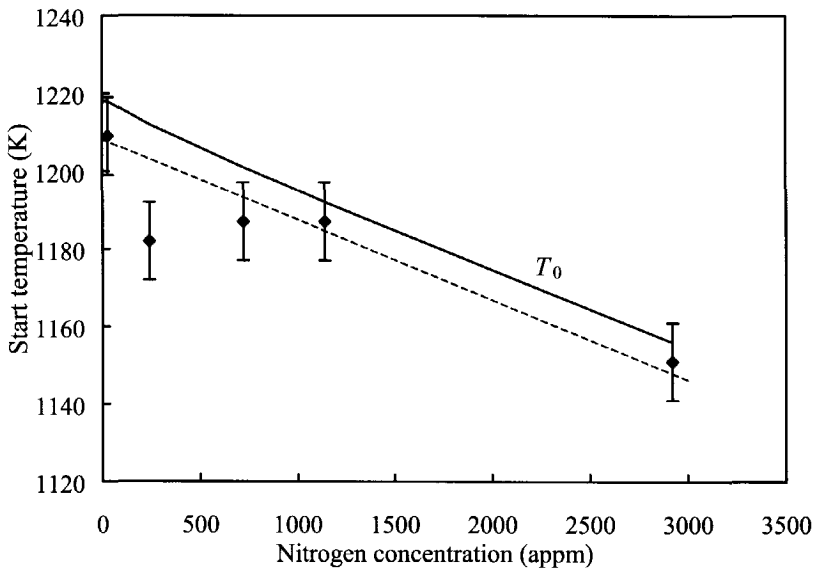
Figure 5.3 The experimentally determined start temperature, T_s, and the T_0–temperature (solid line) vs. the nitrogen concentration. The dashed line indicates a constant undercooling of 10 K.

Figure 5.3 shows the experimentally determined ferrite–start temperatures (T_s) together with the calculated T_0–temperature. Considering the experimental inaccuracy of the determination of T_s, it is concluded that the undercooling, $\Delta T = T_0 - T_s$, is not strongly influenced by the nitrogen concentration and therefore the undercooling is estimated to be constant at 10 K. For the 1Si260N sample the undercooling is taken as 35 K, as observed from the measurement.

The model fraction curves are calculated using the tetracaidecahedron geometry and a mobility–controlled interface velocity [4]. The interface velocity v is given by [2]

$$v = M \cdot \Delta G \ ,$$
(5.2)

in which

$$M = M_0 \cdot \exp\left(-\frac{Q}{RT}\right),$$
(5.3)

73

is the interface mobility, with M_0 the pre–exponential factor, Q the activation energy, R the universal gas constant and T the temperature. The driving force for the transformation, ΔG, is given by the difference between the austenite and the ferrite Gibbs free energies. The Gibbs free energy of the austenite as well as the Gibbs free energy of the ferrite phase is calculated at nominal compositions. In other words, it is assumed that there is no partitioning during the transformation.

For all the calculations the austenite–grain size, the nucleus density n_n, and the activation energy Q are kept constant, irrespective of the nitrogen content, at respectively 120 μm, $195 \cdot 10^{10}$ m^{-3}, and 140 kJ/mol (see chapter 4 for the determination of n_n and the choice for Q). M_0 is used as the only variable to fit the data.

Figure 5.4 shows the model fraction curves compared to the experimental fraction curves. The fits for the 1Si20N, 1Si260N, 1Si740N, 1Si1180N samples are good. For the 1Si2940N sample the correspondence between the experimental and model fraction curves is less accurate. A better agreement between experimental and model fraction curve can not be obtained by varying M_0. Neither can a change in undercooling improve the correspondence. For the other samples the fit is very accurate, especially for the first part of the ferrite formation. Discrepancies between the model and experimental fraction curves occur rather at the end of the ferrite formation. The model uses the difference in Gibbs free energy between the austenite and ferrite as a driving force, under the assumption that no redistribution of alloying elements occurs. Therefore the discrepancy at the end of the transformation is possibly caused by a pile–up of nitrogen at the interface. This causes the kinetics of the nitrogen diffusion to play a role in the overall transformation kinetics, resulting in a reduction of the transformation rate. The transformation kinetics of 1Si2940N are even more strongly reduced. Considering the high nitrogen content of this sample, it is possible that, besides the nitrogen diffusion, precipitates of silicon nitride also play a role. At the onset of the ferrite formation, in the 1150 – 1125 K temperature interval, Si_3N_4 precipitates are thermodynamically unstable and will not precipitate. However, Si_3N_4 precipitates can be present at the temperatures involved if they have not gone into solution during austenitisation.

Table 5.3 shows the M_0– and ΔT–values used to obtain the model fraction curves. For all samples, the M_0–values are used to calculate the mobility M at T_m, which is the temperature at which 50 % ferrite is formed. These mobilities are compared to the mobility M_{base} of the base alloy assuming the mobility is only temperature dependent ($M_0 = 0.250$ molm/Js, $Q = 140$ kJ/mol).
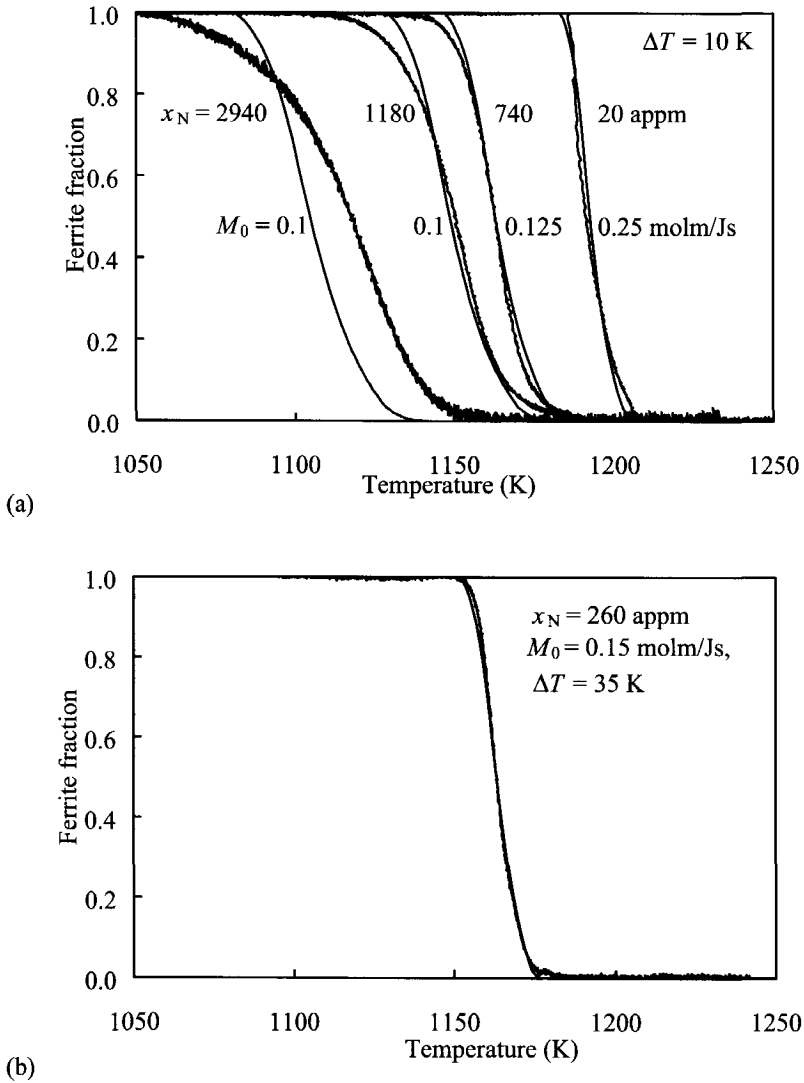
(a)

(b)

Figure 5.4　*The experimental and model ferrite–fraction curves. a) The 1Si20, 740, 1180 and 2940N samples, with $\Delta T = 10$ K, and b) the 1Si260N sample with $\Delta T = 35$ K. The 1Si260N–curve is given seperately because of the overlap with 1Si740N.*

75

Figure 5.5 shows the deviation of the obtained mobilities M from this theoretical value as M/M_{base} vs. the nitrogen concentration. The open symbols with the dashed error bars indicate the results M/M_{fit} of chapter 4 (see figure 4.7). The data of chapter 4 can be described by an exponential relationship. It is seen that the 1Si260N sample coincides with this trend. For higher nitrogen concentrations the interface mobility is still decreasing, however the change in mobility is not as strong as for nitrogen concentrations smaller than 500 appm. Apparently the relation between the mobility and the nitrogen concentration found in chapter 4 is only valid for nitrogen concentrations smaller than about 500 appm.

The relatively high mobility factors for the higher nitrogen concentrations (the mobility does not decrease as fast as with the first 500 appm nitrogen) indicate a contribution of an additional process influencing the transformation kinetics. The deviation of the transformation kinetics at higher nitrogen concentrations can either be caused by Si_3N_4 precipitates or by the diffusion of nitrogen. Although the transformation–start temperatures during heating or cooling did not show any anomalies (figure 5.2), it is possible that Si_3N_4 precipitates have formed during the nitriding treatment according to the phase diagram (figure 5.1b). If part of the nitrogen is precipitated, there will be less nitrogen left in solution. This means that in the model calculations the driving force is underestimated. This in turn causes an overestimation of the intrinsic mobility of the interface. Although the presence of Si_3N_4 precipitates that have not gone into solution during the austenitisation treatment is a likely explanation, the cause for the relatively high mobilities can equally well be related to the diffusion of nitrogen. Partitioning of nitrogen, and a build–up of the nitrogen concentration at the austenite/ferrite interface, causes lower driving forces than are used in the calculations, leading to an overestimation of the mobility factor.

Table 5.3   The values used for the model parameters undercooling, ΔT, and the pre–exponential factor, M_0.

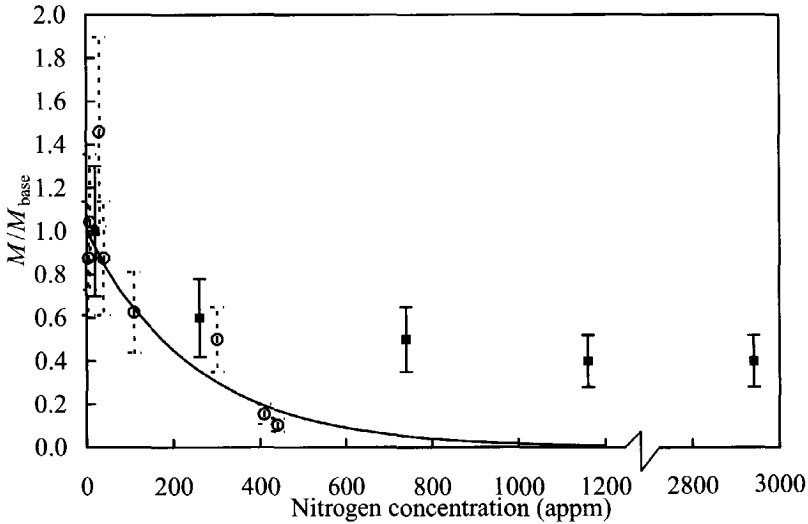| Sample	ΔT (K)	M_0 (molm/Js)
1Si20N	10	0.25
1Si260N	35	0.15
1Si740N	10	0.125
1Si1180N	10	0.1
1Si2940N	10	0.1

Figure 5.5   *The deviation of the mobilities from the value M_{base} for the base alloy, all calculated at $T = T_m$. The open symbols and dashed error bars indicate the equivalent results, M/M_{fit}, of chapter 4.*

5.4. Conclusions

Internal nitriding treatments of an Fe–1at.%Si alloy resulted in samples with various nitrogen concentration. The austenite to ferrite transformation kinetics are retarded and slowed down by the nitrogen. The austenite to ferrite transformation was modelled using the interface–mobility model. It was found that the entire transformation range can be satisfactorily modelled up to nitrogen levels of about 500 appm (see also chapter 4). The intrinsic mobility does strongly depend on the nitrogen content, reducing to about 10 % of the original value for 500 appm. For nitrogen concentrations higher than 500 appm the first part of the ferrite formation is still accurately modelled. However, the variation in intrinsic mobility deviates from the trend between the intrinsic mobility and the nitrogen concentration observed for nitrogen concentrations up to 500 appm. Towards the end of the

transformation the discrepancy between experimental and model fraction curves increases. Both the deviation of M_0 *vs.* nitrogen concentration and the discrepancy towards the end of the transformation curve suggests that for the determination of the driving force, for samples with nitrogen concentrations higher than 500 appm, long range diffusion of nitrogen should be taken into account.

References

1   J.J. Wits, T.A. Kop, Y. van Leeuwen, J. Sietsma, S. van der Zwaag: *Mat. Sci. Eng. A.*, A283 (2000) 234.

2   J.W. Christian: The Theory of Transformations in Metals and Alloys, 2nd edition (Pergamon Press, Oxford, 1981), 476.

3   G.P. Krielaart, S. van der Zwaag, *Mater. Sci. Techn.* 14 (1998) 10.

4   Y. van Leeuwen, S.I. Vooijs, J. Sietsma, S. van der Zwaag: *Metall. Mater. Trans.*, 29A (1998) 2925.

5   T. Gladman: The Physical Metallurgy of Microalloyed Steels, 1st ed., Institute of Materials, London, 1997, 144.

6   H.H. Podgurski, H.E. Knechtel, *Trans. TMS–AIME*, 245 (1969) 1595.

7   M.H. Biglari, C.M. Brakman, M.A.J. Somers, W.G. Sloof, E.J. Mittemeijer, *Z. Metallk.* 84 (1993) 124.

8   T.A. Kop, J. Sietsma, S. van der Zwaag, accepted for publication in *J. Mat. Sci.*(2000).

6

Modelling the austenite to ferrite phase transformation in low carbon steels in terms of the interface mobility

The kinetics of the phase transformation between the high temperature fcc–phase austenite and the low temperature bcc–phase ferrite as it occurs during controlled cooling of hot rolled low carbon steels is described using a physical model that considers austenite grain size, nucleus density, composition effects, and the austenite/ferrite interface mobility. The model is verified against experimental dilatometry data for three lean carbon–manganese steel grades. The model yields adequate reproductions of the transformation kinetics. Ferrite grain coarsening during the transformation appears to have a significant effect on the final microstructure.

6.1. Introduction

A crucial step in the production process of low–carbon steel strip is the decomposition of austenite during cooling after hot rolling. It is during this phase transformation that the microstructure is formed. The microstructure determines the properties of the material, not only by means of the phases present, but also through the dimensions (grain–size distribution, morphology) of the microstructural components. Being a thermally activated process of nucleation and growth, the phase transformation strongly depends on the time/temperature profile to which the material is subjected. In general, the occurrence of an undercooling due to fast cooling results in an enhanced nucleation rate at lower temperatures, which in turn leads to a fine ferritic/pearlitic microstructure, of which the grain sizes are also influenced by the grain–coarsening process. The formation of these phases, depending on a balance between nucleation rate and growth rate, is a complex process, difficult to control. In order to improve the control of the microstructure formation in low–carbon steels, several types of models have been developed to describe the kinetics of the austenite decomposition.

A number of empirical or semi–empirical models has been presented in the literature, of which the description of transformation kinetics by the Johnson–Mehl–Avrami scheme [1–2] is among the most widely applied. A model that is more physically based, relating to the kinetics of carbon diffusion during the transformation, is the almost classical model developed by Zener [3]. This model takes into account that, in the case of alloys with a carbon content above 0.02 wt.%, the ferrite phase cannot contain all the carbon. Consequently, at the ferrite/austenite interface the austenite enriches in carbon. Zener assumes this pile–up of carbon to result in local equilibrium at the ferrite/austenite interface and models the phase–transformation kinetics by assuming the carbon diffusion in the austenite phase to be rate determining. An implicit assumption in this model is that the actual lattice transformation from fcc austenite to bcc ferrite is fast enough to be of no significance to the transformation rate. Notwithstanding the great merits of this diffusion–control model, it is not suited to describe the phase transformation in ultra–low carbon steels and interstitial–free steels, which are becoming increasingly important. Evidently in these steels carbon diffusion plays a less prominent role, so for adequate modelling it is necessary to take the kinetics of the lattice transformation itself into account. The concept of interface mobility, reflecting these kinetics, has been defined in general terms by Christian [4].

The interface mobility determines the interface velocity as a function of the driving force for transformation given by the Gibbs free–energy difference between the austenite and ferrite phases. In most commonly used alloys the transformation rate is determined by the balance between interface mobility and carbon diffusion, leading to so–called mixed–mode models accounting for both these phenomena. An example of a phase–transformation model incorporating the influence of the interface mobility on the kinetics of the austenite–to–ferrite transformation can be found in recent work by Krielaart *et al.* [5]. In this model, the interface velocity is assumed to be proportional to the local driving force for transformation, which in turn is dependent on both the development of the transformation and the diffusion characteristics. In order to "translate" the interface velocity to macroscopic transformation kinetics, the initial austenite microstructure is modelled by a model austenite grain having the shape of a tetrakaidecahedron, and ferrite is assumed to nucleate at grain corners and grain boundaries [6]. The model has been shown to yield good results for the phase transformation in iron alloys containing substitional alloying elements [7].

In this chapter the phase–transformation kinetics at different cooling rates are determined for three commercial low–alloy steels with carbon contents between 0.05 and 0.10 wt.%. The measurements are performed by means of dilatometry, and the resulting development of the fraction ferrite as a function of temperature during cooling is simulated by means of the interface mobility model. An assessment of the influence of carbon diffusion, transformation stresses, and ferrite nucleation and grain coarsening is made.

6.2. Theory

The factors playing a role in the austenite (γ) to ferrite (α) phase transformation can be divided into three categories: (1) nucleation and coarsening, determining the ferrite grain density; (2) interface migration, and (3) geometry of the austenite and the ferrite. This section will discuss the model in terms of these three features.

6.2.1. Nucleation

Nucleation is a process that is experimentally difficult to investigate. Extensive studies have been performed among others by Enomoto and Aaronson [8], regarding the so-called classical nucleation theory. Notwithstanding these scientific efforts, many aspects concerning the nucleation kinetics still lack experimental evidence. An additional complication for studies on nucleation is caused by grain coarsening. During the last decade several papers have been published concerning the question of the coarsening of ferrite grains during the transformation. Priestner and Hodgson [9] investigated the coarsening behaviour of a deformed niobium steel and indicated that the coarsening of ferrite grains already starts in the beginning of the transformation. Bengochea *et al.* [10] show that at least in the later stages of the transformation the competition between coarsening and the kinetics of the formation of ferrite are important in determining the final grain size. This conclusion was also based on niobium containing steels with retained strain being present at the start of the transformation. From their work it follows that if the nucleus density is estimated from the final microstructure an error of at least one order of magnitude is made. Hodgson *et al.* [11] indicate that in the absence of niobium (and at low retained strains) the nucleation –instead of coarsening– may be the decisive step in determining the final ferrite grain size. This conclusion was obtained by comparing ferritic grain sizes from continuous and discontinuous cooling experiments on low carbon steels.

In this chapter, the nucleus density is derived from optical microscopy on both the austenite and the final ferrite microstructure. From the average grain sizes in both microstructures, the number ratio of austenite and ferrite grains, and hence the number of nuclei per austenite grain, is deduced. In applying this scheme, we assume as a first approximation that grain coarsening does not occur in the ferrite. It is assumed that nucleation is taking place instantaneously at a certain temperature, *viz.* upon entering the two–phase region, where the austenite becomes instable; in other words, no undercooling due to nucleation is introduced.

In the model austenite grain, the ferrite nuclei are positioned at grain corners, assuming heterogeneous nucleation to be predominant (see section 6.2.3).

6.2.2. Interface migration

A detailed description of the progression of the interface during the transformation requires a profound knowledge of the local conditions at the interface. However, since these conditions cannot be monitored in detail as a function of time and temperature, for the model the choice has been made to link the transformation kinetics to the average thermodynamical properties of the bulk of the material. The model used to accomplish this was first introduced by Christian [4]. Christian derives the net frequency ω of atoms jumping from the austenite region to the ferrite region to be given by

$$\omega = f^* \exp\left(-\frac{Q}{RT}\right)\left[1 - \exp\left(-\frac{\Delta G^{\gamma/\alpha}}{RT}\right)\right], \tag{6.1}$$

where f^* is the characteristic frequency of the atoms, R the gas constant, T the temperature, Q the activation energy and $\Delta G^{\gamma/\alpha}$ the Gibbs free–energy difference between the austenite and ferrite phases, taking into account their compositions. Since every atom jumping across the interface shifts the interface locally over a distance δ, the atomic diameter, the interface velocity v can be calculated according to

$$v = \omega \cdot \delta = M_0 \exp\left(-\frac{Q}{RT}\right) \cdot \Delta G^{\gamma/\alpha}, \tag{6.2}$$

using the condition that $\Delta G^{\gamma/\alpha} \ll RT$. $M_0 = \dfrac{f^* \delta}{RT}$ is a pre–exponential factor describing the mobility of the interface.

All in all, the model uses three quantities to describe the phase transformation: the activation energy Q, the free–energy difference $\Delta G^{\gamma/\alpha}$ and the pre–exponential factor M_0. The activation energy Q is expected to be similar to the activation energy for grain–boundary diffusion, as it is the energy barrier for atoms "entering" the interface. Its value is expected to be comparable to the value for recrystallisation in pure iron. Hillert experimentally determined this value to be 147 kJ/mol [12]. In a study by Krielaart and Van der Zwaag [13] into the transformation behaviour of binary Fe–Mn alloys a similar value (140 kJ/mol) was found.

For the calculation of the driving force $\Delta G^{\gamma/\alpha}$, for which the thermodynamic database programme MTData is used, the alloys are treated as Fe–C–Mn systems. Since the diffusion rate of manganese atoms is much lower than that of carbon atoms, it is assumed that only the carbon in the system redistributes during the transformation, while the manganese content remains equal in both the ferrite and the austenite phase. This situation is often referred to as para–equilibrium. It implies that the Fe–Mn atom ratio in the two phases remains constant throughout the transformation, which reduces the system to a quasi–binary system M–C, where M stands for a metal atom, either Fe or Mn.
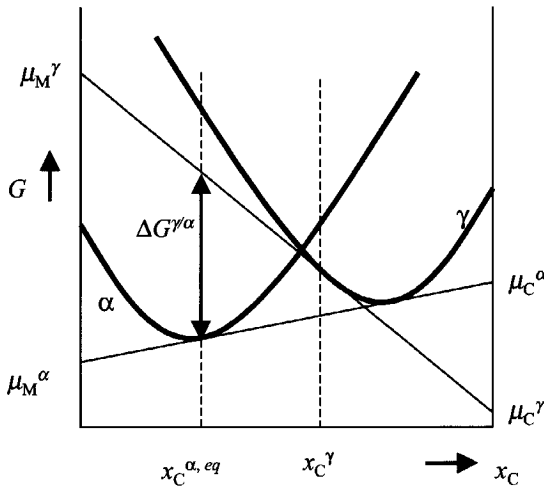

Figure 6.1. Schematic representation of the determination of the driving force for transformation, $\Delta G^{\gamma/\alpha}$.

In order to calculate the driving force for the transformation, the chemical potentials of the atoms are considered. The summation of the chemical potentials of all the elements constituting a system yields the free energy of the system. Under the assumption of para–equilibrium this summation can be written as

$$G^i = (1 - x_C^i)\mu_M^i(x_C^i) + x_C^i \mu_C^i(x_C^i), \qquad (6.3)$$

with i being either α or γ, and μ^i_M and μ^i_C the chemical potentials of the metal and the carbon atoms respectively. μ^i_M and μ^i_C for a certain phase and composition can be obtained by taking the tangent of the free–energy curve of the phase in question at the appropriate composition (figure 6.1). The values of this tangent at $x_C = 0$ and $x_M = 0$ provide μ_M and μ_C respectively. The driving force for transformation can be calculated by summing the differences in the chemical potentials in α and γ for the atoms crossing the interface, according to

$$\Delta G^{\gamma/\alpha} = x_C^{\gamma/\alpha}\Delta\mu_C + \left(1 - x_C^{\gamma/\alpha}\right)\Delta\mu_M , \qquad (6.4)$$

where $x_C{}^{\gamma/\alpha}$ is the carbon fraction of the atoms crossing the γ/α–interface, and $\Delta\mu_A = \mu_A^\gamma(x_C^\gamma) - \mu_A^\alpha(x_C^\alpha)$. The composition of the atom flux crossing the γ/α–interface is equal to the composition in the ferrite phase, which is assumed to be equal to the equilibrium concentration $x_C{}^{\alpha,eq}$. The carbon content in the austenite phase $x_C{}^\gamma$ is assumed to be homogeneous throughout the whole phase and is calculated by

$$x_C^\gamma = \frac{x_0 - f^\alpha x_C^{\alpha,eq}}{1 - f^\alpha} , \qquad (6.5)$$

with x_0 the average carbon concentration of the alloy and f^α the ferrite fraction. This method is commonly referred to as the "mean field" approach. It should be noted that $x_C{}^\gamma$ changes substantially during the transformation, while $x_C{}^{\alpha,eq}$ remains roughly constant at 0.02 wt%.

In this paper the pre–exponential factor M_0 is obtained by fitting the model to experimentally determined macroscopic data.

6.2.3. Geometry model

Equation (6.2) describes the velocity of an α/γ–interface. In order to verify this equation, experimental data on the phase transformation are needed, for which dilatometry is used in this study. This method yields the volume fraction ferrite formed from austenite as a function of temperature. In order to calculate the three–dimensional volume fraction of ferrite from the one–dimensional interface velocity, a three–dimensional geometrical model

is required. Such a model actually accomplishes the translation from the microscopic transformation behaviour to the macroscopic observation of the ferrite fraction.
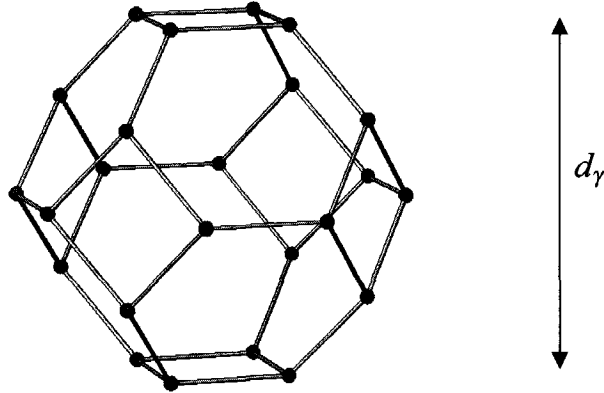

Figure 6.2   A tetrakaidecahedron as the model representation of an austenite grain.

In this paper the tetrakaidecahedron is used as a typical, regular Voronoi cell (see figure 6.2) to model the austenite grain geometry. As was shown in earlier work, due to its geometrical properties the tetrakaidecahedron is an ideal representation of an austenite grain for modelling the transformation behaviour [6]: the grain corners enable the modelling of heterogeneous nucleation as it is often reported in the literature [14–15], and by resizing the grain the influence of the austenite grain size on the transformation kinetics can be incorporated. It was shown in ref. [6] that the choice of model geometry for the austenite microstructure has significant effects on the calculated transformation kinetics.

In the model described here the ferrite phase is modelled to grow from the corners of the tetrakaidecahedron, at which nucleation is assumed to occur. The velocity v is given by eq. (6.2), being independent of the direction of the growth, and the ferrite will thus grow as segments of spheres. In every time step the ferrite fraction is determined by means of numerical integration.

6.3. Experimental

The transformation kinetics in three different lean C–Mn steel grades were investigated. The composition of the alloys is given in Table 6.1. The transformation kinetics were measured using a Bähr 805A dilatometer, on cylindrical specimens, 10 mm long with a diameter of 4 mm. The specimens were austenitised at 1223 K and subsequently cooled at a cooling rate of either 0.05, 0.3, or 10 K/s. Alloy A has also been measured at a cooling rate of 60 K/s. Apart from the temperature–control thermocouple, a second thermocouple, placed at 4 mm from the first, was used to check the temperature gradient along the length of the specimen. The measured temperature gradient was always smaller than 5 K.

Table 6.1   Compositions of the alloys used in this investigation in wt.% (at%).

	C	Mn	Si	Cu	Cr	Ni	Mo	Sn	P	S
alloy A	0.103 (0.48)	0.490	0.006	0.009	0.018	0.021	0	0	0.010	0.014
alloy B	0.072 (0.33)	0.365	0.007	0.010	0.024	0.024	0.002	0	0.012	0.013
alloy C	0.055 (0.26)	0.237	0.008	0.009	0.023	0.024	0	0.002	0.011	0.013

The volume fraction ferrite has been determined from the measured length change, taking into account the carbon enrichment of the austenite during the transformation and the difference between the specific volumes of ferrite and pearlite [16].
In order to determine the austenite grain size, samples for optical microscopy were prepared by thermal etching. The ferrite grain size was determined after etching with 2% nital. The determination of both the ferrite and austenite grain sizes was carried out by means of the mean linear intercept method.

6.4. Results and Discussion

Figure 6.3 shows two micrographs of the etched ferritic microstructure of alloy A after austenitisation and cooling at 0.05 and 60 K/s, respectively. The microstructure resulting from the slow cooling shows distinct bands of pearlite. The microstructure attained with

the high cooling rate has a more random distribution of pearlite in the ferrite matrix. This feature is also observed for the alloys B and C. Table 6.2 gives the results of the microstructural analysis for the three steel grades after cooling at the different rates, with d_i the average grain size in phase i. The resulting nucleus density n_n is calculated by $n_n = (1/d_\alpha)^3$.

Table 6.2   Microstructural data for the austenite and ferrite phase, as determined by optical microscopy, d_γ is the average austenite grain diameter, d_α the average ferrite grain diameter and n_n the nucleus density.

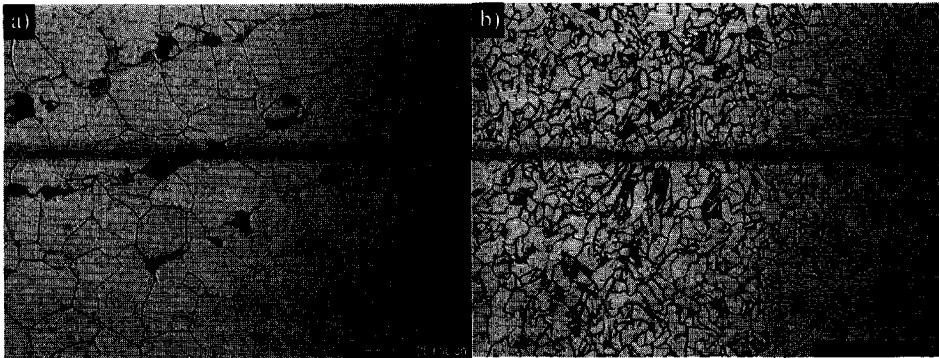|		0.05 K/s		0.3 K/s		10 K/s		60 K/s	
	d_γ (µm)	d_α (µm)	n_n (10^{13}m^{-3})	d_α (µm)	n_n (10^{13}m^{-3})	d_α (µm)	n_n (10^{13}m^{-3})	d_α (µm)	n_n (10^{13}m^{-3})
A	11	20	13	15	30	8	195	6	462
B	11	25	6.4	25	6.4	8	195	–	–
C	10	30	3.7	26	5.7	16	24	–	–

Figure 6.3   Microstructure of alloy A, after cooling with a) 0.05 K/s, and b) 60 K/s.

Figure 6.4 shows the measured ferrite volume fractions f^α for alloy A as a function of temperature. In this graph five curves are depicted. Four curves correspond to continuous cooling at 0.05, 0.3, 10 and 60 K/s, the fifth curve is determined in a second experiment at a cooling rate of 0.3 K/s. During this experiment a 30 minute isothermal hold at 1061 K was introduced. The curves belonging to the two lowest cooling rates coincide for $f^\alpha > 0.5$. The transformation in the 0.3 K/s experiment starts at a slightly lower temperature than in the 0.05 K/s experiment. Due to the larger driving force the growth process is faster, and

the 0.3 K/s curve joins the 0.05 K/s curve at $f^{\alpha} \approx 0.5$. From here on the transformation rate, as defined by volume fraction transformed per unit of temperature, is the same for the two cooling rates. The fact that the same development of the ferrite fraction occurs, can be explained by the transformation following the equilibrium state. In order to check this, the second experiment at 0.3 K/s has been interrupted for 30 minutes at 1061 K. The fractions ferrite as a function of temperature for the two 0.3 K/s experiments coincide over the complete temperature range, as can be seen in figure 6.4.
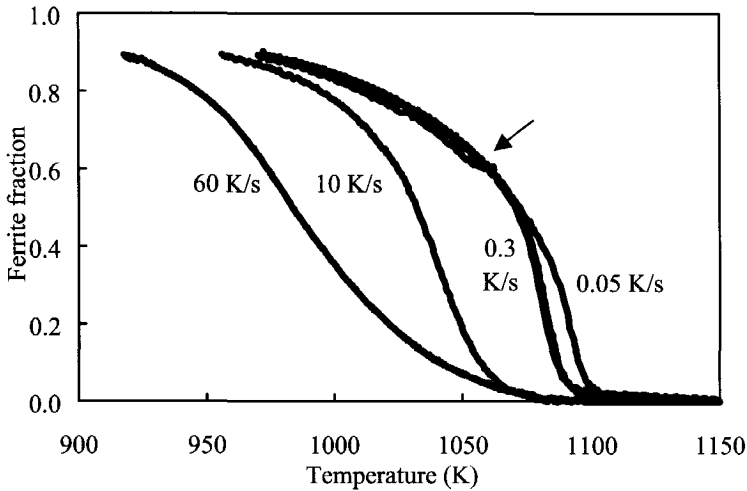

Figure 6.4   Transformation curves, derived from dilatometry results, for steel grade A at controlled cooling rates of 0.05, 0.3, 10 and 60 K/s. An additional fraction curve corresponding to a cooling rate of 0.3 K/s, in which a 30 minute isothermal hold at 1061 K was performed, is included. This curve coincides completely with the continuous cooled, 0.3 K/s, fraction curve. The observed ferrite fraction during the isothermal hold is indicated by the arrow.

During the isothermal period, indicated by the arrow, there is no significant deviation of the fraction curve. The change in fraction which is observed during this period is caused by instrumental fluctuations. The transformation rate that appears in figure 6.4 gives the development of the ferrite fraction with temperature, or df^{α}/dT. This quantity gradually decreases with increasing cooling rate. The transformation rate with respect to time

(df^{α}/dt) increases with the cooling rate, caused by the increased undercooling that strongly enhances the driving force for transformation.

Figure 6.5 gives the experimentally determined ferrite fractions (thick lines) and the modelled curves (thin lines) for the alloys A, B and C. In the calculations, the nucleus density and the austenite grain size as given in table 6.2 are used, and the activation energy Q is set to 140 kJ/mol. The mobility parameter M_0 is used as the single parameter to optimise the agreement between model and experimental curves. The resulting values are listed in table 6.3.

Table 6.3   The M_0–values (in molm/Js) used for the model curves in figures 6.5a–c.

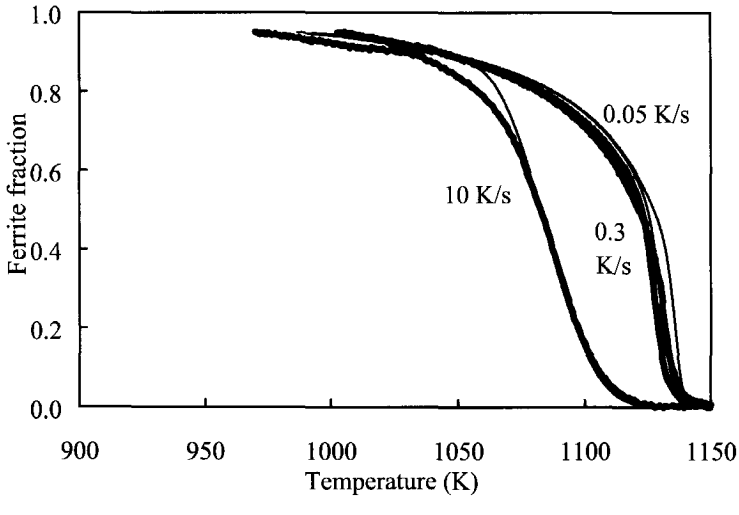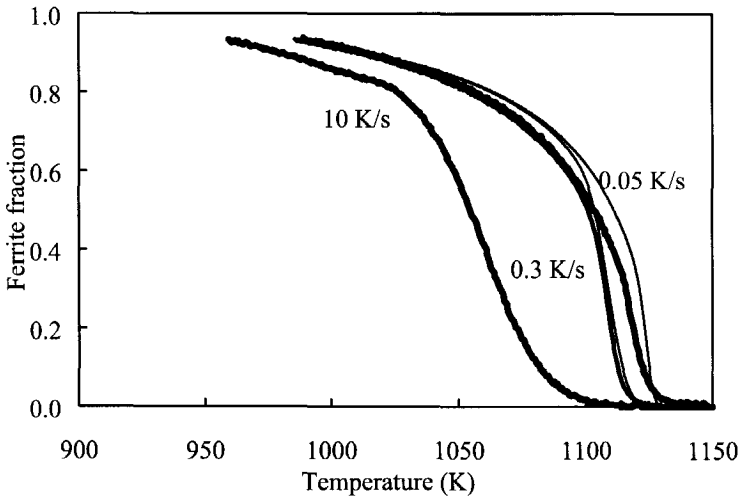|	0.05 K/s	0.3 K/s	10 K/s	60 K/s
alloy A	0.03	0.04	0.09	0.28
alloy B	0.03	0.04	0.09	–
alloy C	0.03	0.06	0.18	–

(a)

(b)

(c)
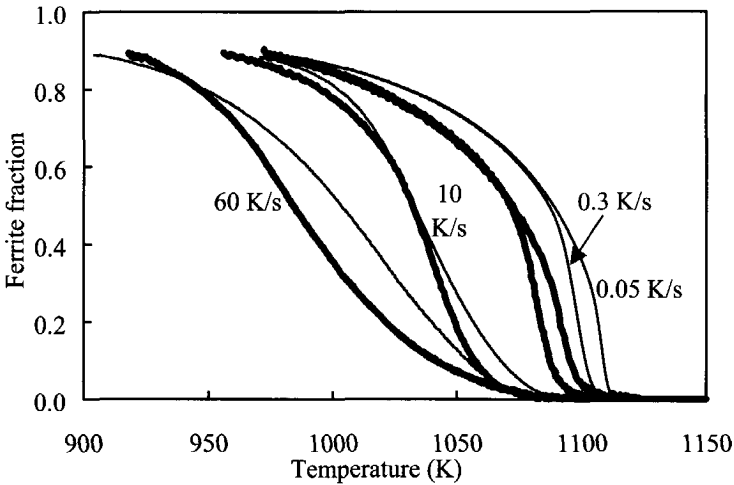
Figure 6.5   Experimentally   determined   (thick   lines)   and   simulated   (thin   lines) transformation curves at cooling rates of 0.05, 0.3, 10 and 60 K/s for steel grade a) A, b) B, and c) C.

The shape of the model transformation curves for all cooling rates corresponds well to the experimental fraction curves. In general, for all three alloys the correspondence between

model and experiment is remarkable. All three alloys show the coincidence of the fraction curves for the two lowest cooling rates used, both in the experimental and in the model curves. It is seen, however, that the equilibrium fraction ferrite in the model curves is shifted towards higher values compared with the measured fraction. This difference is largest for alloy A (relatively high carbon and manganese concentrations) and smallest for alloy C (low carbon and manganese concentrations). For higher ferrite fractions the experimental and modelled fraction curves seem to approach each other. However on a temperature scale the difference between the modelled and the experimental fractions remains the same. The reason for this temperature shift between the experimental determined and calculated absolute ferrite fraction is unclear. Figure 6.6 shows the calculated driving force for the transformation in alloy A at the four different cooling rates. It is seen that the driving force strongly increases with increasing cooling rate, due to an increased lagging of the ferrite fraction with respect to the equilibrium fraction. At the two lowest cooling rates, after an early maximum in the driving force, the transformation proceeds according to equilibrium, and the driving force levels off to a small value that is related to the time step in the simulations.

A relative comparison between the three alloys shows the highest transformation start temperatures for steel grade C. This occurs both for the experimental and the calculated fraction curves. Furthermore it is seen that for the higher cooling rates the correspondence between the experimental and calculated fraction curves for the carbon and manganese rich steel grade is less accurate. This is possible due to the fact that in the calculations nucleation is assumed to take place instantaneously at the Ae_3-temperature. Since manganese is known to retard the nucleation kinetics, this assumption is expected to become less adequate for the steel grades in the order A, B, C.

Considering the M_0-values (table 6.3) two trends can be observed: the value of M_0 increases with increasing cooling rate and with decreasing carbon content. These trends should be considered in view of the fact that M_0 is used as the only parameter to optimise the agreement between model and experimental curves; consequently, all factors influencing the overall transformation kinetics, but which have been disregarded in the model, will influence its value. The three main factors, *viz.* the diffusivity of carbon, the build–up of stresses at the α/γ–interface, and the differences between the actual nucleus density and the density derived from the microstructures, will now be discussed.
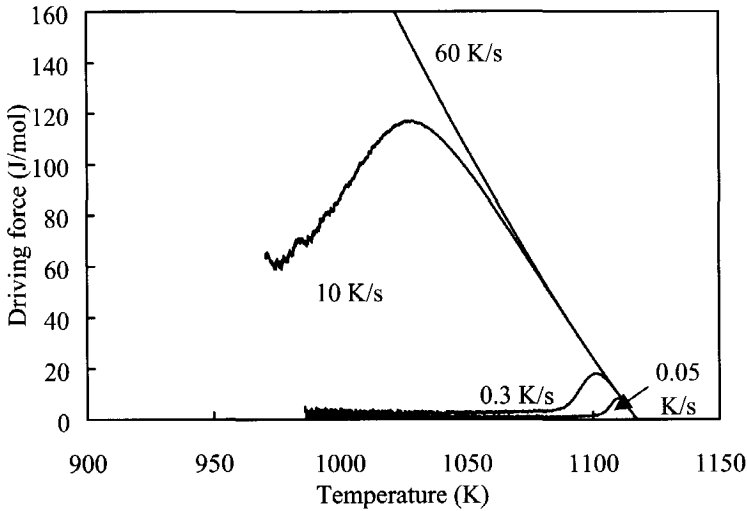
Figure 6.6   The calculated driving forces corresponding to the model curves for alloy A in figure 6.5a.

For the model assumption that the carbon is homogeneously distributed in the austenite to be valid at each moment in time, it is required that the carbon diffusion is infinitely fast compared with the γ/α–interface mobility. If the finite carbon diffusion plays a role in the determination of the γ/α–interface velocity, it causes a carbon pile–up in the austenite in front of the transforming interface, leading to a lower driving force. This implies a slower transformation, and in the calculations a slower transformation is described by a lower M_0–value. A carbon pile–up at the interface is more likely to occur at higher cooling rates, since there will be less time for carbon to diffuse into the bulk, and with higher initial carbon concentrations, since the carbon concentration gradient will be less pronounced.

Ferrite has a larger specific volume than austenite, therefore during the transformation the material expands. This will occur via stresses surrounding the ferrite grains, which effectively corresponds to a lower driving force for the transformation, and thus causes a slower transformation. The effect of stress build–up at the interface is expected to increase with increasing cooling rate, since there is less time for recovery of the stress, and with increasing alloying content, since alloying elements slow down the recovery process.

Considering the nucleus density the following remarks can be made. The more nuclei are present, the faster the transformation will proceed. If, due to grain coarsening, the nucleus

93

density derived by the present method (relating the α– and γ–microstructures) is too low, a too high velocity is attributed to the interface, since in the calculations the same overall transformation kinetics is to be achieved by a smaller number of ferrite grains. Grain coarsening is expected to be enhanced when more nuclei are formed, *i.e.* at higher cooling rates and lower alloying contents.

It is shown in the present study that the austenite to ferrite transformation is well described by the transformation model, in which the most important parameters, such as the austenite grain geometry, the nucleus density, and the driving force, based on chemical composition and temperature, are incorporated. An evaluation of the mobility of the interface with respect to cooling rate and carbon content indicates the grain coarsening to play a significant role in the transformation kinetics. This is derived from the increase of M_0 with increasing cooling rate and decreasing carbon concentration, a tendency that is expected from an increasing underestimation of the nucleus density, as discussed above. The effects of finite carbon diffusion and transformation stresses would lead to an opposite tendency.

6.5. Conclusions

An austenite to ferrite transformation model based on the concept of interface mobility has been tested for three commercial steel grades at cooling rates between 0.05 and 60 K/s. The model satisfactorily predicts the transformation rate at all cooling rates, including the ranges in which the transformation follows the equilibrium. For an optimal description of the fraction ferrite as a function of temperature for this series of experiments, a slight variation in M_0–values is used. The increasing tendency of M_0 with increasing cooling rate and decreasing carbon content appears to be caused by an underestimation of the nucleus density due to grain coarsening.

References

1   J.W. Johnson, R.F. Mehl: *Trans. A.I.M.E.*, 135 (1939) 416.
2   M. Avrami: *J. Chem. Phys.*, 7 (1939) 1103, 8 (1940) 212, 9 (1941) 177.
3   C. Zener: *J. Appl. Phys.*, 20 (1949) 950.

4   J.W. Christian: The Theory of Transformations in Metals and Alloys, 2nd edition (Pergamon Press, Oxford, 1981), 476.

5   G.P. Krielaart, J. Sietsma, S. van der Zwaag: *Mater. Sci. Eng.*, A237 (1997) 216.

6   Y. van Leeuwen, S.I. Vooijs, J. Sietsma, S. van der Zwaag: *Metall. Mater. Trans.*, 29A (1998) 2925.

7   S.I. Vooijs, Y. van Leeuwen, J. Sietsma, S. van der Zwaag: *Metall. Mat. Trans.*, 31A (2000) 379.
        J.J. Wits, T.A. Kop, Y. van Leeuwen, J. Sietsma, S. van der Zwaag: *Mat. Sci. Eng. A.*, A283 (2000) 234.

8   M. Enomoto, H.I. Aaronson: *Metall. Trans.*, 17A (1986) 1381, 1385, 1399.

9   R. Priestner, P.D. Hodgson: *Mat. Sci. Techn.*, 8 (1992) 849.

10   R. Bengochea, B. Lopez, I. Gutierrez: *Metal. Mat. Trans.*, 29A (1998) 417.

11   P.D. Hodgson, R.M. Trail, R.K. Gibbs, J.Grace, C.H.J. Davies: 2nd International conference on Modelling of Metal Rolling Processes, London 9–11 December 1996, eds. J.H. Beynon, P. Ingham, H. Teichert, K. Waterson (The Institute of Materials, 1996) 345.

12   M. Hillert: *Metall. Trans.*, 6A (1975) 5.

13   G.P. Krielaart, S. van der Zwaag: *Mater. Sci. Techn.*, 14 (1998) 10.

14   W. Huang, M. Hillert: *Metall. and Mater. Trans.*, 27A (1996) 480.

15   Ch. Zurek, E. Sachova, H.P. Hougardy: Abschlussbericht Project COSMOS (Max–Planck–Institut für Eisenforschung GmbH, Düsseldorf, Germany, 1993).

16   T.A. Kop, J. Sietsma, S. van der Zwaag: Dilatometric Analysis of Phase Transformations in Hypo–eutectoid Steels, to appear in *J. Mat. Sci.* (2000).
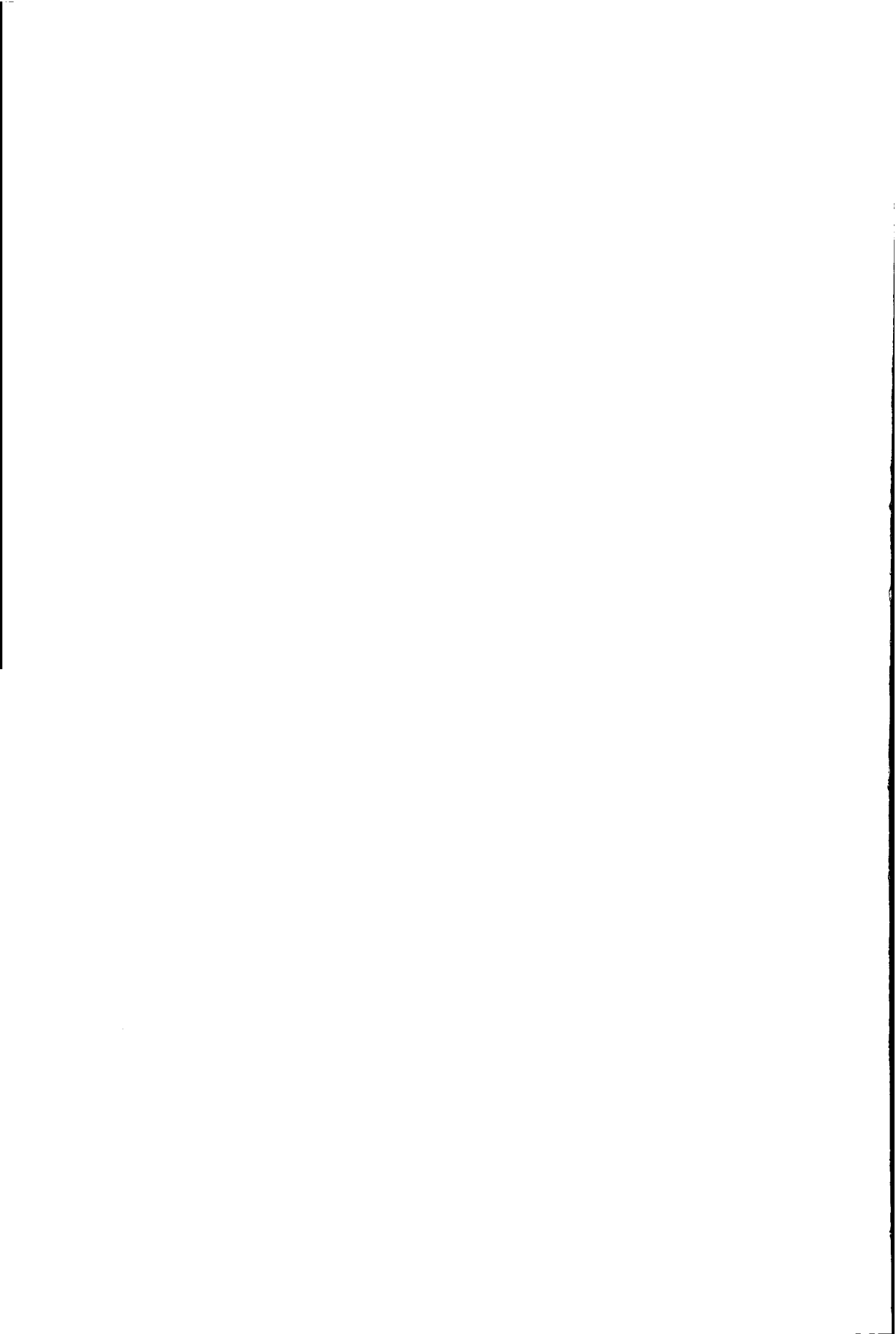
7

Some observations on the effect of austenitisation conditions on the transformation kinetics in an HSLA steel and related C–Mn steels

The dependence of the transformation kinetics of an HSLA steel and related C–Mn steels on the austenitisation conditions have been investigated using calorimetry and dilatometry. It is observed that the ferrite–start temperature depends both on the manganese content and on the amount of niobium in solution. Calculations of the transformation kinetics based on an interface–mobility model applied in a tetrakaidecahedron austenite–grain geometry are used to investigate the background of the observed changes in transformation kinetics.

7.1. Introduction

Transformation kinetics in modern construction steels are rather complex. The austenite to ferrite phase transformation depends on the chemical composition of the steel, on the austenite microstructure before transformation and on the applied cooling rate. The microstructure that results after transformation depends on the combined effect of the above–mentioned factors.

The effects of chemical composition are threefold. Carbon, the main interstitial alloying element, will pile up at the migrating austenite/ferrite interface due to the limited carbon solubility in ferrite, thereby reducing the local driving force for transformation. Substitutional elements like manganese and silicon also have a strong effect on the transformation kinetics. High concentrations of substitutional elements give rise to deeper undercooling, thereby giving rise to the formation of Widmanstätten ferrite and bainite rather than allotriomorphic ferrite. Some alloying elements form precipitates at austenitisation temperatures. These precipitates can inhibit grain growth, thereby causing a reduced austenite grain size.

The starting microstructure for the transformation, which is characterised by the austenite grain size and the amount of alloying elements either in solute solution or in precipitated form, depends on the preceeding time–temperature path. It is well known that there is a relation between the reheat temperature and the austenite grain size. In the case of HSLA steels the time–temperature path also determines the amount and size of the precipitates [1–2]. High temperature plastic deformation has a large influence on both the austenite grain size and the amount and spatial distribution of precipitates [3–4].

The microstructure obtained when cooling down the austenite depends on the cooling rate. At low cooling rates there will be enough time for the formation of allotriomorphic ferrite. In this regime the chemistry of the system has a distinct influence on the nucleation and growth behaviour. At higher cooling rates there will be less time for the formation of allotriomorphic ferrite, and a transition to Widmanstätten ferrite formation will occur [5]. After ferrite formation there will be pearlite or bainite/martensite formation.

From the above it is clear that in an HSLA steel the chemistry and the austenite grain size are highly coupled. There are not many papers in the literature which actually study the growth kinetics of ferrite quantitatively and try to separate the influence of solute or precipitated niobium on nucleation or growth kinetics [6–8]. In the paper by Cochrane and Morrison [6] it is argued that precipitation before transformation accelerates the allotriomorphic ferrite formation. Thomas and Michal [7] have found a decrease in the

ferrite–start temperature for niobium contents less than 0.04 wt.%, and an increasing ferrite–start temperature for higher niobium concentrations. Lee *et al.* [8] model and discuss the growth kinetics on the basis of the classical nucleation and diffusional growth theories. It is concluded that the solute niobium slows down the ferrite–start temperature and that solute and precipitated niobium have the same effect on the progress of the ferrite formation.

In the work presented here a comparison between the transformation kinetics of a niobium containing steel and similar C–Mn steel grades without niobium is effectuated. Furthermore, several series of experiments on the niobium containing steel are performed to separate the effects of precipitated niobium and niobium in solution. Experiments to determine the transformation kinetics are performed using both Differential Thermal Analysis (DTA) and dilatometry, while microstructural data is obtained using optical microscopy and Transmission Electron Microscopy (TEM).

An analysis of the transformation kinetics is performed in terms of an interface mobility model which incorporates microstructural features such as austenite grain size and nucleation site density [9].

7.2. Theory

A key property for the effect of niobium on the formation of both the austenite and the ferrite microstructure is the solubility product of niobium–(nitro)carbide [10]. In the present study we will concentrate on NbC as the precipitating phase. The solubility product k for NbC is defined by

$$k = [\text{Nb}][\text{C}], \tag{7.1}$$

in which [A] denotes the concentration of element A in solution in the iron lattice. Most commonly, [A] is expressed in weight percentages. The solubility product has an Arrhenius–like temperature dependence, which is expressed by the equation

$$k = k_0 \exp\left(-\frac{Q_S}{RT}\right), \tag{7.2}$$

with k_0 denoting a pre–exponential factor, Q_S an activation energy, R the gas constant and T the temperature. From equation (7.1) and the total amount of niobium in the alloy the weight percentage of Nb present as NbC–precipitate, c_{NbC}, can be readily derived.
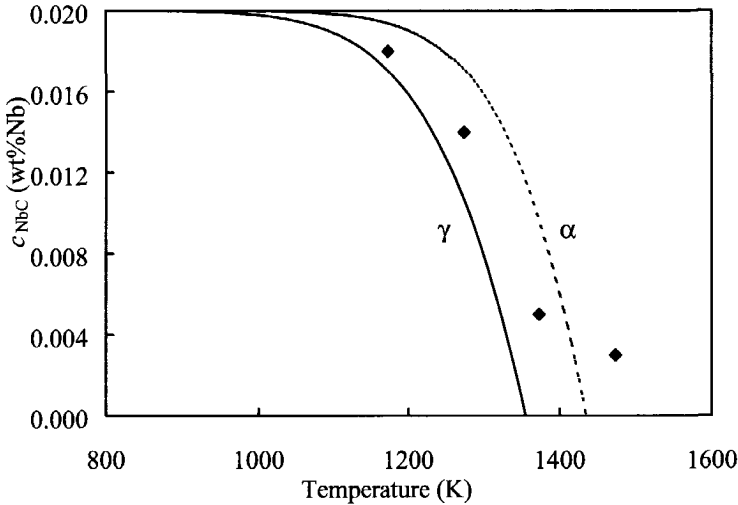

Figure 7.1   Equilibrium concentration of niobium–carbide precipitates in austenite (γ) and ferrite (α) as a function of temperature. The symbols denote the experimentally determined values.

Several sets of the parameters k_0 and Q_S for NbC in ferrite and in austenite have been proposed in the literature, as summarised recently by Gladman [11]. Whereas the actual values for k_0 and for Q_S show considerable differences, the resulting values for k as a function of T show that the variation in k in the austenite temperature range (1000 K < T < 1300 K) is limited to ± 30%. For ferrite (800 K < T < 1200 K) the differences increase up to ± 60%. In this work we will adopt the values $k_0 = 1380$ (wt.%)^2 and $Q_S = 148$ kJ/mol for the austenite phase, which were derived from the SGTE thermodynamic database. The parameters for the solubility product of NbC in ferrite have the values $k_0 = 31600$ (wt.%)^2 and $Q_S = 194$ kJ/mol. For the HSLA steel grade used in this work it follows that for T > 1350 K all niobium dissolves in the austenite phase (figure 7.1). In the ferrite phase the solubility is less than in the austenite phase. At temperatures at which ferrite is stable the formation of niobium carbide precipitates is thermodynamically favourable.

There are several models available to describe the austenite to ferrite phase transformation. In the work presented here the aim is to obtain a better understanding of the physical processes occurring during –and thereby governing– the austenite to ferrite phase transformation. Therefore a model based on physical grounds is used. A first quantity to consider in the model is the size and the shape of the austenite grain. The austenite grains have irregular three–dimensional shapes, corresponding with a Voronoi tesselation, which on average contain approximately 15 faces. Van Leeuwen *et al.* [9] describe a model which is based on a tetrakeidecahedron, which can be regarded as an average austenite grain shape. In this geometry, nucleation can be simulated to take place at specific sites, for instance the austenite grain corners, from which the nuclei grow spherically into the austenite grain. The fraction ferrite as a function of time is determined by numerical integration.

In order to simulate the growth of the ferrite grains, the interface mobility model as described by Krielaart *et al.* [12], after Christian [13], is used. The interface velocity v is given by the product of the interface mobility M and the driving force for transformation, $\Delta G^{\gamma/\alpha}$, according to

$$ v = M \cdot \Delta G^{\gamma/\alpha} = M_0 \exp\left(\frac{-Q}{RT}\right) \cdot \Delta G^{\gamma/\alpha} , \tag{7.3} $$

where M_0 is a pre–exponential factor, Q the activation energy for movement of the atoms in the boundary region, and $\Delta G^{\gamma/\alpha}$ is the difference in Gibbs free energy between the austenite and the ferrite. In this work we will adopt this definition of interface velocity. The driving force can be calculated using a thermodynamic database, which takes into effect the contributions of manganese and carbon. The manganese is assumed to be homogeneously distributed throughout the material. Furthermore it is assumed that the carbon redistributes during the austenite to ferrite transformation, and that the carbon is distributed homogeneously throughout the austenite phase. The total amount of niobium present in the system is too small to have a noticeable influence on the phase diagram and the resulting driving force. The principal influence of the chemical composition is thus incorporated.

If precipitates are present, they can influence the transformation kinetics, for instance by exerting a pinning force on the austenite/ferrite interface, effectively reducing M_0. According to the classical Zener approach [14] the Zener drag or Zener retardation

pressure P_z, experienced by a moving interface and caused by a distribution of precipitates, is given by

$$P_z = \frac{3}{4} \cdot \beta \cdot \frac{f \cdot \gamma}{r}, \tag{7.4}$$

where β is a correction factor, γ is the interfacial energy, f the volume fraction of precipitates and r the size of the precipitates. Spherical incoherent precipitates were assumed and the problem is treated only geometrically. In this case β equals 1. In later studies the correction factor β was introduced [15]. This factor can vary between 0.1 and 2.3, depending on the geometry of the precipitates and the shape of the deforming grain boundary.

The parameters describing the interface mobility, M_0 and Q, are mathematically strongly dependent when equation (7.3) is fitted to experimental data on the kinetics of the phase transformation. The approach adopted in this study is to keep the activation energy at a fixed value and to vary the pre–exponential factor to optimise the agreement between experimental and modelled fraction curves. For the activation energy a value of 140 kJ/mol is used. This value corresponds to the activation energy for austenite recrystallisation [16] and to the value used by Krielaart and Van der Zwaag for the austenite to ferrite transformation in binary Fe–Mn alloys [12]. Factors that do influence the transformation kinetics but have not been incorporated in the model will affect the value of the pre–exponential factor, M_0.

In the calculations it is assumed that nucleation takes place instantaneously at a certain temperature during cooling from the austenitisation temperature. The undercooling, ΔT, is defined as the difference between this temperature and the Ae_3–temperature. The undercooling, which is a measure for the delay in nucleation, is also varied to optimise the correspondence between calculated and measured data.

7.3. Experimental

The compositions of the steel grades used in this investigation are given in table 7.1. Grade Mn12Nb is the HSLA steel, and contains a small amount of niobium, 0.02 wt.%, and furthermore as main alloying elements 1.20 wt.% manganese and 0.136 wt.% carbon. The

other grades do not contain niobium, but differ in manganese, carbon and silicon concentration. The grades are coded according to the manganese content. The compositions lead to a variation in the equilibrium fractions as a function of temperature, as can been seen in figure 7.2.

Table 7.1   Chemical composition of alloys in wt%.

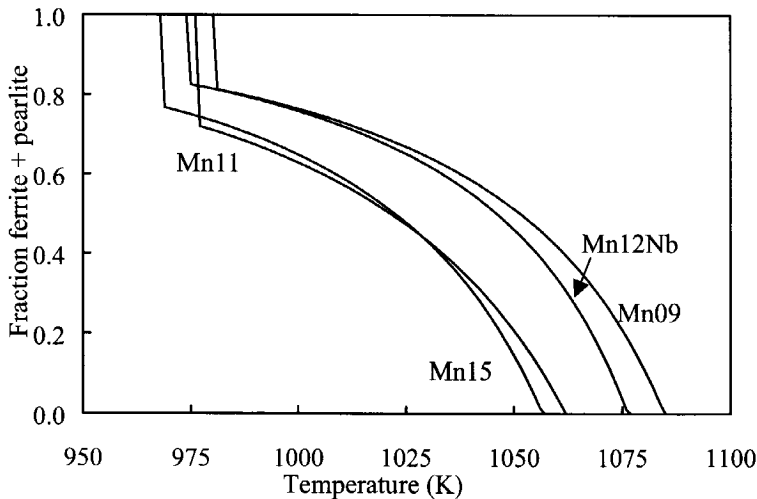| Alloy	C (at.%)	Mn	Si	Nb	Al	Cr	Ni	N	P
Mn12Nb	0.136 (0.63)	1.20	0.017	0.020	0.053	0.025	0.027	0.0036	0.016
Mn09	0.147 (0.68)	0.93	0.009	0.002	0.043	0.027	0.026		0.011
Mn11	0.210 (0.98)	1.10	0.320	<0.005	0.028	<0.02	0.020	0.0077	0.011
Mn15	0.173 (0.80)	1.46	0.178	–	0.031	–	0.026	0.0064	–

Figure 7.2   Equilibrium ferrite plus pearlite fraction as a function of temperature for the steel grades presented in table 7.1.

In this figure the total fraction of ferrite plus pearlite for the different steel grades is shown as a function of temperature in the ferrite/austenite region. The fractions are calculated using the thermodynamic database program MTData assuming para–equilibrium and taking into account contributions of manganese, silicon and carbon. The relatively low Ae_3–temperature of the Mn11 alloy is caused by the relatively high carbon concentration.

For the quantitative analysis of the fractions solute and precipitated niobium as a function of the austenitisation temperature, samples were electrochemically brought into solution using an EDTA solution. In this process the precipitates do not dissolve. The electrolyte is filtered using a filter with a 100 nm pore size. The residue is mixed with Na_2SO_4. This mixture is melted and dissolved in a solution of sulphuric and oxalic acid. The niobium concentration of this solution as well as the niobium concentration in the electrolyte are determined using a Perkin Elmer Inductive Coupled Plasma – Optical Emission Spectrometer (ICP–OES).

To obtain data on the transformation kinetics, dilatometry experiments were performed using a Bähr 805A/D dilatometer. Cylindrical samples of 4.0 mm diameter and 10.0 mm length were clamped between quartz push–rods. The samples were heated by induction and the temperature was registered by S–type thermocouples. The temperature gradients along the length of the samples remained within 10 K. Cooling rates were controlled to be constant over the entire transformation range. For the higher cooling rates an N_2–flow was used. The dilatation data was analysed using a method that accounts for the difference in specific volume between ferrite and cementite [17]. Three series of experiments were performed. The first series was performed at different austenitisation temperatures, ranging from 1173 K to 1423 K, in order to determine the dependence of the austenite grain size and the subsequent transformation kinetics on the austenitisation temperature. The samples were heated at a rate of 50 K/min, held for 20 minutes at the austenitisation temperature, and cooled at 20 K/min. To investigate the influence of different austenitisation times, a second series of experiments was performed, consisting of heating at 5 K/s to 1423 K, an isothermal hold for 5, 20 or 40 minutes and subsequent cooling at 20 K/min. Finally, two different types of two–step annealing experiments were made. The samples were first annealed at 1423 K to dissolve the niobium–carbide precipitates, and the second anneal was performed at a temperature below the precipitation start temperature (1350 K) to allow for re–precipitation of the niobium carbide. Analogous experiments were performed without the second anneal, yielding samples with the same austenite grain size, but a different amount of niobium in solution. The first type of the two–step annealing experiments –heat treatment A– consisted of heating at a rate of 50 K/min, annealing for

20 minutes, cooling at 20 K/min to 1273 K, holding for 0 or 30 minutes and subsequent cooling at 20 K/min. The other heat treatment –heat treatment B– consisted of heating at 5 K/s, annealing for 40 minutes, cooling at 10 K/s to 1033 K, holding for 0, 30 or 60 minutes and subsequent cooling at 20 K/min.

The experiments with varying austenitisation temperature as well as one of the two–step annealing experiments were also performed on a Perkin–Elmer DTA–7 apparatus. Discs with a diameter of 3.0 mm and a height of 2 mm were used. Special care was taken to prevent decarburisation by using a purified N_2–gas flow through the sample chamber.

Microstructural data was obtained using optical microscopy. 2% nital was used to reveal the ferritic/pearlitic microstructures. The prior austenite grain boundaries were revealed using both a thermal etching technique and a technique based on the partial transformation of the sample. The grain sizes were determined using the mean linear intercept method.

The TEM foils were prepared by mechanical grinding, electropolishing and ion–milling. A Philips CM30 TEM was used to detect niobium–carbide precipitates. Both bright and dark field techniques were applied.

7.4. Results and discussion

7.4.1. Experimental

Figure 7.1 shows c_{NbC} in the austenite and in the ferrite phase as a function of temperature, calculated from the solubility products for the HSLA–steel investigated in this study. The fraction precipitated niobium after austenitisation at the indicated temperatures (followed by a quench to room temperature) as found by the chemical analysis is depicted as well. The measured fractions correspond well with the calculated results, although the experimental concentrations are slightly higher than the theoretical values. The theoretical values describe the equilibrium case. The experimentally observed concentrations however, are influenced by the kinetics of the dissolution of the niobium carbides. It can be seen that above 1350 K most niobium is dissolved in the austenite phase. At this temperature a bimodal austenite grain size distribution is observed in optical microscopy. This bimodal austenite grain size distribution is due to the transition of grain growth inhibited by pinning by the precipitates to normal grain growth after the dissolution of the precipitates, as is described in [18]. For the steel grades without niobium no bimodal austenite grain size distribution is found. Combining figures 7.1 and 7.2 it can been seen

that according to equilibrium predictions all niobium should be precipitated before the austenite to ferrite transformation starts, since the Ae_3–temperature for Mn12Nb is 1078 K.
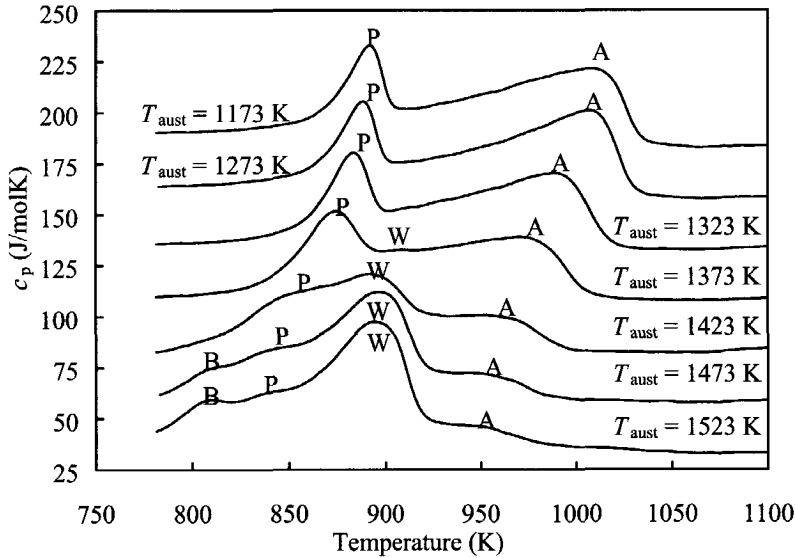

Figure 7.3   The measured specific heat curves (plus a multiple of 25 J/molK) during cooling at 0.3 K/s for austenitising Mn12Nb at different temperatures as measured with the DTA. The labels A, W, P, and B correspond to the formation of allotriomorphic ferrite, Widmanstätten ferrite, pearlite and bainite respectively.

Figures 7.3 and 7.4 show the effect of the austenitisation temperature on the transformation kinetics as observed by DTA and dilatometry. Figure 7.3 shows the DTA measurements and figure 7.4 shows the measured dilatation and the resulting fraction development during the transformation for alloy Mn12Nb. The DTA measures the specific heat and the transformation enthalpies. Therefore the sensitivity for the ferrite formation becomes larger at lower temperatures. The sensitivity for the pearlitic reaction is even larger, caused by the formation of the covalent cementite structure. The height of a peak is a measure for the average rate of the transformation, df/dT [19]. In figure 7.3 a multiple of 25 J/molK is added to each measured heat curve in order to clarify the relative changes between the curves belonging to different austenitisation temperatures.
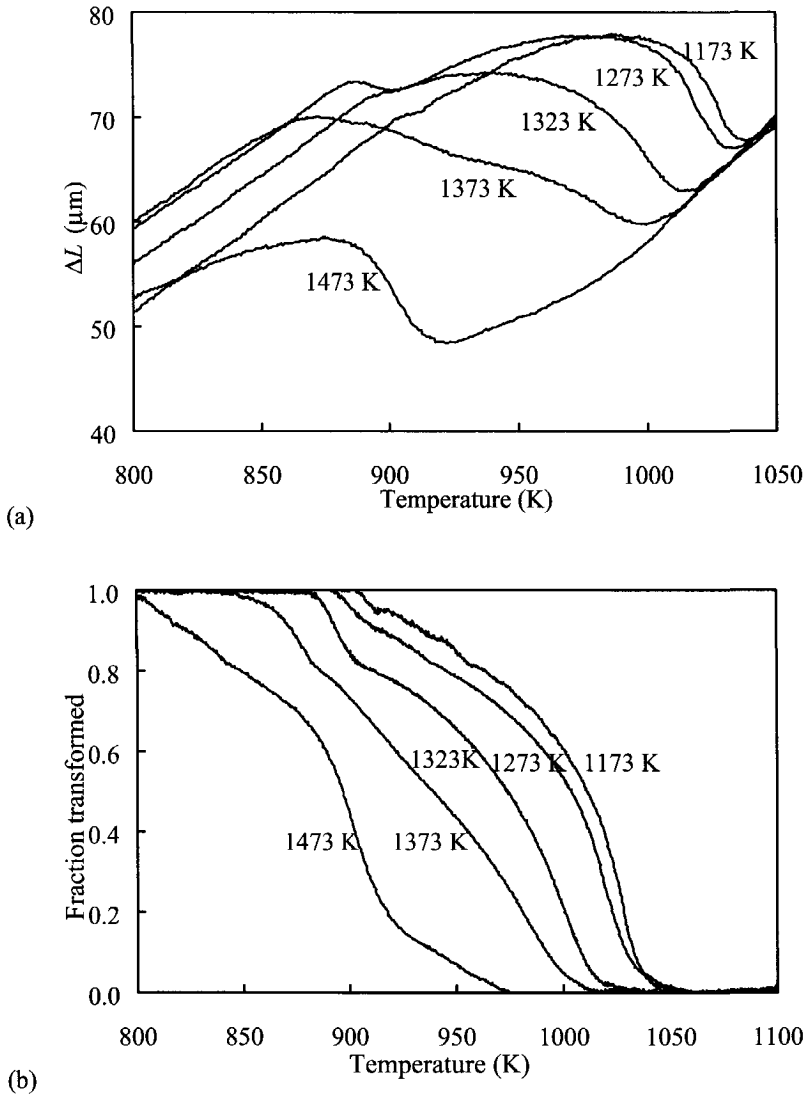
Figure 7.4   *a) The dilatation curves, and b) the fractions transformed of Mn12Nb during cooling at 0.3 K/s after austenitisation at different temperatures. The austenitisation temperature is indicated.*

In the DTA signal corresponding to the lowest austenitisation temperature, 1173 K, two peaks, labelled A and P, are observed. It is seen that the allotriomorphic ferrite formation

(peak A) starts at 1050 K. The second peak, corresponding with the pearlite formation starts at 905 K (peak P). The heat effect measured after the highest austenitisation temperature indicates four different processes. The peak corresponding to the allotriomorphic ferrite formation is still present, shifted towards lower temperatures and smaller with respect to the A–peak after the lowest austenitisation temperature. The largest peak in this curve, peak W, starting at 925 K, corresponds to the formation of Widmanstätten ferrite. This peak partly overlaps with the peak corresponding to the pearlite formation. The peak at 810 K, labelled B, corresponds to bainite formation. The peak labelling was applied on the basis of microstructural analysis of the fully transformed samples. Figure 7.3 shows that increasing the austenitisation temperature shifts the ferrite start temperature towards lower temperatures. Furthermore, it is seen that at higher austenitisation temperatures the formation of Widmanstätten ferrite becomes favourable due to the fact that less allotriomorphic ferrite is formed. The appearance of the Widmanstätten phase coincides with the niobium–carbide precipitates being dissolved (*i.e.* above 1350 K).

The dilatation signal (figure 7.4a) can be used to obtain data concerning the phase fractions, since the phase transformation results in volume changes. The volume change corresponding to the austenite to ferrite transformation depends on the carbon concentration of the austenite, and since the volume change corresponding to the austenite to pearlite transformation is normally less than the volume change of the austenite to ferrite transformation, the pearlite formation is less clearly observable. Nevertheless the dilatation signal shows the same features as the DTA results. Figure 7.4a gives the measured change in length. The dilatation curves are shifted along the ΔL–axis such that they coincide in the austenite region and highlight the shift in transformation start temperature. The absolute length change is difficult to measure accurately and depends on the sample preparation (chapter 3). Figure 7.4b shows the fraction curves obtained from the dilatation measurements. For the specimen austenitised at 1173 K both allotriomorphic ferrite and pearlite formation are detectable in the dilatation signal. The specimen austenitised at 1473 K shows some allotriomorphic ferrite formation before a transition to Widmanstätten ferrite occurs. Note that the formation of Widmanstätten ferrite, which was visible as a peak in the DTA–signal, shows as an increase of the length–change rate in dilatometry. In this sample both pearlite and bainite are formed. In the dilatation signal however it is not possible to distinguish the pearlite from the bainite formation.
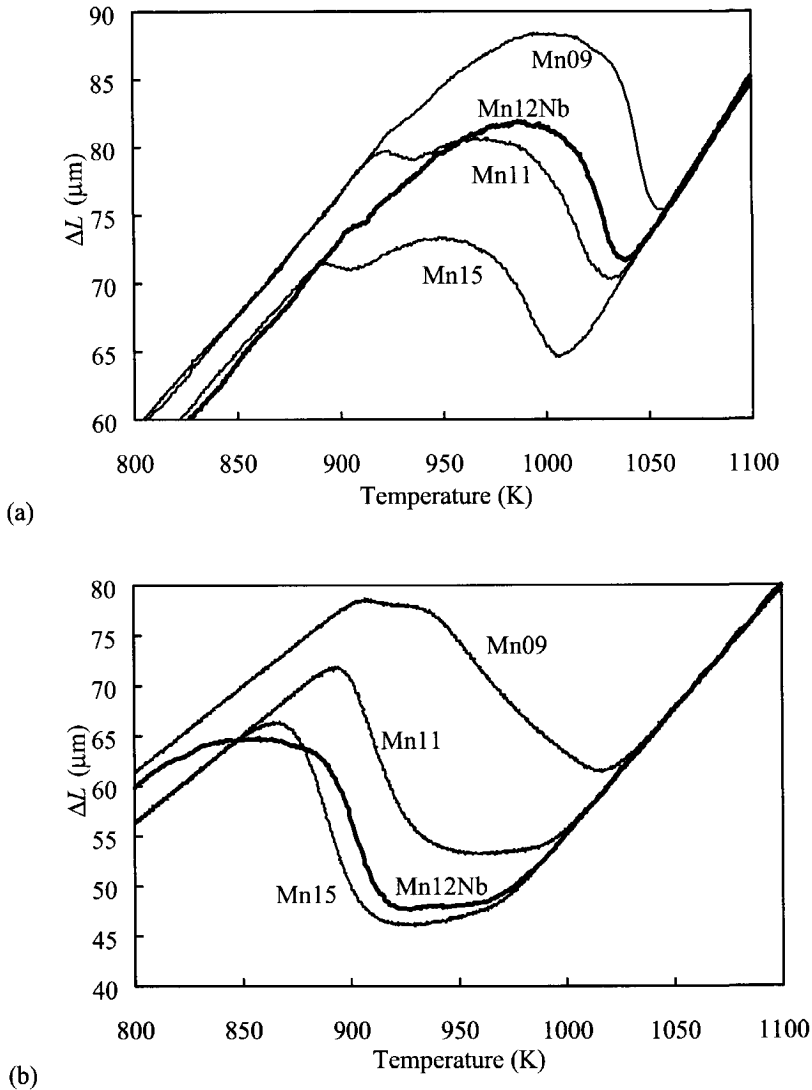
(a)

(b)

Figure 7.5   Dilatation curves for the four steel grades investigated after austenitisation a) at 1173 K, and b) at 1423 K.

Figure 7.5a shows the dilatation curves of the steel grades investigated, all austenitised at 1173 K and subsequently cooled at a rate of 0.3 K/s. They indicate that the average transformation rate of the steel grades is approximately the same. The transformation

products are allotriomorphic ferrite and pearlite. Comparing the dilatation curves with the equilibrium fraction curves of figure 7.2, it is seen that the Mn15 alloy has the largest undercooling. This indicates that the retarding influence of manganese is larger than the influence of the carbon. Figure 7.5b shows the dilatation curves after austenitisation at 1423 K. The transformation behaviour of Mn09 is quite similar as before. There is a rapid formation of allotriomorphic ferrite followed by the formation of pearlite. The other three alloys, however, show a slower formation of ferrite and a transition to the formation of Widmanstätten ferrite. The shift in ferrite–start temperature of Mn12Nb is quite large in comparison to the shift in ferrite–start temperature of Mn11 when the transformation kinetics after austenitisation at 1173 K and 1423 K are compared. Furthermore, there is a prominent retardation in the pearlite formation of the Mn12Nb alloy. Figure 7.6 summarises the above. The shift of the experimentally determined start temperature relative to the equilibrium A_3–temperature for the steel grades investigated is plotted against the austenitisation temperature. The dashed lines as well as the low temperature part of the Mn12Nb line are all parralel and are intended as a guide to the eye. For the non–niobium containing alloys there is a gradual dependence between the undercooling and the austenitisation temperature, whereas in the Mn12Nb alloy an additional retardation is observed for austenitisation above 1323 K.
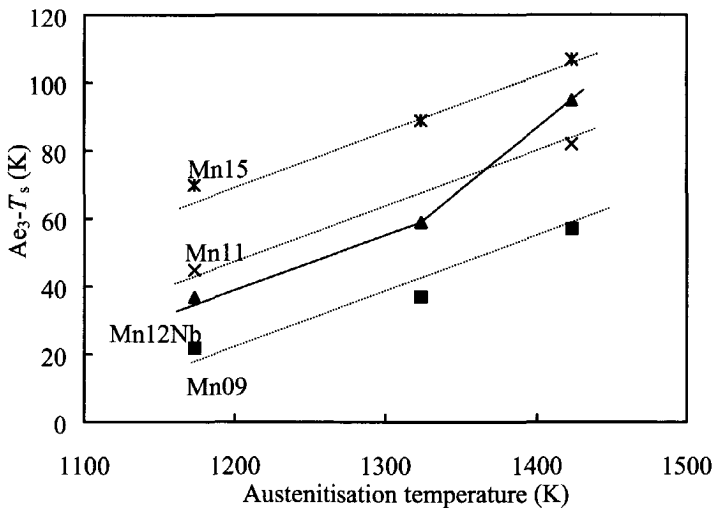

Figure 7.6   The shift of the experimental determined start temperature (T_s) relative to the equilibrium A_3–temperature vs. the austenitisation temperature for the steel grades investigated.
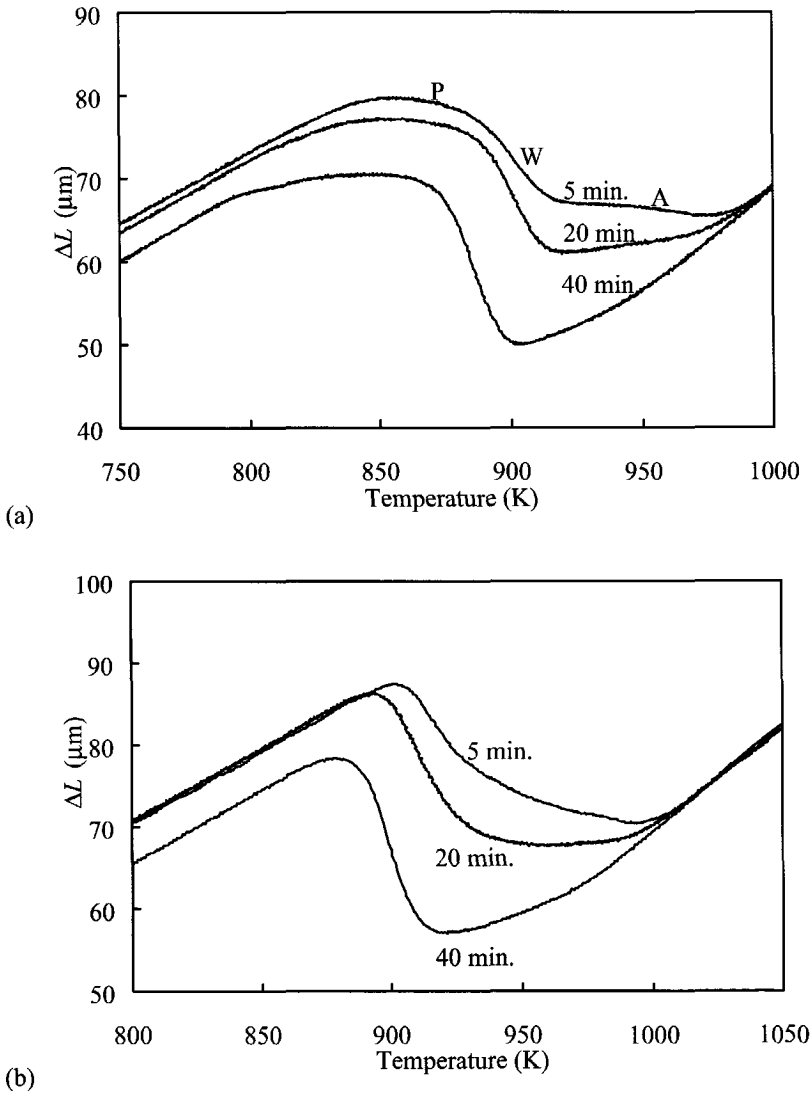
Figure 7.7   Dilatation curves resulting from different austenitisation times at 1423 K when a cooling rate of 0.3 K/s is applied for a) steel grade Mn12Nb, and b) steel grade Mn11.

The relation between the austenite grain size and the ferrite–start temperature is also observed when analysing the effect of the austenitisation time, as is seen in figure 7.7a for the Mn12Nb alloy and in figure 7.7b for Mn11. Both figures show a delay in the ferrite–start temperature. In table 7.2 the austenite grain sizes of Mn12Nb are given, and it is seen that longer austenitisation times indeed lead to an increase in austenite grain size. A further comparison of figures 7.7a and 7.7b shows that even after a short austenitisation time, the ferrite growth rate in the Mn12Nb steel is effectively reduced. Furthermore due to the slow pearlite formation in the Mn12Nb steel, the transition of Widmanstätten ferrite to pearlite formation is clearly visible for this grade. An increase in cooling rate also leads to an increased undercooling, as can be seen in figure 7.8. This however is not caused by the austenite grain size, but by the time available for nucleation. Another interesting feature in figure 7.8 is the transition from ferrite formation to Widmanstätten ferrite formation, which depends both on the transformation temperature and the amount of allotriomorphic ferrite formed.
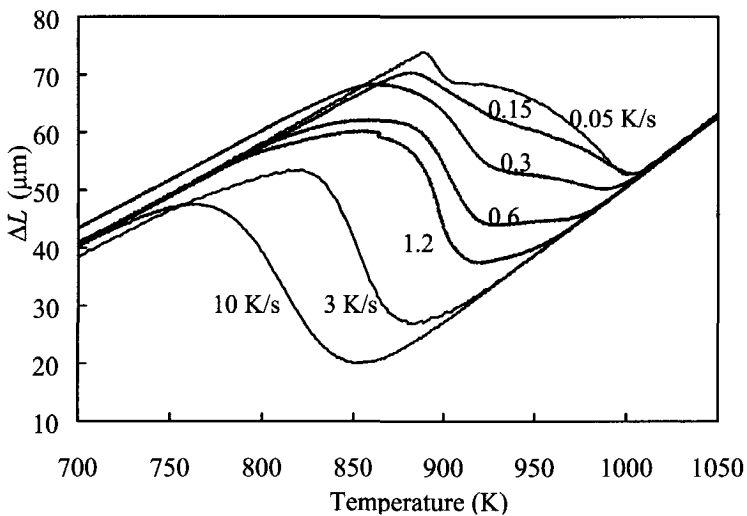

Figure 7.8   Dilatation curves for Mn12Nb for various cooling rates after austenitisation at 1423 K.
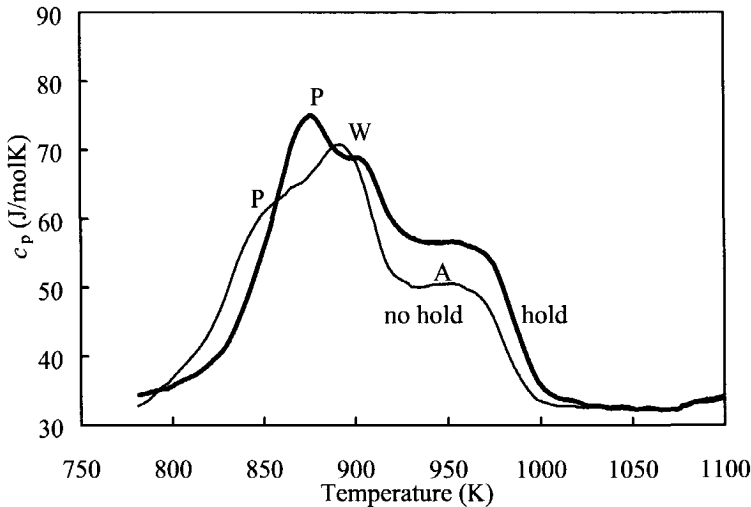
Figure 7.9   Specific heat curves for Mn12Nb. The peaks correspond to allotriomorphic ferrite, Widmanstätten ferrite and pearlite formation. Both curves correspond to samples austenitised at 1423 K. One sample was additionally held at 1273 K for 30 minutes before further cooling.

Figure 7.9 and 7.10 show the DTA and dilatation measurements of the two–step annealing experiments. The holding temperature was chosen at 1273 K, such that precipitation of the niobium in NbC, which had gone into solute solution during austenitisation at 1423 K, is thermodynamically favourable. In order to determine the influence of the niobium, in figure 7.10 the fraction curves for Mn11 for identical heat treatments are also shown. For the Mn11 alloy there is no influence of the additional holding at 1273 K. This indicates that the austenite grain size does not change during the 1 hour hold. In the fraction curves corresponding to the niobium containing alloy there is a shift along the temperature axis; after the additional hold the ferrite–start temperature is increased. The amount of allotriomorphic ferrite formed is larger and the amount of Widmanstätten ferrite smaller. The specific heat curves show the same features. The shift in start temperature is less clearly visible, but the shift towards less Widmanstätten ferrite formation and thereby a reduced contribution to the heat effect of the Widmanstätten ferrite compared to the contribution of pearlite is clear. Figure 7.10 shows that the ferrite–start temperature after the additional hold is approximately 10 K higher than in the experiment without the intermediate hold. This corresponds to an undercooling of 85 K. Considering figure 7.6, it

113

can be concluded that the net effect of the niobium causes a retarding effect on the ferrite nucleation. The shift in start temperature is expected to be related to a change in the amounts of solute niobium and niobium carbides. Figure 7.11 shows the fractions transformed after holding at 1033K, near the Ar_3–temperature, for alloys Mn12Nb and Mn11. The difference in average growth rate of the allotriomorphic ferrite between the curves in figure 7.10 and 7.11 are due to the difference in austenite grain size, which is due to the variation in austenitisation time as was seen in figure 7.7. Apart from this difference the same observations are made as in figure 7.10: the additional hold for the Mn12Nb causes a reduction in undercooling while the second isotherm has no influence on the transformation kinetics of the Mn11 alloy.

The TEM was used to compare the precipitation characteristics of the austenitisation treatments at 1423 K with and without the additional hold at 1033 K. Neither heat treatment led to precipitation on prior austenite grain boundaries nor to precipitation at the γ/α–interface during transformation. The heat treatment without the additional hold resulted in a distribution of fine niobium–carbide precipitates. The heat treatment with the additional hold resulted, besides the fine precipitates, in numerous coarser particles. The coarseness of the precipitates indicates that they have been formed before the transformation occurred. Evidence of increased nucleation due to presence of the precipitates is not observed. The delay in transformation–start temperature after the austenitisation above the precipitation–start temperature is probably due to the niobium in solution.

7.4.2. Model

The model calculations focus on the behaviour of Mn12Nb. The results of the modelling are summarised in tables 7.2 to 7.4. Figure 7.10 shows an example of the model results. Both the undercooling, ΔT, and the pre–exponential factor, M_0, are varied, such that the modelled curves fit the part of the experimental fraction curves which corresponds to the allotriomorphic ferrite formation. The modelled curves are not smooth since a limited grit of 40×40×40 is used in the numerical model.
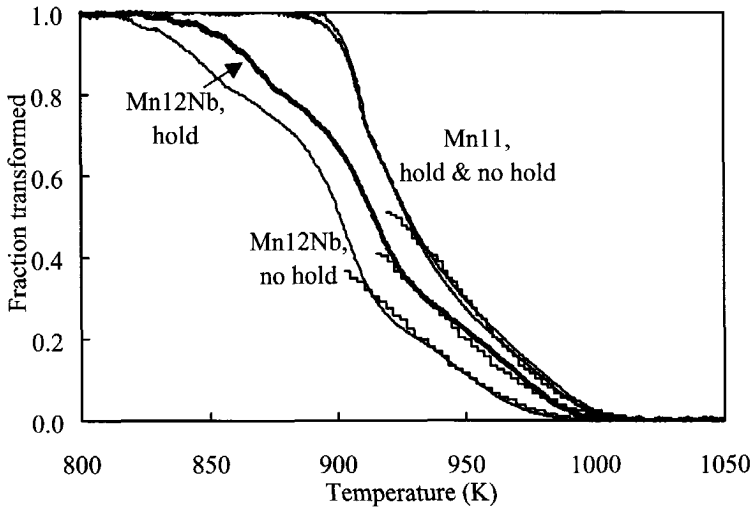
Figure 7.10 Fraction transformed for Mn12Nb and Mn11 after austenitising at 1423 K, with and without hold at 1273 K. The modelled allotriomorphic ferrite fractions are also given.
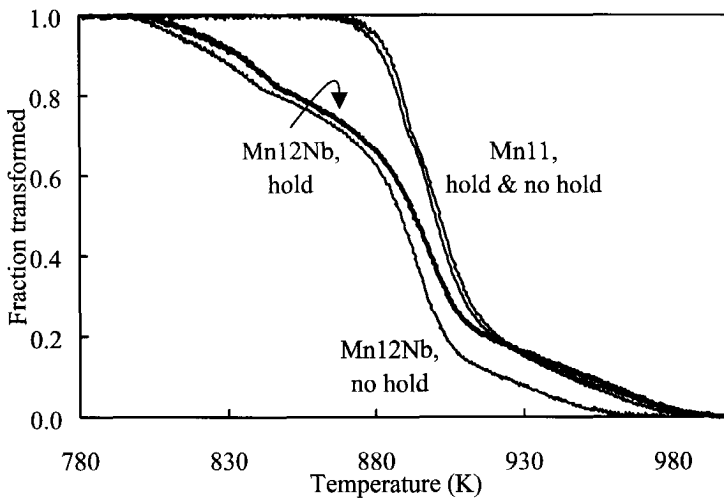

Figure 7.11 Fraction transformed for Mn12Nb and Mn11 after austenitising at 1423 K, with and without hold at 1033 K.

Table 7.2 M_0, ΔT and d_γ as a function of the austenitisation time at 1423 K for the Mn12Nb steel grade. The corresponding experimental dilatation curves are shown in figure 7.7a.

t_{aus} (min.)	M_0 (molmm/Js)	ΔT (K)	d_γ (μm)
5	18	60	193
20	22	70	245
40	30	100	309

Table 7.3 M_0 and ΔT as a function of the cooling rate after austenitisation at 1423 K for the Mn12Nb alloy. The corresponding experimental dilatation curves are shown in figure 7.8.

β (K/s)	M_0 (molmm/Js)	ΔT (K)
0.15	9	35
0.3	16	45
0.6	28	55
1.2	50	70

Table 7.2 shows both an increasing M_0 and ΔT with increasing austenitisation temperature. The increase in ΔT is caused by the lower density of heteregenous nucleation sites, due to the increase in d_γ. The increase in M_0, which corresponds with a higher interface velocity, might seem to contradict figure 7.7, where for the higher austenitisation temperature a lower df/dT was found. It should be noted however, that not only M_0, but also the nucleus density influences the overall df/dT. The nucleus density however is hard to determine accurately. In all calculations, the number of 24 nuclei per austenite grain, corresponding to all the corners of the tetrakaidecahedron, was used. As an example of the influence of this choice, a calculation for the experiment consisting of the 40 minutes austenitisation treatment, with more nuclei, *viz.* 40 per austenite grain, leads to $M_0 = 23$ molmm/Js when ΔT is kept at 100 K.

Table 7.3 shows both an increasing M_0 and ΔT with increasing cooling rate. In these experiments, the austenite grain size from which the allotriomorphic ferrite forms is the same for each cooling rate. The shift in undercooling can therefore not be attributed to the austenite grain size, and is most likely related to the time available for nucleation. The model calculations show a large cooling–rate dependence of the pre–exponential factor,

implying a change in interface mobility. The main reason for this trend in M_0 is the increasing nucleus density, due to the lower ferrite–start temperature.

Table 7.4 M_0 and ΔT resulting from the two–step annealing experiments A and B. The corresponding experimental fraction curves are shown in figures 7.10 and 7.11.

Alloy	Holding temperature (K) & time (min.)	M_0 (molmm/Js)	ΔT (K)
Mn12Nb	1033 / 60	20	50
	1033 / 30	21	60
	1033 / 0	23	80
	1273 / 30	18	40
	1273 / 0	19	60
Mn11	1273 / 0	33	16
	1273 / 30	33	16

The data in table 7.4 are interesting since the holding experiments provide a means to separate the direct effect of the niobium on the transformation kinetics from austenite grain size effects. It is seen that the additional hold causes an increase in undercooling (see also figure 7.10). The growth rate however does not seem to be influenced significantly. The variation in M_0 is not significant. Figure 7.12 shows the driving force for the transformation for the experiment with the one–hour hold at 1033 K. It is seen that due to the low temperatures at which the transformation occurs, relatively large driving forces are involved, even for the low cooling rate used. One of the possible mechanisms by which the transformation could be slowed down is the pinning of the interface by precipitates. This pinning would result in a modification of the driving force as given by the difference in free energy between the ferrite and the austenite. The order of magnitude for the pinning force can be calculated using equation (7.4). Assuming $\gamma = 0.2$ J/m^2 for an austenite/ferrite interface, $f = 2 \cdot 10^{-4}$, $r = 5 \cdot 10^{-9}$ m, $\beta = 1$ it follows that the pinning force is 0.04 J/mol. This value changes slightly for other values of β, γ, f or r, but it can always be neglected when compared to the driving forces involved. In table 7.4 the M_0 and ΔT values following from the fitting of the data of the Mn11 steel grade after austenitisation at 1423 K are also shown. The ΔT–value is the lowest found in this work, which once more indicates the

delay of nucleation in the niobium containing steel after austenitisation above the niobium–carbide dissolution temperature. Furhtermore it is seen that the interface mobility of Mn11 is higher than that of Mn12Nb.
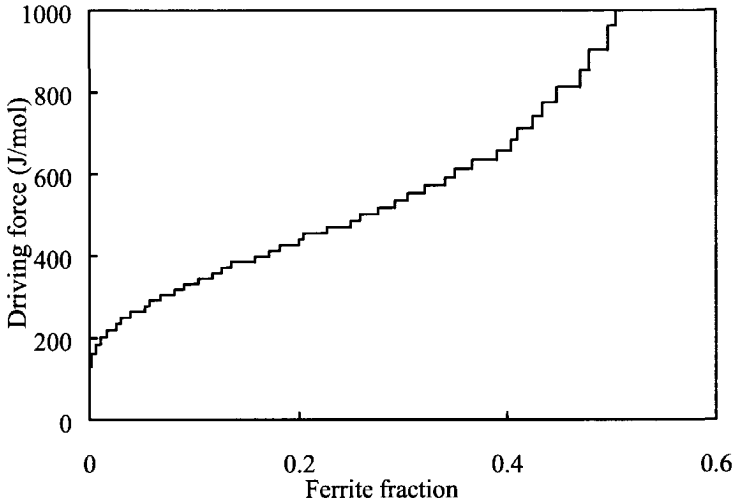

Figure 7.12   The driving force for transformation vs. allotriomorphic ferrite fraction as calculated for the two–step annealing experiment on Mn12Nb in which a 1 hour hold at 1033 K was applied.

7.5. Conclusions

A comparison of the transformation kinetics of an HSLA steel grade and related C–Mn alloys shows that, for the niobium containing steel, increasing the austenitisation temperature leads to a lower ferrite–start temperature and a transition to Widmanstätten ferrite formation. Also longer austenitisation times, leading to a reduction of heteregeneous nucleation sites, or higher cooling rates, delay nucleation and shift the transformation towards lower temperatures. The nucleus density however seems to increase. For the non–niobium containing alloys a retardation effect of manganese on the nucleation is observed. Also niobium in solution has a strong influence on the nucleation of ferrite as is shown by the shift of the ferrite–start temperature of the HSLA steel after an additional hold below the precipitation–start temperature, together with the relatively large shift of the undercooling as a function of the austenitisation temperature compared with the non–

niobium containing alloys. The interface velocity of the austenite–ferrite interface itself is not changed by the change in the ratio between the amount of niobium in precipitates and the amount of niobium in solution.

References

1   W.J. Liu, E.B. Hawbolt, I.V. Samarasekera, Conf. Proc. "*Mathematical Modelling of Hot rolling of steel*", Hamilton, Canada, 26–29 Augustus (1990), The Canadian Institute of Mining and Metallurgy, Montreal, 477.

2   P.A. Manohar, D.P. Dunne, T. Chandra, C.R. Killmore, *ISIJ International* 36 (1996) 194.

3   B. Dutta, E. Valdes, C.M. Sellars, *Acta Metall. Mater.* 40 (1992) 653.

4   S.H. Park, S. Yue, J.J. Jonas, *Metall. Trans. A* 23A (1992) 1641.

5   R.L. Bodnar, S.S. Hansen, *Metall. Mat. Trans. A* 25A (1994) 665.

6   R.C. Cochrane, W.B. Morrison, Conf. Proc., "*Steels for line pipe and pipeline fittings*" London, 21st–23rd October, (1981), The Metals Society, London pp. 70.

7   M.H. Thomas, G.M. Michal, *Proc. Int. Conf. on Solid to Solid Phase Transformations*, ed. H.I. Aaronson, D.I. Laughlin, R.F. Sekerka, L.M. Wayman, The Metallurgical Society of AIME, Warrendale, Pennsylvania, August 10 (1981), 469.

8   K.J. Lee, J.K. Lee, K.B. Kang, O. Kwon, *ISIJ International* 32 (1992) 326.

9   Y. van Leeuwen, S.I. Vooijs, J. Sietsma, S. van der Zwaag, *Met. Mat. Trans. A* 29A (1998) 2925.

10   H. Nordberg, B. Aronsson, *J.I.S.I.* 206 (1968) 1263.

11   T. Gladman, *The physical metallurgy of microalloyed steels*, Institute of Metals, London, 1996.

12   G.P. Krielaart, S. van der Zwaag, *Mat. Sci. Tech.* 14 (1998) 10.

13   J.W. Christian; *The theory of transformations in metals and alloys*, 2nd edition, 476 (1981) Pergamon Press, Oxford.

14   C. Zener as quoted by C.S. Smith, *Trans. AIME* 175 (1948) 15.

15   C.H. Wörner, P.M.Hazzledine, *JOM* 44 (No. 9) (1992) 16.

16   M. Hillert, *Metall. Trans.* 6A (1975) 5.

17   T.A. Kop, J. Sietsma, S. van der Zwaag, accepted for publication in *J. Mat. Sci.* (2000).

18   E.J. Palmiere, C.I. Garcia, A.J. DeArdo, *Met. Mat. Trans. A* 25A (1994) 277.

19   H.J. Borchardt, F. Daniels, *J. Am. Chem. Soc.* 79 (1957) 41.

Summary

The conventional hot strip rolling process consists of the following major steps: steel slabs are heated to the soaking temperature, rolled to the final thickness in the roughing and finishing mill, and finally a controlled cooling treatment, followed by the coiling step, is applied. Influencing either directly or indirectly the austenite to ferrite phase transformation, each process step can influence the final properties of the end product. This thesis concentrates on the kinetics of the austenite to ferrite phase transformation, which in general occurs during the cooling treatment. In the first part of this thesis the applicability of dilatometry to obtain accurate data on the austenite to ferrite transformation kinetics is studied. In the second part of the thesis an interface mobility model is presented and the validity of the model is tested in various cases utilising experimental dilatometry data.

Dilatometry is a useful technique to obtain experimental data concerning transformation kinetics in ferrous alloys. This technique is commonly used in cooling experiments to study the austenite decomposition of hypo–eutectoid steel grades. A dilatation measurement at a constant cooling rate, dT/dt, results in the observation of the sample length change $vs.$ temperature. A dilatation curve of a sample transforming from austenite to ferrite consists of two parts that are approximately linear with temperature, corresponding with the thermal expansion behaviour of austenite and ferrite/pearlite respectively, and a non–linear part which corresponds with the volume change caused by the phase transformation. In the standard analysis of the dilatation signal two assumptions are made: the dilatation behaviour of the sample is isotropic, and the observed change in length, relative to the extrapolated expansion behaviour of the austenite and the ferrite/pearlite, is proportional to the fraction transformed austenite. When proportionality between the change in length and the change in phase fractions is assumed, two factors are neglected. First during the pro–eutectoid ferrite formation the austenite enriches in carbon. This causes that the austenite–length reference level deviates from the extrapolated austenite thermal expansion behaviour, since the austenitic atomic volume also depends on the carbon concentration. Furthermore, the atomic volume of the ferrite formed is considerably different from that of the pearlite formed. Not taking into account these two effects can lead to an error in the determined ferrite fraction of up to 25 %. In Chapter 2 a method is presented that takes into account the two above–mentioned factors. In order to determine both the ferrite fraction and the pearlite fraction, in the analysis the temperature

range of the transformation is divided into a ferrite–formation range and a pearlite–formation range. Two possible criteria for this division are discussed, and it is shown that the choice between these two does not have an essential influence on the results; in both cases a satisfactory analysis can be performed.

Chapter 3 discusses the validity of the assumption concerning the isotropic dilatation behaviour. In general the material used to study the austenite decomposition has been continuously casted and hot–rolled. This process quite often results in spatial inhomgeneities in the concentration of the alloying elements, which can lead to the formation of banded ferrite/pearlite structures. Dilatation measurements are performed on cylindrical samples with the longitudinal axis either parallel or normal to the bands of ferrite and pearlite, and show rather different results for those heat treatments, which lead to a banded ferrite/pearlite microstructure. Under those conditions the standard methods of deriving the fractions transformed from the dilatation signal are not applicable. A model describing the anisotropic dilatation behaviour for such an evolving banded structure is presented. The model reproduces the experimentally observed differences as a function of the band orientation semi–quantitatively. The model calculations indicate that the description of the anisotropic dilatation behaviour during transformation of a forming banded structure should be based on a time dependent model rather than on models that do not account for the phase transformation history. Furthermore, the implications for the determination of the fraction transformed are discussed.

The model that is used extensively in this thesis to describe the austenite to ferrite transformation is a single–grain model involving interface–controlled mobility. The grain has a tetracaidecahedron geometry. In the calculations the ferrite nuclei, which are placed on the grain corners or grain faces of the austenite grain, grow at a certain rate. The velocity of the austenite/ferrite interface is determined by the intrinsic mobility of the interface and the driving force for the transformation. The driving force for the transformation depends on the temperature and on the chemical composition of the phases at the interface. The intrinsic mobility of the interface is determined by the kinetics of the austenite to ferrite lattice transformation. For the interface mobility, M, an Arrhenian temperature dependence is assumed:

$$M = M_0 \cdot \exp\left(-\frac{Q}{RT}\right).$$

Q, R en T are respectively the activation energy, the gas constant and the temperature. M_0 is a pre–exponential factor. Chapters 4 to 7 investigate the applicability of the model to describe the austenite to ferrite transformation kinetics for iron alloyed with various elements.

In chapter 4 the transformation from austenite to ferrite in binary substitutional Fe–X alloys, where X represents successively 1 or 2 % of Co, Cu, Mn, Cr or Al, is investigated experimentally. The driving force for the transformation is calculated assuming the chemical compositions of both the austenite and ferrite phase to be equal to the initial composition, *i.e.* no partitioning is assumed. The assumption of an Arrhenian temperature dependence of the interface mobility is found to give a consistent picture of the observations, which were made over a temperature range of about 250 K. For the activation energy for atoms crossing the interface a value of 140 kJ/mol was used. The unintentional presence of interstitial nitrogen is shown to have a significant effect on the mobility, as large as a factor 8 at concentration levels on the order of 10^{-4}.

In chapter 5 the inferred relation between nitrogen content and the mobility of the austenite/ferrite interface is explored further. Samples of an Fe–1at.%Si alloy were given various internal nitriding treatments, leading to samples containing nitrogen concentrations between 20 and 3000 appm. Dilatometric measurements indicate a clear shift in the transformation curves. The transformation is shifted to lower temperatures and is slowed down with higher nitrogen contents. For nitrogen concentrations smaller than 500 appm there is a good agreement between experimental and model fraction curves, using an exponential relation for the nitrogen dependence of the pre–exponential mobility factor, M_0. For higher nitrogen levels M_0 decreases less rapidly. Moreover, only the first part of the ferrite formation is accurately modelled. Towards the end of the transformation the discrepancy between experimental and model fraction curves increases. This suggests that for the determination of the driving force in the case of higher nitrogen concentrations the diffusion of nitrogen should be taken into account.

In chapter 6 the transformation behaviour of three lean–carbon manganese steels is investigated. The relatively large amount of interstitial carbon present necessitates a different approach for the calculation of the driving force than was followed in chapter 4 and 5. The interstitial carbon is assumed to redistribute infinitely fast during the transformation. The carbon compositions at the transforming interface are thus assumed to be the equilibrium concentration in the ferrite and the average concentration in the austenite. The experimental fraction curves are modelled using the intrinsic mobility factor M_0 as the adjustable variable. The interface model yields adequate reproductions of the

experimentally determined transformation kinetics, with only a slight variation in M_0. It is found that M_0 increases slightly with increasing cooling rate and decreasing carbon concentration. This variation is evaluated in the light of the diffusivity of carbon, the build–up of stresses at the austenite/ferrite interface, and the nucleus density. The trends in M_0 can be explained by wrong input for the nucleus density, which can be caused by ferrite grain coarsening. It is argued that the apparent ferrite nucleus density determined from the ferrite grain size in the completely transformed sample underestimates the nucleus density, probably caused by ferrite grain coarsening taking place during the transformation.

The dependence of the transformation kinetics of a High Strength Low Alloy steel and comparable C–Mn steels on the austenitisation conditions has been investigated using both dilatometry and calorimetry (chapter 7). It is observed that the ferrite–start temperature depends both on the manganese content and on the amount of niobium in solution. Application of the interface–mobility model showed that the micro–alloying element niobium has no influence on the intrinsic mobility of the interface.

This thesis shows that for the accurate determination of fractions transformed the possible appearance of anisotropic dilatation behaviour and the indirect effects of carbon should be taken into account, and that the combination of the tetracaidecahedron representative single grain concept and the austenite/ferrite interface mobility model proves to be a valuable tool to study the austenite to ferrite transformation kinetics.

Samenvatting

Het conventionele warmwalsproces voor bandstaal omvat de volgende belangrijke productiestappen: de stalen plakken worden in een oven opgewarmd tot de austeniteertemperatuur, voorgewalst, uitgewalst tot de uiteindelijke dikte, en tenslotte wordt een gecontroleerd koeltraject doorlopen, waarna de band opgewikkeld wordt. Al deze productie stappen beïnvloeden direct of indirect de austeniet naar ferriet fasentransformatie, en daardoor de resulterende mechanische eigenschappen van de uiteindelijke staalplaat. Dit proefschrift richt zich op de kinetiek van de austeniet naar ferriet fasentransformatie. In het eerste deel van het proefschrift wordt het gebruik van dilatometrie voor het verkrijgen van nauwkeurige data betreffende de fracties austeniet en ferriet als functie van tijd en temperatuur bediscussieerd. In het tweede deel wordt een model gepresenteerd dat de austeniet naar ferriet transformatie beschrijft. Dit model is gebaseerd op de mobiliteit van het austeniet/ferriet grensvlak en wordt getest aan de hand van experimentele dilatometrische data voor verschillende staalkwaliteiten.

Dilatometrie, de meting van de lengteverandering van een proefstuk, is een geschikte techniek om data betreffende de transformatiekinetiek van vaste stof fasentransformaties te verkrijgen. In staalonderzoek wordt deze techniek vaak toegepast om de austenietdecompositie van hypo–eutectische legeringen tijdens afkoelen te bestuderen. Een dilatatie meting bij constante afkoelsnelheid, dT/dt, resulteert in een gemeten lengteverandering als functie van de temperatuur. Een dilatatiecurve van een proefstuk dat van austeniet naar ferriet transformeert zal bestaan uit twee delen die bij benadering lineair zijn als functie van de temperatuur, corresponderend met het thermisch–expansie gedrag van de austeniet danwel ferriet/perliet, en een niet lineair deel dat correspondeert met de volumeverandering die tijdens de transformatie plaatsvindt. De standaardanalyse van het dilatatiesignaal is gebaseerd op twee aannames: de dilatatie van het proefstuk is isotroop en de waargenomen lengteverandering, ten op zichte van het geëxtrapoleerde uitzettingsgedrag van de austeniet en de ferriet/perliet, is evenredig met de fractie getransformeerde austeniet. Deze tweede aanname leidt in het geval van koolstof–houdend materiaal tot het verwaarlozen van twee factoren. Ten eerste verrijkt de austeniet in koolstof tijdens de ferrietvorming. Dit leidt ertoe dat het referentie austeniet–lengteniveau afwijkt van het geëxtrapoleerde austenietgedrag, omdat het austenietvolume mede bepaald wordt door de koolstofconcentratie. Bovendien leidt de aanwezigheid van koolstof tot de

vorming van perliet, hetgeen een ander atomair volume heeft dan ferriet. Het verwaarlozen van deze twee factoren kan leiden tot een fout van 25 % in de bepaalde ferrietfractie. In hoofdstuk 2 wordt een analysemethode die wel rekening houdt met de twee voornoemde factoren gepresenteerd. Om zowel de ferriet– als de perlietfractie te bepalen, dient de analyse in twee stappen plaats te vinden. Hiervoor moet de temperatuuras gesplitst worden in een range behorende bij de ferrietvorming en een range voor de perlietvorming. Twee mogelijke criteria voor deze splitsing worden besproken. Het blijkt dat beide criteria tot vergelijkbare resultaten leiden.

Hoofdstuk 3 onderzoekt de juistheid van de aanname van isotroop dilatatiegedrag. Het bepalen van de juistheid van deze aanname is van belang voor onderzoek aan warmgewalste constructie staalsoorten waar bij niet te hoge austeniteer–temperaturen en beperkte afkoelsnelheden vaak een gelaagde ferriet/perliet microstructuur ontstaat. Dilatatiemetingen zijn uitgevoerd aan cilindrische proefstukken waarvan de cilinderas hetzij parallel aan of loodrecht op de ferriet– en perlietlagen is. Het blijkt dat de aanname van isotroop dilatatiegedrag niet juist is. Een model gebaseerd op de interacties tussen de lagen wordt gebruikt om het anisotrope dilatatiegedrag te verklaren. De invloed die het anistrope dilatatiegedrag op de bepaling van de getransformeerde fracties heeft wordt belicht.

Om de kinetiek van de austeniet naar ferriet fasentransformatie te beschrijven wordt gebruik gemaakt van een één–korrel model, waarin de groeisnelheid van de ferriet wordt bepaald door de austeniet/ferriet grensvlakmobiliteit. De austenietkorrel is een regelmatig veertienvlak. In de berekeningen worden de ferrietkiemen op de hoekpunten van de korrel geplaatst. Iedere kiem groeit vervolgens met een bepaalde snelheid die bepaald wordt door de intrinsieke mobiliteit van het grensvlak en de drijvende kracht voor de transformatie. De drijvende kracht voor de transformatie is afhankelijk van de temperatuur en van de chemische samenstelling aan het bewegende grensvlak. De intrinsieke mobiliteit van het grensvlak is afhankelijk van de kinetiek van de omvorming van de atoomstapeling van de kubisch vlakken–gecentreerde structuur naar de kubisch ruimtelijk–gecentreerde structuur. Voor de temperatuursafhankelijkheid van de mobiliteit, M, wordt een Arrhenius–verband verondersteld:

$$M = M_0 \cdot \exp\left(-\frac{Q}{RT}\right).$$

Q, *R* en *T* staan respectievelijk voor de activeringsenergie, de gasconstante en de temperatuur. M_0 is een pre–exponentiële factor. Het onderzoek in hoofdstuk 4 tot en met 7 betreft de toepasbaarheid van dit model voor de beschrijving van de austeniet naar ferriet transformatie van ijzer gelegeerd met verschillende soorten legeringselementen.

In hoofdstuk 4 is de transformatiekinetiek van austeniet naar ferriet in binaire substitutionele Fe–X legeringen onderzocht, waar X staat voor 1 of 2 % Co, Cu, Mn, Cr of Al. De drijvende kracht voor de transformatie is berekend onder de aanname dat de concentraties in de austeniet en de ferriet gedurende de gehele transformatie gelijk zijn aan de beginconcentratie. Met andere woorden, er wordt aangenomen dat er geen herverdeling van legeringselementen plaatsvindt. De aanname van een Arrhenius–verband voor de temperatuurafhankelijkheid van de grensvlakmobiliteit, geeft een goede beschrijving van de waarnemingen, die een temperatuur–range van meer dan 250 K beslaan. Voor de activeringsenergie voor atomen die het grensvlak oversteken is een waarde van 140 kJ/mol gebruikt. Kleine hoeveelheden stikstof, die als verontreiniging in de proefstukken aanwezig is, blijken een grote invloed op de mobiliteitsfactor te hebben. De mobiliteit daalt met een factor 8 door een stikstofconcentratie in de orde van 10^{-4}.

In hoofdstuk 5 is het verband tussen de stikstofconcentratie en de mobiliteit verder onderzocht. Proefstukken van een Fe–1at.%Si legering hebben een nitreerbehandeling ondergaan teneinde het stikstofgehalte te variëren van 20 tot 3000 appm. Dilatatiemetingen aan de resulterende reeks proefstukken laten een duidelijke verschuiving van de transformatiecurven zien. De transformatie verschuift naar lagere temperaturen en verloopt langzamer. Voor stikstofconcentraties tot ongeveer 500 appm is er een goede overeenkomst tussen de experimentele en de gemodelleerde fractiecurven, waarbij de stikstofafhankelijkheid van de pre–exponentiële mobiliteitsfactor, M_0, met een exponentiële functie beschreven kan worden. Verder wordt uit de waarnemingen afgeleid dat voor hogere stikstofgehaltes de diffusie van stikstof een belangrijkere rol gaat spelen en er niet meer volstaan kan worden met een berekening van de drijvende kracht, gebaseerd op de aanname dat er geen herverdeling van legeringselementen plaatsvindt.

In hoofdstuk 6 worden drie C–Mn staalsoorten onderzocht. Een andere aanpak voor de berekening van de drijvende kracht is nodig in vergelijking met hoofdstuk 4 en 5 vanwege het relatief hoge interstitieel–koolstof gehalte. Er wordt aangenomen dat de koolstof behalve in de ferriet ook in de austeniet oneindig snel diffundeert in vergelijking met de beweging van het austeniet/ferriet grensvlak. De koolstofconcentratie aan het transformerende grensvlak in de austeniet is de gemiddelde koolstofconcentratie in de austeniet en de concentratie in de ferriet is gelijk aan de evenwichtsconcentratie van

127

koolstof in ferriet. De pre–exponentiële mobiliteitsfactor, M_0, is gebruikt als de variabele parameter om de experimentele fractiecurven te modeleren. Het model geeft een goede beschrijving van de experimentele resultaten met slechts een geringe variatie in M_0. M_0 neemt toe met toenemende afkoelsnelheid en met afnemende koolstofconcentratie. Een eventuele samenhang tussen deze trends en de diffusie van koolstof, de opbouw van spanningen aan het austeniet/ferriet grensvlak en de kiemdichtheid is onderzocht. De trends in M_0 suggereren dat de ferrietkiem dichtheid zoals bepaald uit de ferriet korrelgrootte te laag is, en dat er waarschijnlijk tijdens de ferrietvorming ook ferrietvergroving optreedt.

In hoofdstuk 7 is de invloed van de austeniteercondities op de transformatiekinetiek van een HSLA (High Strength Low Alloy) staal en vergelijkbare C–Mn staalsoorten onderzocht met behulp van dilatometrie en calorimetrie. De ferriet–start temperatuur blijkt zowel van het mangaangehalte als van de hoeveelheid niobium in oplossing af te hangen. Toepassing van het grensvlakmobiliteitsmodel leidt tot de conclusie dat het micro–legeringselement niobium geen invloed heeft op de mobiliteit van het austeniet/ferriet grensvlak.

Dit proefschrift laat zien dat nauwkeurige bepaling van fracties getransformeerd met behulp van dilatometrie mogelijk is mits rekening gehouden wordt met eventueel anisotroop dilatatiegedrag en de invloed van koolstof op de verschillende atomaire volumina, en dat de combinatie van het concept van een representatieve 14–vlaks austenietkorrel en een grensvlakmobiliteitsmodel geschikt is om de austeniet naar ferriet fasentransformatie te bestuderen en te beschrijven.

Dankwoord

Tot slot wil ik hier mijn dank betuigen aan hen die mij de mogelijkheid hebben geboden om mijn promotieonderzoek uit te voeren en aan hen die direct of indirect hebben bijgedragen aan de werkvreugde.

Allereerst wil ik de volgende organisaties bedanken; het Innovatief Onderzoek Programma Metalen, het Prioriteiten Programma Materialen, Corus Research and Development en de Technische Universiteit Delft. Zij boden de financiële middelen waarmee, en het kader waarin, het onderzoek uitgevoerd kon worden.

Het beschreven werk is uitgevoerd onder toeziend oog van Sybrand van der Zwaag en Jilt Sietsma, in samenwerking met collega promovenda Yvonne van Leeuwen, en de afstudeerders Simone Vooijs, Peter Remijn en Jeroen Wits. Mijn hartelijke dank voor jullie werk dat in belangrijke mate bijgedragen heeft aan het verwezenlijken van dit proefschrift.

Tevens gaat mijn dank uit naar de collega's van het Laboratorium voor Materiaalkunde, en in het bijzonder naar de mensen van ondersteunende diensten en de vakgroepen Fysische Chemie en Materiaalkunde en Productie Technologie.

Om niet in een oneindige opsomming van namen te vervallen zal ik slechts enkele namen noemen. Mijn dank gaat uit naar onder andere de volgende mensen die door hun enthousiasme ervoor gezorgd hebben dat het iedere dag weer een plezier was om aan het werk te gaan. De mannen van het eerste uur Marco, Bert, Fred en Jörgen, voor het middenstuk Arjan, Mieke, Martin, Simone en Pieter, en voor de eindspurt Jilt, Dave, Roland, Erik Peekstok, Willem Maarten en Wilma.

Tot slot wil ik de scheiko's uit Leiden, mijn huisgenoten, de drummers en danseressen, de klimmers, en mijn familie bedanken, misschien wel niet zo zeer voor hun bijdrage aan dit proefschrift, als wel voor het verhogen van de algehele levensvreugde.

Curriculum Vitae

Theo A. Kop

geboren op 12 juli 1973 te Rotterdam

1985 – 1991   VWO, Dalton Scholengemeenschap Erasmus College te Zoetermeer.

1991 – 1995   Scheikunde studie aan de Rijksuniversiteit Leiden. Afstudeerrichting Vaste Stof Chemie. Afstudeerproject "Structure determination of A_2BO_4 compounds with $CaFe_2O_4$ or K_2NiF_4-related structures" uitgevoerd onder begeleiding van dr. D.J.W. IJdo.

1994 – 1995   Industriële stage bij SCCC (Societé de Coulée Continue de Cuivre, bedrijf dat koperdraad produceert) in Frankrijk. Project *"La dissolution d'oxygène dans le liquide du cuivre"* uitgevoerd onder begeleiding van de heer M. Ly en prof. M. Onillon (Université de Bordeaux).

1995 – 2000   Promotie-onderzoek "A dilatometric study of the austenite/ferrite interface mobility" uitgevoerd in de sectie "Microstructuurbeheersing in Metalen" van het Laboratorium voor Materiaalkunde aan de Technische Universiteit Delft, onder begeleiding van prof. dr. ir. S. van der Zwaag en dr. ir. Jilt Sietsma.

2000   Wetenschappelijk medewerker bij Philips Research te Eindhoven.

List of publications

Journal papers

P. Jacques, E. Girault, T. Calin, N. Geerlofs, T. A. Kop, S. van der Zwaag, F. Delannay, *Bainite transformation of low carbon Mn–Si TRIP–assisted multiphase steels: influence of silicon content on cementite precipitation and austenite retention*, Materials Science and Engineering A273-275 (1999) 475–479

J.J. Wits, T.A. Kop, Y. van Leeuwen, J. Sietsma, S. van der Zwaag, *A study on the austenite–to–ferrite phase transformation in binary substitutional iron alloys*, Materials Science and Engineering A283 (2000) 234–241

T.A. Kop, Y. van Leeuwen, J. Sietsma, S. van der Zwaag, *Modelling the austenite to ferrite phase transformation in low carbon steels in terms of the interface mobility*, Iron and Steel Institute Japan International, Vol. 40 (2000) 713–718

T.A. Kop, J. Sietsma, S. van der Zwaag, *Dilatometric Analysis of phase transformations in hypo-eutectoid steels*, accepted for publication in Journal of Materials Science (2000)

T.A. Kop, P.G.W. Remijn, V. Svetchnikov, J. Sietsma, S. van der Zwaag, *Some observations on the effect of austenitisation conditions on the transformation kinetics in an HSLA steel and related C–Mn steels*, accepted for publication in Journal of Materials Science (2000)

T.A. Kop, J. Sietsma, S. van der Zwaag, *The influence of nitrogen on the ferrite/austenite interface mobility in Fe–1%Si*, submitted to Materials Science and Engineering A (2000)

T.A. Kop, J. Sietsma, S. van der Zwaag, *The anisotropic dilatation behaviour of hot rolled steels showing a banded structure*, submitted to Materials Science and Technology (2000)

Conference papers

T.A. Kop, J. Sietsma, S. van der Zwaag, *The transformation kinetics of construction steels; a combined dilatometric and DTA approach*, Proceedings of the 5th European Conference on Advanced Materials, Processes and Applications (EUROMAT 97) "Materials, Functionality & Design", Vol. 1: Metals and Composites, L.A.J.L. Sarton, H.B. Zeedijk (eds.), The Netherlands Society for Materials Science, Zwijndrecht, 1997, p. 537–540.

T.A. Kop, F.D. Tichelaar, J. Sietsma, S. van der Zwaag, *In-situ Observation of the Growth of Ferrite from Austenite in the Transmission Electron Microscope*, Proceedings of the 5th European Conference on Advanced Materials, Processes and Applications (EUROMAT 97) "Materials, Functionality & Design", Vol. 4: Characterization and Production/Design, L.A.J.L. Sarton, H.B. Zeedijk (eds.), The Netherlands Society for Materials Science, Zwijndrecht, 1997, p. 39–42.

T.A. Kop, J. Sietsma, S. van der Zwaag, *Ferrous phase transformation kinetics: a combined dilatometric-calorimetric approach*, Accelerated Cooling/Direct Quenching of Steels, Proceedings of Materials Solutions '97 on Accelerated Cooling/Direct Quenching of Steels, Indiana Convention Center, Indiana, 15-18 September 1997, R. Asfani (ed.), ASM International, Materials Park, Ohio, 1997, p. 159–165.

T.A. Kop, P.G.W. Remijn, J. Sietsma, S. van der Zwaag, *The effect of the austenitisation temperature on the transformation kinetics of an Nb-containing steel*, Proceedings of the International Conference on Microalloying in steels, J.M. Rodriguez-Ibabe, I. Gutiérrez, B. López (eds.), Trans Tech Publications Ltd, Switzerland, 1998 (Materials Science Forum 284-286), p. 193–200.

Y. van Leeuwen, T.A. Kop, J. Sietsma, S. van der Zwaag, *Phase transformations in low-carbon steels; modelling the kinetics in terms of the interphase mobility*, J. Phys. IV France, 9 (1999) Pr-9-401–409.
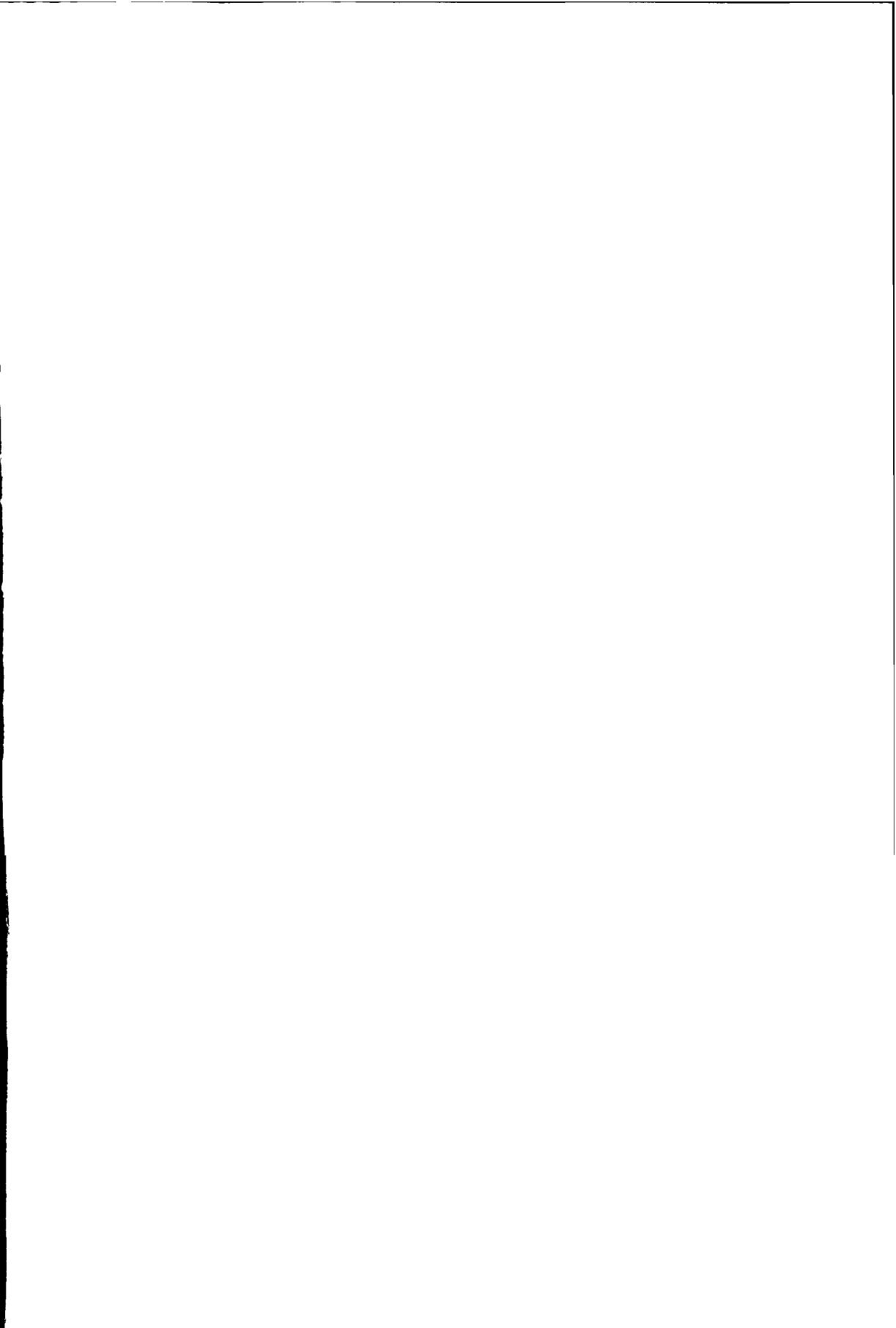
A dilatometric study of the austenite/ferrite interface mobility

This thesis contributes to the development of a model for the austenite to ferrite phase transformation. The model is based on physical and microstructural features, thereby aiming to enlarge the insight into the physical processes occurring. By doing so, the results and insight gained are helpful in the development of new steel grades and steel production processes. The model describes the transformation via a nucleation and growth process. The growth is assumed to be controlled by the intrinsic mobility of the austenite/ferrite interface. Data on the austenite to ferrite transformation kinetics are mainly determined using dilatometry.

In the first part of this thesis the applicability of dilatometry for the determination of fractions transformed during the austenite decomposition of steel is treated in detail. The second part concentrates on the transformation kinetics of different steel systems.

Delft University of Technology